AIRCRAFT ACCIDENT REPORT 2/2014

ACCIDENT INVESTIGATION DIVISION

Civil Aviation Department
The Government of
Hong Kong Special Administrative Region

Report on the accident to AgustaWestland AW139
Registration B-MHJ operated by East Asia Airlines Limited
at Hong Kong Victoria Harbour
on 3 July 2010

Hong Kong
July 2014

In accordance with Annex 13 to the ICAO Convention on International Civil Aviation and the Hong Kong Civil Aviation (Investigation of Accidents) Regulations, the sole objective of this investigation is the prevention of aircraft accidents. It is not the purpose of this activity to apportion blame or liability.

民航處
CIVIL AVIATION DEPARTMENT
香港特別行政區政府
The Government of the Hong Kong Special Administrative Region

香港大嶼山香港國際機場
東輝路1號民航處總部
Civil Aviation Department Headquarters
1 Tung Fai Road, Hong Kong International Airport,
Lantau, Hong Kong

電話 Tel: (852) 2910 6363
圖文傳真 Fax: (852) 2501 6040
檔案編號 Our ref:
來函編號 Your ref:

6 June 2014

The Honourable C Y Leung, GBM, GBS, JP
The Chief Executive
Hong Kong Special Administrative Region
People's Republic of China

Dear Sir,

In accordance with Regulation 10(6) of the Hong Kong Civil Aviation (Investigation of Accidents) Regulations, I have the honour to submit the report by Mr K C MAN, an Inspector of Accidents, on the circumstances of the accident to an AgustaWestland AW139 helicopter, registration B-MHJ at Hong Kong Victoria Harbour on 3 July 2010.

Yours faithfully,

(Norman S M LO)
Director-General of Civil Aviation

Intentionally Left Blank

TABLE OF CONTENTS Page

GLOSSARY OF ABBREVIATIONS

AACM	Civil Aviation Authority of Macao Special Administrative Region
AAIB	United Kingdom Air Accidents Investigation Branch
AD	Airworthiness Directive
ADELT	Automatically Deployable Emergency Locator Transmitter
AGL	Above Ground Level
AHRS	Lateral Acceleration
Altitude	The vertical distance of an aircraft above mean sea level
AMS	Aircraft Maintenance Schedule
AMSL	Above Mean Sea Level
ANRM	Air Navigation Regulation of Macao
ANSV	Agenzia Nazionale per la Sicurezza del Volo of Italy
ATS	Air Traffic Service
AW	AgustaWestland
°C	Degree Celsius
C of A	Certificate of Airworthiness
CA	Continuing Airworthiness
CAD	Hong Kong Civil Aviation Department
Cloud base	The base of the lowest cloud layer at any particular location, measured as a vertical distance above the surface
C of G	Centre of Gravity
COSPAS/SARSAT	Cosmicheskaya Sistyema Poiska Avariynich Sudov / Search and Rescue Satellite
CVR	Cockpit Voice Recorder
DSC	Differential Scanning Calorimetry
EAA	East Asia Airlines Limited

EASA	European Aviation Safety Agency
ELT	Emergency Locator Transmitter
ENAC	Ente Nazionale per l'Aviazione Civile
FDR	Flight Data Recorder
FEM	Finite Element Analysis
FESEM	Field Emission Scanning Electron Microscope
FOCC	Flight Operations Control Centre
FSCC	Fire Services Communication Centre
FSD	Fire Services Department
GAG	Ground Air Ground
GFRC	Glass Fibre Reinforced Composite
GFS	Government Flying Service
HKO	Hong Kong Observatory
HKPF	Hong Kong Police Force
HUMS	Health and Usage Monitoring System
IAS	Indicated Airspeed
ICAO	International Civil Aviation Organisation
ILRS	Interlaminar Radial Stress
ILSS	Interlaminar Shear Stress
ILTS	Interlaminar Transverse Stress
IMC	Instrument Meteorological Conditions
JAA	Joint Aviation Authorities
JAR	Joint Airworthiness Requirements
kg	kilogram
KHz	Kilohertz
km/hr	Kilometer per hour
kt	knot

°M	Degrees Magnetic
MFPR	Multi-Purpose Flight Recorder
MHz	Megahertz
mm	millimeter
MPa	Megapascal
MRCC	Maritime Rescue Co-ordination Centre
m/s	meter per second
MTOW	Maximum Take Off Weight
nm	nautical mile
PF	Pilot Flying
PLB	Personal Locator Beacon
P/N	Part Number
PNF	Pilot Not Flying
QinetiQ	A defence, aerospace and security expert company provided forensic engineering service to CAD
RCCC HK	Regional Command and Control Centre of Hong Kong Island
RCCC MAR	Regional Command and Control Centre Marine
RPM	Revolution Per Minute
SB	Service Bulletin
SEM	Scanning Electron Microscope
S/N	Serial Number
SOP	Standard Operating Procedures
SVFR	Special Visual Flight Rules
TCDS	Type Certificate Data Sheet
Tg	Glass Transition Temperature
TGB	Tail Gearbox
TSO	Technical Standard Order

UKCAA	United Kingdom Civil Aviation Authority
UTC	Coordinated Universal Time
με	microstrain
μm	micrometer
VFR	Visual Flight Rules
VHF	Very High Frequency
VMC	Visual Meteorological Conditions
Vv	Vertical Descent Velocity

ACCIDENT INVESTIGATION DIVISION

CIVIL AVIATION DEPARTMENT

Aircraft Accident Report 2/2014

Registered Owner:	East Asia Airlines Limited
Operator:	East Asia Airlines Limited
Aircraft Type:	AgustaWestland AW139
Nationality:	Chinese
Registration:	B-MHJ
Place of Accident:	Hong Kong Victoria Harbour
	Latitude: 22º 17' 28" N Longitude: 114º 08' 56" E
Date and Time:	3 July 2010 at 0400 hrs (1200 hrs)
	All times in this Report are in UTC with Hong Kong local time in parenthesis

Intentionally Left Blank

SYNOPSIS

The helicopter took off from Sheung Wan / Sky Shuttle Heliport in Hong Kong at 0400 hrs (1200 hrs). Approximately 2 minutes after takeoff, shortly after the crew had completed the post-takeoff checks while climbing on a north-westerly heading at approximately 350 ft Above Mean Sea Level (AMSL) and at about 70 kt Indicated Airspeed (IAS), the tail rotor assembly detached from the helicopter. The commander immediately entered into autorotation and subsequently made a controlled ditching into the harbour. All pilots and passengers were rescued by the nearby vessels. Six of the 11 passengers received treatment for minor injuries.

The accident was notified to the Accidents Investigation Division of the Hong Kong Civil Aviation Department (CAD) by the Fire Services Communication Centre (FSCC) of the Fire Services Department (FSD) at 0405 hrs (1205 hrs) on 3 July 2010. The investigation team, comprising a team of CAD Inspectors of Accidents, started the investigation immediately. Two days later, investigators from the Civil Aviation Authority of Macao Special Administrative Region (AACM), Agenzia Nazionale per la Sicurezza del Volo of Italy (ANSV) and AgustaWestland (AW), the aircraft manufacturer joined the investigation team.

The investigation identified that the failure of the White Blade was caused by the reduction of torsion box stiffness at the blade root radii area, which when associated with manufacturing strap defects at maximum acceptable values in production specification, caused the Interlaminar Radial Stress (ILRS) to exceed the maximum allowable limit, resulting in matrix delamination onset and then propagation under Interlaminar Shear Stress (ILSS) and complete failure of the blade.

The investigation team has made two safety recommendations on the AW139 tail rotor blades.

1 FACTUAL INFORMATION

1.1 History of the Flight

1.1.1 On 3 July 2010, the helicopter was operated by East Asia Airlines Limited (EAA) to perform shuttle flights between Macao and Hong Kong. The accident flight EA 206A, with a callsign of 'East Asia 2', was scheduled to depart Sheung Wan / Sky Shuttle Heliport at 0400 hrs (1200 hrs) with 2 crew members and 11 passengers onboard. The commander was the pilot flying (PF) in the right seat. The first officer was the pilot not flying (PNF) in the left seat, assisting the commander in carrying out flight procedures. The crew conducted the flight in accordance with the Flight Time Limitations Scheme of the operator. The same crew had flown the flight from Macao to Hong Kong prior to the accident flight. A rotors-running turnaround without refueling was carried out at the Heliport. The previous flight was normal.

1.1.2 The helicopter lifted off at 0400 hrs (1200 hrs) and was climbing away from the Heliport on a north-westerly heading, tracking towards Green Island. When passing approximately 350 ft AMSL, the crew had completed the post-takeoff checks. Shortly afterwards, both pilots heard a loud bang from the rear of the helicopter followed by sense of airframe vibrations. At the same time, the commander found that he had no authority on the pedal controls and determined that the tail rotor of the helicopter had failed. Immediately, the commander put the helicopter into autorotation. Whilst in autorotation, he commanded the first officer to shut down both engines in accordance with the emergency procedures. The first officer shut down the engines after two more commands from the commander. Also, the commander transmitted a MAYDAY call on the company frequency. The commander made a controlled ditching with the helicopter maintained in a level attitude and low forward speed at touchdown. Once the helicopter touched the water, all the four emergency floatation bags inflated automatically.

1.1.3 While the helicopter remained floating at a slightly nose down attitude, both pilots exited the cockpit through the emergency exit windows on their respective cockpit doors. The commander then opened the starboard passenger door from the outside. Both pilots instructed and assisted the passengers to evacuate from the helicopter. After ensuring that nobody

remained on board, the commander left the helicopter. All pilots and passengers were rescued by the nearby vessels. The 11 passengers were taken to hospital for medical examination. Six passengers received treatment for minor injuries. All passengers were discharged from hospital on the same day.

1.2 Injuries to Persons

1.2.1 There were 13 persons onboard including two pilots and 11 passengers. Their injury status is shown in the table below. There was no injury to any other person.

Injuries	Flight crew	Passengers	Total in Helicopter
Fatal	0	0	0
Serious	0	0	0
Minor	0	6	6
Nil Injury	2	5	7
TOTAL	2	11	13

1.2.2 Six of the 11 passengers were admitted to hospital for medical treatment on minor injuries such as arm bruise or dizziness. They were discharged from hospital on the same day.

1.3 Damage to Aircraft

1.3.1 The cabin of the helicopter was intact. All occupant seats were neither damaged nor distorted. The cockpit doors and cabin doors were intact without deformation and their function was normal.

1.3.2 The following parts were found missing from the helicopter wreckage:

(a) The top section of the vertical fin.

(b) The tail rotor and tail gearbox assembly and the associated drive shaft, control rods and cover fairings.

(c) The two cockpit door window transparencies.

(d) Left-hand nose window transparency panel.

(e) Two vent air scoops.

1.3.3 A detailed description of damage found on the relevant helicopter components is contained in Section 1.12 – Wreckage and Impact Information.

1.4 Other Damage

1.4.1 Apart from the helicopter, there was no damage sustained by other objects.

1.5 Personnel Information

1.5.1 Pilot in Command

Sex / Age:	Male, aged 45 years	
Licences:	Airline Transport Pilot's Licence (Helicopters) issued by AACM, no limitations	
Aircraft ratings:	AW139	
Last Licensing Flight Test on type:	2 May 2010	
Last Operator Proficiency Check on type:	2 May 2010	
Medical Certificate:	Class 1, valid until 24 January 2011. No restrictions.	
Flying Experience:	Total helicopter:	6153 hours
	Total on type:	377 hours
	Total on type as pilot-in-command (PIC):	307 hours

1.5.2 Co-pilot

Sex / Age:	Male, aged 36 years	
Licences:	Airline Transport Pilot's Licence (Helicopters) issued by AACM, no limitations	
Aircraft ratings:	AW139	
Last Licensing Flight Test on type:	23 June 2010	
Last Operator Proficiency Check on type:	23 June 2010	
Medical Certificate:	Class 1, valid until 4 November 2010. No restrictions.	
Flying Experience:	Total helicopter:	4729 hours
	Total on type:	531 hours

1.6 Aircraft Information

1.6.1 Aircraft Data

1.6.1.1 General Information

(a) The AW AW139 helicopter holds a Type Certificate EASA.R.006 issued by the European Aviation Safety Agency (EASA). It is a medium-sized, single main rotor and single tail rotor helicopter that is powered by two Pratt and Whitney Canada PT6C-67C turbine engines and is equipped with retractable landing gears.

(b) The helicopter was delivered following manufacture to the operator. Detailed data are as follows:

Aircraft manufacturer:	AW
Aircraft model:	AW139
Aircraft serial number:	31222
Year of manufacture:	2008
Nationality and Registration Marks:	B-MHJ
Certificate of Registration:	Certificate of No. 03/09 issued on 22 January 2009
Name of the Owner:	East Asia Airlines Limited
Name of the Operator:	East Asia Airlines Limited
Certificate of Airworthiness (C of A):	Certificate of No. 03/09 issued on 24 February 2009
Validity of C of A:	The C of A was last renewed on 12 February 2010 with an expiry date of 23 February 2011

1.6.1.2 Aircraft History

(a) At the time of the accident, the total flying hours since manufacture of the helicopter was 1467:36 hours. The total flying hours of the latest periodic inspections were as follows:

Periodic Inspection (Latest carried out)	Date	Total Flying Hours	Next Due (Total Flying Hours)
25 Hours Inspection	1 July 2010	1459:55	1484:55
50 Hours Inspection	15 June 2010	1430:59	1480:59
100 Hours Inspection	8 June 2010	1402:38	1506:38
300 Hours Engine Inspection	19 June 2010	1441:07	1741:07
300 Hours	22 June 2010	1441:09	1741:09
600 Hours	24 March 2010	1149:37	1749:37
1200 Hours	24 March 2010	1149:37	2349:37

(b) The helicopter was maintained and in compliance with the Maintenance Schedule of reference: MS/AW139/SS Rev.05 approved by AACM. There was no evidence of overdue items.

(c) All EASA Airworthiness Directives (AD) for AW AW139 were reviewed. There were three ADs related to the helicopter tail section and the required inspections were carried out with no overdue. All other ADs were found well controlled in accordance with the AD list of SkyTech, the

organisation contracted by EAA to provide continuing airworthiness management of the AW139 fleet.

(d) There were no outstanding deferred defects recorded for the helicopter.

1.6.2 Engine Data

1.6.2.1 The helicopter was equipped with two Pratt & Whitney Canada PT6C-67C engines. The two engines were installed new on the helicopter:

(a) Engine No. 1 of Serial No. KB0456

(b) Engine No. 2 of Serial No. KB0452

1.6.2.2 No abnormalities of engine operation were reported prior to the accident.

1.6.3 Tail Rotor Data

1.6.3.1 The history of the major tail rotor components are listed below. Where applicable, none of their total time had exceeded the respective retirement life.

Component	Part No.	Serial No.	Manufacturer	Total Time (flying hours)	Retirement Life
Tail Rotor Assembly	3G6420A00133	Q283	AGUSTA	1467:36	Not applicable
Tail Rotor Blade (Red)	3G6410A00131	Q1088	AGUSTA	1467:36	10000 flying hours
Tail Rotor Blade (White)	3G6410A00131	Q1059	AGUSTA	1467:36	10000 flying hours
Tail Rotor Blade (Blue)	3G6410A00131	Q1093	AGUSTA	1467:36	10000 flying hours
Tail Rotor Blade (Yellow)	3G6410A00131	Q1085	AGUSTA	1467:36	10000 flying hours
Tail Rotor Elastomeric Damper (Red)	3G6420V00455	LK1858	LORD CORPORATION	388:41	Nil
Tail Rotor Elastomeric	3G6420V00455	LK1871	LORD CORPORATION	363:49	Nil

Component	Part No.	Serial No.	Manufacturer	Total Time (flying hours)	Retirement Life
Damper (White)					
Tail Rotor Elastomeric Damper (Blue)	3G6420V00456	LK1854	LORD CORPORATION	388:41	Nil
Tail Rotor Elastomeric Damper (Yellow)	3G6420V00455	LK1859	LORD CORPORATION	363:49	Nil
Tail Gearbox Assembly	3T6522A00243	TBL6736	WESTLAND TRANS.	1467:36	Overhaul at 5000 flying hours

1.6.4 Weight and Balance Data

1.6.4.1 The computerised loading and Centre of Gravity (C of G) calculation was stated on the load sheet. The calculation indicates that the aircraft was within both longitudinal and lateral C of G limits. The actual take off weight recorded was 5971 kg, which was below the Maximum Take Off Weight (MTOW) of 6400 kg. At this weight, ICAO Class 1 performance was assured.

1.6.5 Minimum Equipment List

1.6.5.1 The helicopter was subjected to an AW139 Minimum Equipment List furnished by Sky Shuttle Helicopters Limited. At the time of the accident, there was no outstanding deferred defect on the aircraft.

1.6.6 Fuel Information

1.6.6.1 The type of fuel used was Jet A-1. It was recorded in the Technical Log Record Sheet, Sheet No. 0168 dated 3 July 2010, that the "Arrive" fuel was 870 kg. As engine operations were normal prior to the accident, fuel samples were not taken for contamination check as there was no such need.

1.6.7 Parts and/or Systems Relevant to the Accident

1.6.7.1 Tail Rotor Assembly – General Construction

(a) Figure 1 shows a general view of the tail rotor and hub assembly used on B-MHJ. The fully-articulated tail rotor consists of four glass-fibre composite blades, which rotate in an anti-clockwise direction (as viewed from the starboard side). The four tail rotor blades were designated in sequence as Red blade, White blade, Blue blade and Yellow blade, in the direction of rotation.

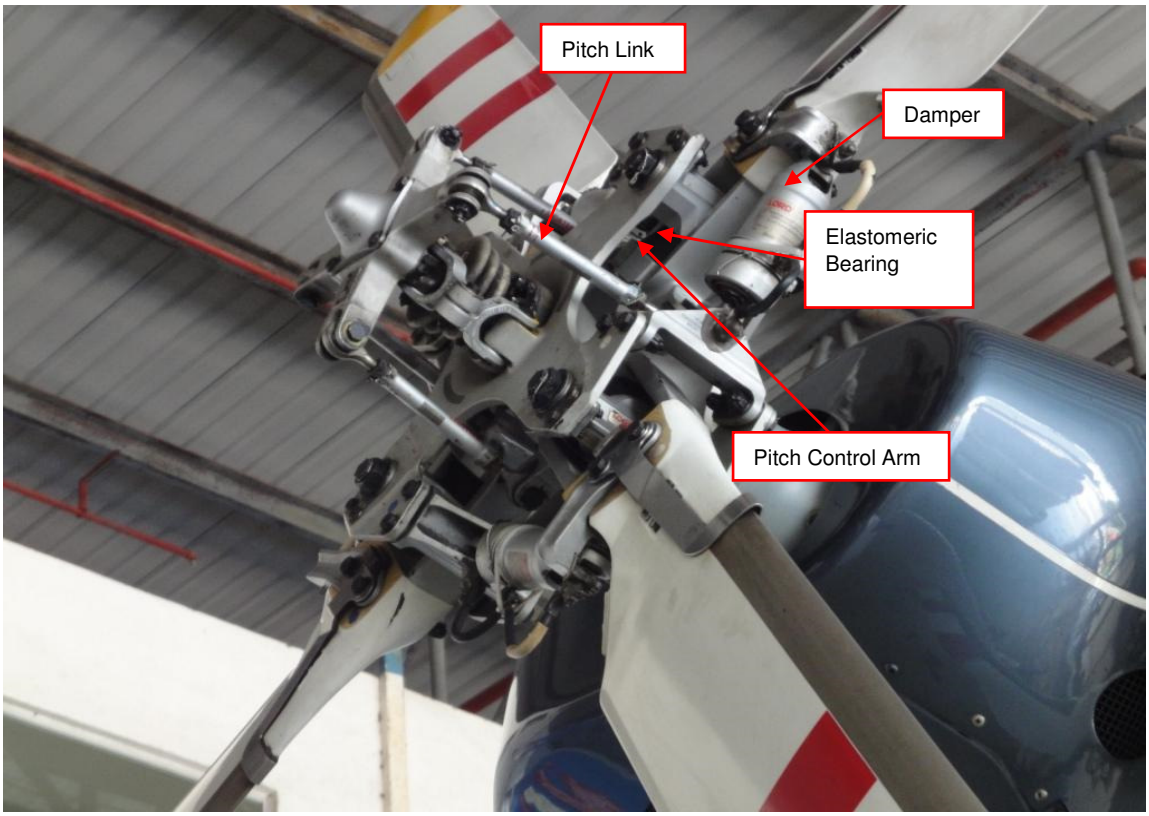

Figure 1 – General view of tail rotor assembly

1.6.7.2 Tail Rotor Blade Installation

(a) Each of the tail rotor blades, with Part Number (P/N) 3G6410A00131, is connected to the tail rotor hub via a spherical elastomeric bearing. The pitch of the tail rotor blades is adjusted through a linkage attached to a pitch control arm bonded to the root of each tail rotor blade. The elastomeric bearing serves to transmit all loads between the tail rotor hub and the tail rotor blade whilst providing freedom, with limits, for the tail

rotor blade to move in flap, in lead-lag, in pitch or any combination thereof. Blade damper attachment lugs allow connection of the dampers to the blades at station 249. Refer to Figure 2 for the schematic diagram.

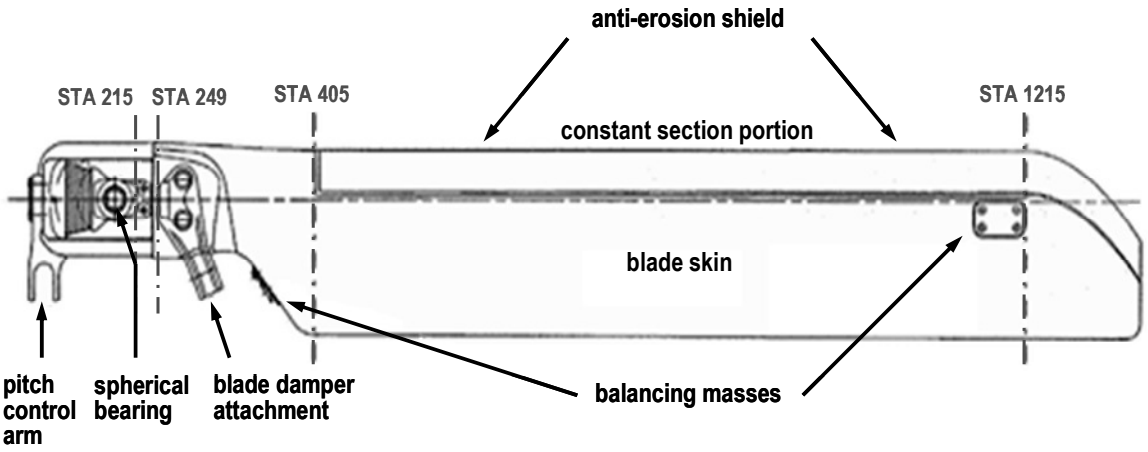

Figure 2 – Tail rotor blade schematic diagram

1.6.7.3 Tail Rotor Blade – Structural Elements

(a) The principal load-bearing element of a tail rotor blade at the root end consists of a spar assembly comprising two straps of unidirectional S-glass composite bonded to, and separated by a filler core. Figure 3 refers. The spar assembly is overwrapped in a ±45°Glass Fibre Reinforced Composite (GFRC) laminate. At the root end, the blade structure loops around the elastomeric bearing. Sacrificial layers of woven GFRC cloth are bonded to the root and machined to match the profiles of the pitch control arm and the elastomeric bearing. The metal pitch control arm is adhesively bonded and is attached to the elastomeric bearing by four bolts; two on each side of the GFRC blade structure.

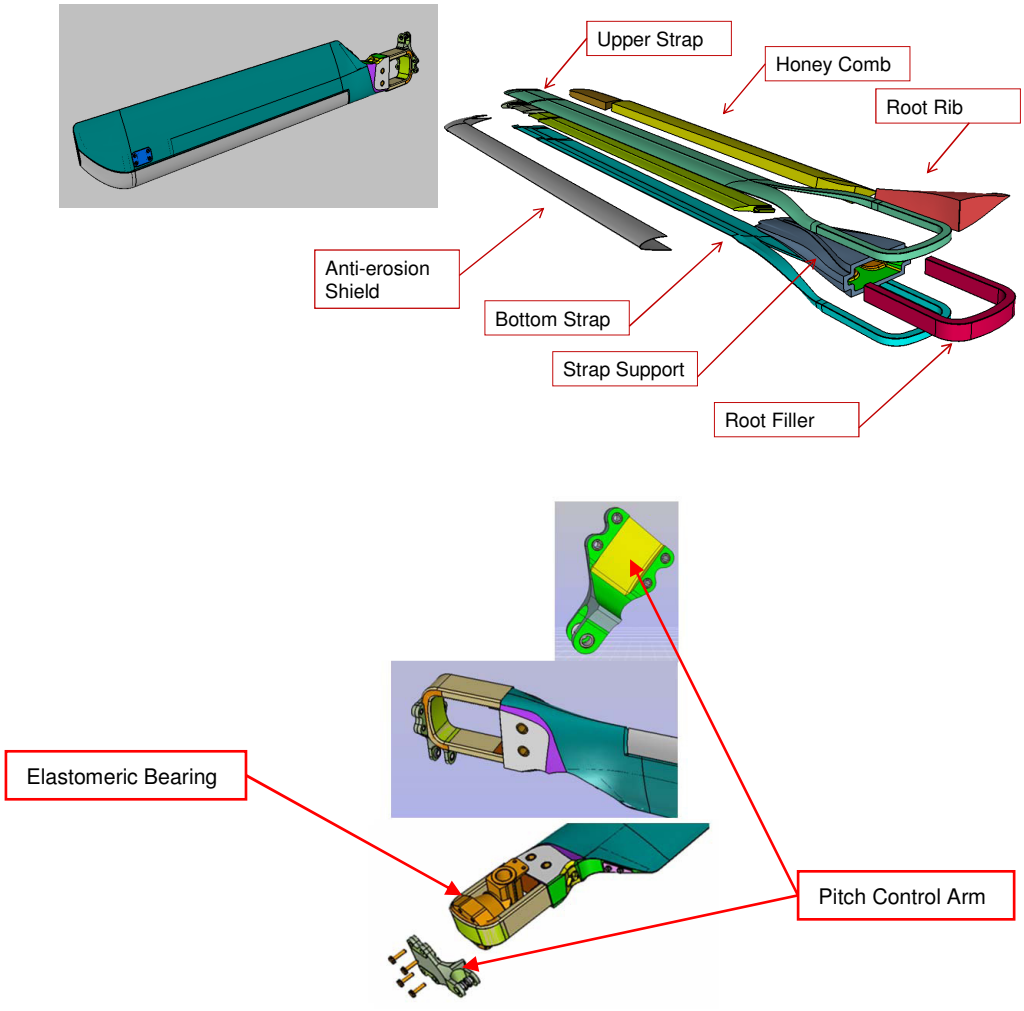

Figure 3 - Tail rotor blade structure

1.6.7.4 White Tail Rotor Blade - Evaluation of Production Defects

(a) According to AW, the top and bottom straps of the White tail rotor blade had been subjected to production defect evaluation in accordance with AW Technical Specifications STAP106 and SRA035/SRA036, where SRA035 and SRA036 were for porosity classification and marcel classification respectively. According to STAP106, marcel is defined as a deviation of the fibers direction from the desired one. The results of evaluation are shown in the table below.

(b) A post accident review of the defect classification in the curved zone of the blade was performed by a different inspector (III Level). The results of the review are also shown in the table below.

(c) As stated by AW, no discrepancies outside the allowable limits have been identified on the straps regarding marcel, porosity and separation.

Tail rotor blade Serial Number	Strap Serial Number	Defect Evaluation	Marcel (Grade)	Porosity (Grade)	Separation (mm)
Q1059	Q1232 (top strap)	During production	1	1	0
		Post accident review	1	1	0
	Q1242 (bottom strap)	During production	3	4	0
		Post accident review	2	4	27

Note: Grade of Marcel from 1 (least severe) to 6 (most severe)
Grade of Porosity from 1 (least severe) to 8 (most severe)

1.6.8 Means of Emergency Evacuation

1.6.8.1 The passenger cabin is fitted with a cabin door on each side of the fuselage. These two cabin doors are normally used for embarkation and disembarkation of passengers. In case of emergency, both doors can be used as emergency exits for passenger evacuation. When the cabin doors cannot be opened, all cabin windows on the doors can be jettisoned to allow rapid evacuation of the passengers. Figure 4 refers.

1.6.8.2 The helicopter is fitted with a cockpit door on each side. The upper part of the door is equipped with a push-out type emergency exit window, allowing rapid evacuation of the flight crew when the cockpit door cannot be opened, typically when the two flotation bags are fully inflated. After ditching, both the commander and the first officer evacuated from the cockpit through their respective emergency exit windows.

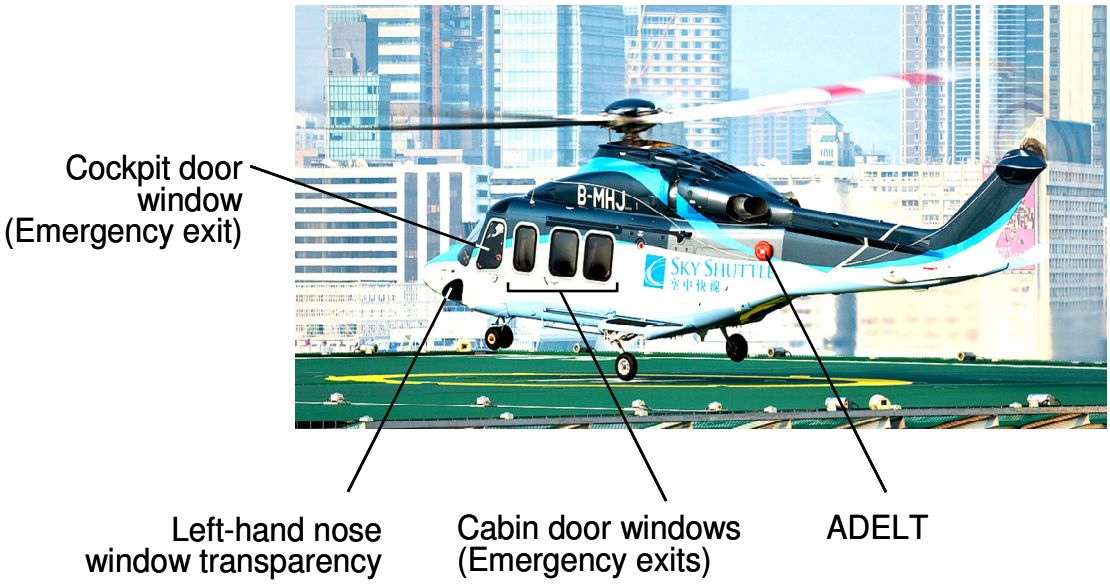

Figure 4 – B-MHJ

1.6.9 Emergency Flotation System

1.6.9.1 The helicopter is equipped with an emergency flotation system consisting of two forward and two aft float assemblies. The sytsem was manufactured by Aero Sekur S.p.A. under the Production Organization Approval issued by ENAC while the design of the system is certified by EASA. Figure 5 refers.

Figure 5 – AW139 Emergency Floatation System

1.6.9.2 The forward left float assembly is installed in a compartment located at the left side of the front fuselage. The assembly includes a pod, a floatation bag and the gas distribution system. The pod is made of composite material and screwed on dedicated frames of the fuselage. The forward left floatation bag consists of three independent sealed chambers. Failure of any of the sealed chambers would not affect the operation of the others. The floatation bag is inflated by helium supplied from the two gas cylinders of the inflation system. When inflated, the floatation bag has a cylindrical shape with hemispherical bulkheads.

1.6.9.3 To ensure proper positioning of the floatation bag along the fuselage, the forward left floatation bag is equipped with an additional chamber, called the 'buck' bag. Figure 6 refers. The buck bag is inflated by helium supplied from the middle sealed chamber of the floatation bag. The forward right float assembly has the same construction as its counterpart on the left side.

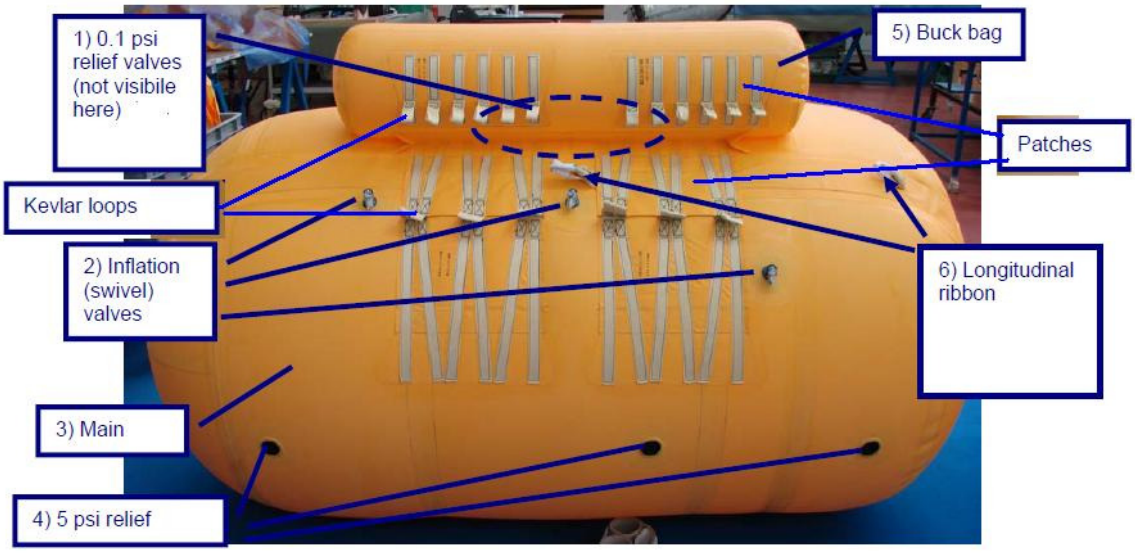

Figure 6 - Forward floatation bag and buck bag

1.6.9.4 The aft left float assembly is installed in a compartment located at the left side of the rear fuselage. The assembly includes a pod, a floatation bag and the gas inflation system. The aft left floatation bag consists of four independent sealed chambers and is inflated by helium supplied from the two gas cylinders of the inflation system. When inflated, it has a truncated cone shape with hemispherical bulkheads. Two 'buck' bags ensure proper positioning of the

floatation bag along the fuselage. The buck bags are inflated by helium supplied from their respective sealed chambers of the floatation bag. The gas inflation system consists of a gas cylinder and the associated discharge valves, flexible hoses and rigid pipe network. The gas cylinder provides helium supply for the inflation of all the four floatation bags. The aft right float assembly has the same construction as its counterpart on the left side.

1.6.9.5 Each floatation bag is made of polyester polyurethane coated Aertex 89810 fabric and attached to the pod by Kevlar girt loops integrated with the floatation bag by means of patches on which ribbons are stitched. The patches are glued on the floatation bag. Figure 7 refers. When a floatation bag is in operation, the pod, which is the composite container that accommodates the floatation bag, transfers the load between the inflated floatation bag and the helicopter when the latter is in buoyant condition. The longitudinal webbings on the floatation bag maintain its shape and size and ensure correct axial load distribution.

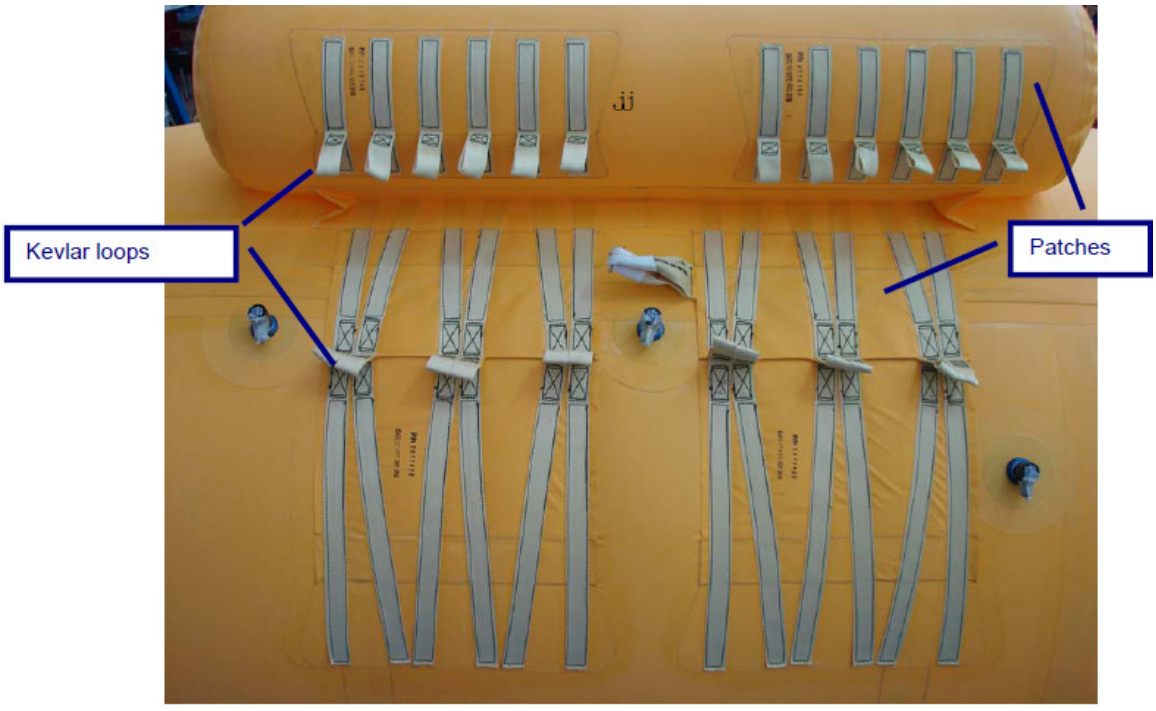

Figure 7 – Kevlar loops and patches

1.6.9.6 Each floatation bag is equipped with inlet non-return swivel valve(s), inflate / deflate valve(s) and pressure relief valve(s) for the inflation, testing and overpressure protection of the floatation bag and buck bag.

1.6.10 Passenger Life Jacket

1.6.10.1 The passenger cabin was certified to carry 12 passengers. They were accommodated in three rows of seats of four. The front row seats are rearward facing while the second and the last row seats are forward facing. Figure 8 refers.

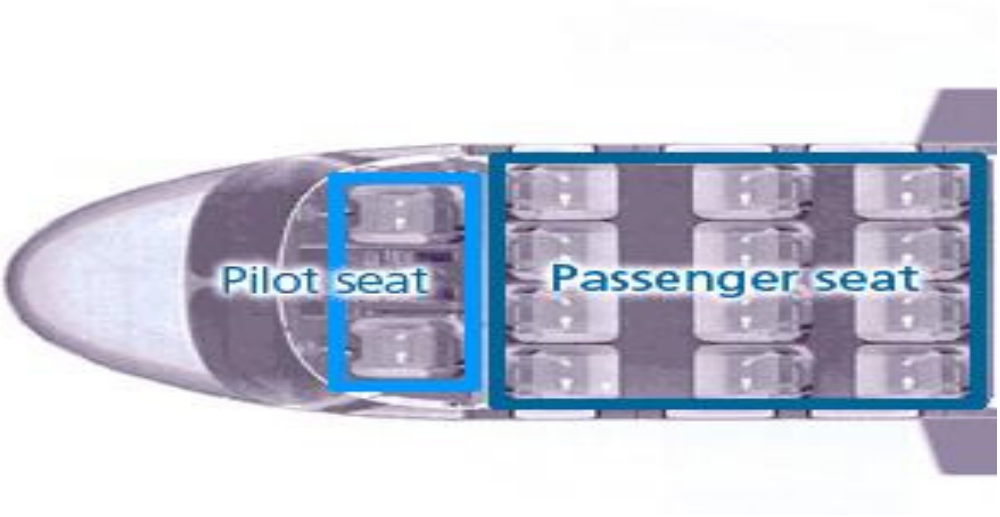

Figure 8 – B-MHJ Seating configuration

1.6.10.2 The flight between Hong Kong and Macao does not require the helicopter to go beyond a distance from land of more than 10 minutes flying time from land at normal cruise speed. The carriage of life jackets was therefore not mandated by Air Navigation Regulation of Macao (ANRM), which was in compliance with ICAO Annex 6 Part III effective in 2010.

1.6.10.3 Despite not legally required, the operator chose to equip the helicopter with crew and passenger life jackets onboard. The crew life jackets are stowed in the centre console between the two crew seats. The passenger life jackets are stowed inside the compartment under the passenger seats and attached to the bottom of the seat panes by Velcro tapes. To get the life jackets, the passenger had to pull down the flap covering the front of the seat compartment and then pull the life jacket off to unlatch the Velcro. Figure 9 refers.

Figure 9 – A typical installation of passenger life jacket

1.6.10.4 Aircraft Maintenance Schedule (AMS) task 09-18 of the helicopter approved by AACM requires daily inspection of the passenger life jackets. The description of the inspection task was "Ensure correctly located, condition and life expiry detail." Every inspection requires the life jacket to be pulled off from its stowed position and then re-installed after the inspection is done.

1.6.11 Safety Instructions Placard

1.6.11.1 Safety instructions placard providing details of brace position to be adopted by passengers, life jacket access and donning procedures, and operation of cabin window transparencies on cabin doors were provided to passengers onboard. Figure 10 refers. AACM requirement for the provisioning of safety instructions placard is published in Article 12(5)(b)(iv), ANRM, which stipulates that:

> *"The position of equipment provided for emergency use shall be indicated by clear markings in or on the aircraft. In particular in every commercial air transport aircraft registered in Macao there shall be:*
> *information provided in passenger emergency briefing cards as to where the life-jackets, escape slides, life-rafts and oxygen masks, if required to be provided by sub-paragraph (2) above, are to be found and instructions as to how they are to be used, including any special instructions for passengers seated near a window or door emergency exit."*

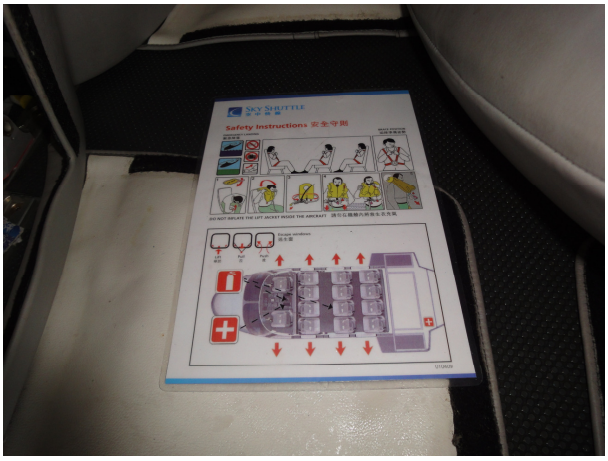

Figure 10 – Safety Instructions Placard

1.6.11.2 Placards showing passenger life jacket location and access were installed at the aft surface of the Cabin Bulkhead upper area, the forward surface of the aft Cabin Bulkhead upper area, and the left and right cabin wall upper areas at STA 3905. Figure 11 refers. AACM requirement for the provisioning of passenger life jacket location placard is published in paragraph 4(2)(a)(3), Fifth Schedule, ANRM which requires the carriage of aircraft equipment Scale B. Scale B(x)(d) stipulates that:

> *"Means of ensuring that the following information and instructions are conveyed to passengers: location and use of life jackets or equivalent individual floatation devices where their carriage is required."*

1.6.11.3 Since the carriage of life-jackets on the helicopter was not mandatory, the provisioning of these placards by EAA was voluntary.

Figure 11 – Passenger life jacket location placard

1.6.12 Safety Demonstration to Passengers

1.6.12.1 The operator conducted safety demonstration to passengers by showing a safety briefing video for view before their boarding. On 20 July 2010, the investigation team observed a safety demonstration at the Sheung Wan / Sky Shuttle Heliport. The safety briefing video was shown at about eight minutes prior to passenger boarding, with Cantonese and Mandarin commentary supplemented by English sub-titles. Before the start of the video, a general announcement was made to draw the attention of the passengers but they were not confined to a location while the video was being played. The video provided the required safety information to passengers, including those concerning the location of the life jackets and the instruction of their use.

1.6.13 ADELT

1.6.13.1 The helicopter was equipped with an Automatically Deployable Emergency Locator Transmitter (ADELT), also known as Crash Position Indicator, mounted externally on the left aft fuselage between station 8150 and 8700. Figure 4 refers.

1.6.13.2 The ADELT is a buoyant unit that interfaces with the full emergency frequency operation at 121.5 MHz and 406 MHz of the international Cosmicheskaya Sistyema Poiska Avariynich Sudov / Search and Rescue Satellite (COSPAS/SARSAT) distress alerting system for locating an aircraft in distress condition. During deployment, the ADELT is ejected from the fuselage. The encoded position uncertainty of the ADELT is plus or minus 4 minutes of Latitude and Longitude.

1.6.14 Health and Usage Monitoring System

1.6.14.1 The helicopter was equipped with a Health and Usage Monitoring System (HUMS), which is a maintenance aid for monitoring the degradations of the helicopter rotors and drive components. All the data is stored inside the HUMS card.

1.6.14.2 The HUMS card was recovered together with the accident helicopter from sea. However, the download of the data was unsuccessful, even after attempts were made to retrieve the data directly from the chips inside the card memory. The

chips were found corroded due to exposure to sea water.

1.6.14.3 The operator downloads HUMS data on a daily basis and the downloaded data is maintained. The investigation team had conducted an examination of the HUMS data of the helicopter from 14 April 2010 up to 2 July 2010, the day before the accident. The examination did not reveal any abnormality on helicopter rotors and drive components.

1.7 Meteorological Information

1.7.1 The weather was generally fine. The cloud base was about 2000 ft and the visibility was 10 km. The height of sea wave was between 1.5 m and 2.0 m, which is categorised as State 4 (Moderate) in accordance with the sea state codes of World Meteorological Organisation. The 1-min wind speed measured at Central Pier adjacent to Sheung Wan / Sky Shuttle Heliport at 0405 hrs (1205 hrs) was 7 kts.

1.8 Aids to Navigation

1.8.1 The accident flight was operated under VFR, during which the aircraft was required to remain clear of cloud and the pilots had to maintain in sight of the surface, so visual contact with the surface was the principle method of navigation.

1.9 Communications

1.9.1 The helicopter was fitted with dual Very High Frequency (VHF) radio communication equipment and the radio was serviceable on the day of the accident. Throughout the flight, the first officer's VHF radio was set to communicate with Hong Kong Air Traffic Service Unit, the Zone Control, on VHF frequency 120.6 MHz while the commander's VHF radio was set to communicate with the Flight Operations Control Centre (FOCC) of the operator at Sheung Wan / Sky Shuttle Heliport on VHF frequency 131 MHz. The Mayday call made by the commander was transmitted on the FOCC frequency

and thus only received by the FOCC. Paragraph 4 (Reporting hazardous conditions), Part II, Eleventh Schedule, ANRM requires that:

> *The pilot-in-command of an aircraft shall, on meeting with hazardous conditions in the course of a flight, or as soon as possible thereafter, send to the appropriate air traffic control unit by the quickest means available information containing such particulars of the hazardous conditions as may be pertinent to the safety of other aircraft.*

1.9.2 The operator's Standard Operating Procedures (SOP) and AW139 In-flight Checklists did not provide instructions and check as to the selection of radio frequency for reporting hazardous conditions to the appropriate air traffic control unit.

1.10 Aerodrome Information

1.10.1 Sheung Wan / Sky Shuttle Heliport (VHSS) is located at the north shore of the Hong Kong Island. It is an elevated helipad, measuring 34.4m x 34.4m in dimensions. The operational period is from 0000 hrs (0800 hrs) to 1459 hrs (2259 hrs). Both VFR and SVFR traffic types are permitted. The departure tracks from the heliport are 080°M or 310°M. The heliport administration is handled by Sky Shuttle Helicopters Limited.

1.11 Flight Recorders

1.11.1 Multi-Purpose Flight Recorder (MPFR)

1.11.1.1 The helicopter was equipped with a Penny & Giles Aerospace Limited Model D51615-102 solid-state Multi-Purpose Flight Recorder (MPFR), capable of retaining 25 hours of flight data recording, 30 minutes of voice recording, 120 minutes of cockpit audio and combined voice recording. The MPFR recorded a total of 658 parameters of flight data.

1.11.1.2 The MPFR was recovered and found undamaged. However, due to water contamination, the download of the flight data via the external download connector was unsuccessful. With the assistance of the specialist of the

helicopter manufacturer, the MPFR was partially disassembled and the flight data was downloaded directly and successfully from its memory module. The MPFR recorded all the data per the design.

1.11.1.3 The total duration of the flight data recorded by the MPFR was 92,909 seconds. The time between the helicopter take-off (04:00:01) and the end of MPFR recording (04:01:21) was 80 seconds. All MPFR data within the period were checked. Abrupt change in recorded parameters of Lateral Acceleration (AHRS), Yaw Rate and Tail Gearbox (TGB) Oil temperature was evident at 04:00:40. See Appendix 1.

1.11.1.4 At the point of ditching, the MPFR recorded that the helicopter banked to the left by 6.5 degrees. Also, the MPFR recorded the following speed parameters:

(a) Ground Speed of helicopter = 24 kt.

(b) Vertical Descent Speed of helicopter = 2.76 m/s.

1.11.2 Cockpit Voice Recorder (CVR)

1.11.2.1 The Cockpit Voice Recorder (CVR) was part of the MPFR. The audio recording system consists of four separate channels, providing recording of the following six audio tracks:

(a) Pilot.

(b) Co-pilot.

(c) Cabin intercommunication system for the last 30 minutes.

(d) Combined audio track of (a) to (c) for the last 120 minutes.

(e) Cockpit Area Microphone for the last 30 minutes with a bandwidth of 6 KHz.

(f) Cockpit Area Microphone for the last 120 minutes with a reduced bandwidth of 3.5 KHz.

1.11.2.2 The CVR captured all the recording per the design and the quality of the recording was good.

1.12 Wreckage and Impact Information

1.12.1 General Description of the Site of the Accident

1.12.1.1 The helicopter ditched into the Victoria Harbour north-west of the Sheung Wan / Sky Shuttle Heliport. See Appendix 2 for the location of the heliport, the point where the tail rotor attachment structure was broken off in flight, and the point where the helicopter ditched into the harbour.

1.12.2 Impact Sequence

1.12.2.1 It was confirmed with a video, as retrieved from a camera mounted on a building nearby the accident site, that the tail rotor together with the tail gearbox were separated from the helicopter prior to helicopter touchdown. According to the flight data record, the entire tail rotor assembly became detached from the helicopter whilst the helicopter was climbing at an altitude of approximately 350 ft.

1.12.2.2 Whilst ditching in Victoria Harbour, the helicopter was maintained in level attitudes and with low forward speed at touchdown. The helicopter was then floating firmly on water. Figure 12 refers.

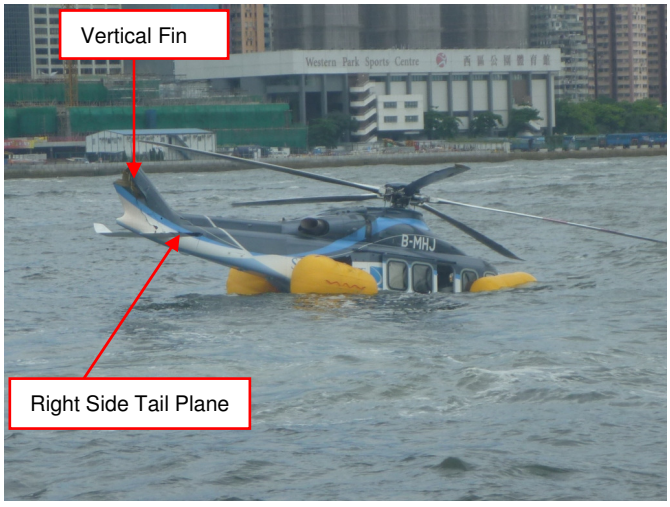

Figure 12 – The helicopter floating in Victoria Harbour

1.12.3 Distribution Pattern of the Wreckage

1.12.3.1 The helicopter was basically intact except substantial damage was found in its tail area. Figure 12 refers.

1.12.4 Damage on Helicopter Fuselage

1.12.4.1 The vertical fin was severed at a point where a hand hole, on the right side of the vertical fin torque box, was located. Post accident inspection revealed that the tail rotor, tail gearbox, the associated tail rotor drive shaft and control rods, and cover fairings on vertical fin were missing. Figure 13 refers.

Figure 13 – Damage on vertical fin (side view)

1.12.4.2 The torque box of the vertical fin was severely damaged. The riveted joint at rear spar right hand side was wedged open. Figure 14 refers. Severe cuts and scratch marks were obvious on the interior surfaces of the torque box structure. Figure 15 refers.

Figure 14 – Damage on vertical fin (rear view)

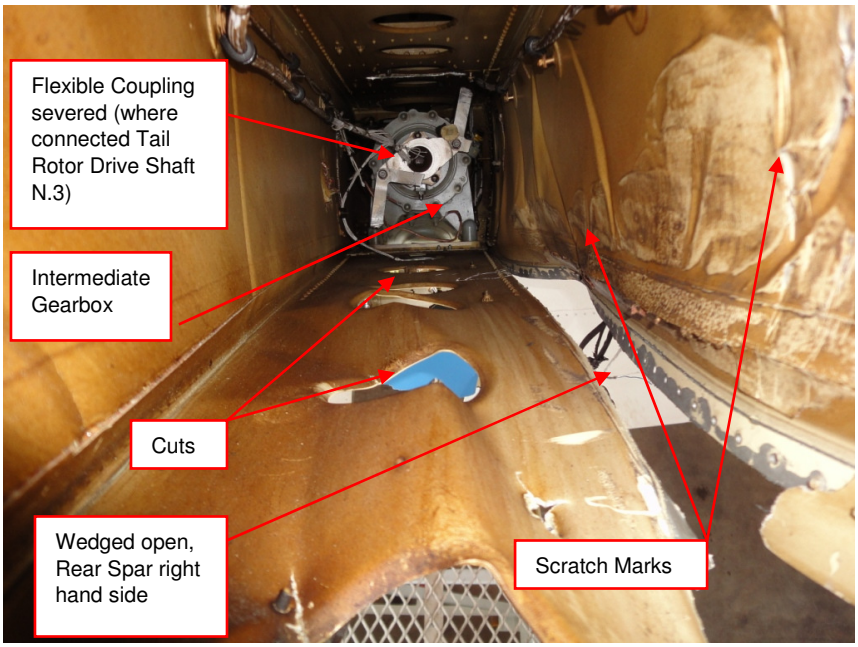

Figure 15 – Damage on vertical fin (view on interior surfaces)

1.12.4.3 Regarding the tail rotor drive system, the flexible coupling that connected the tail rotor intermediate gearbox to the tail rotor drive shaft N.3 was found

severed. Impact marks were found on the flexible coupling. Figure 16 refers.

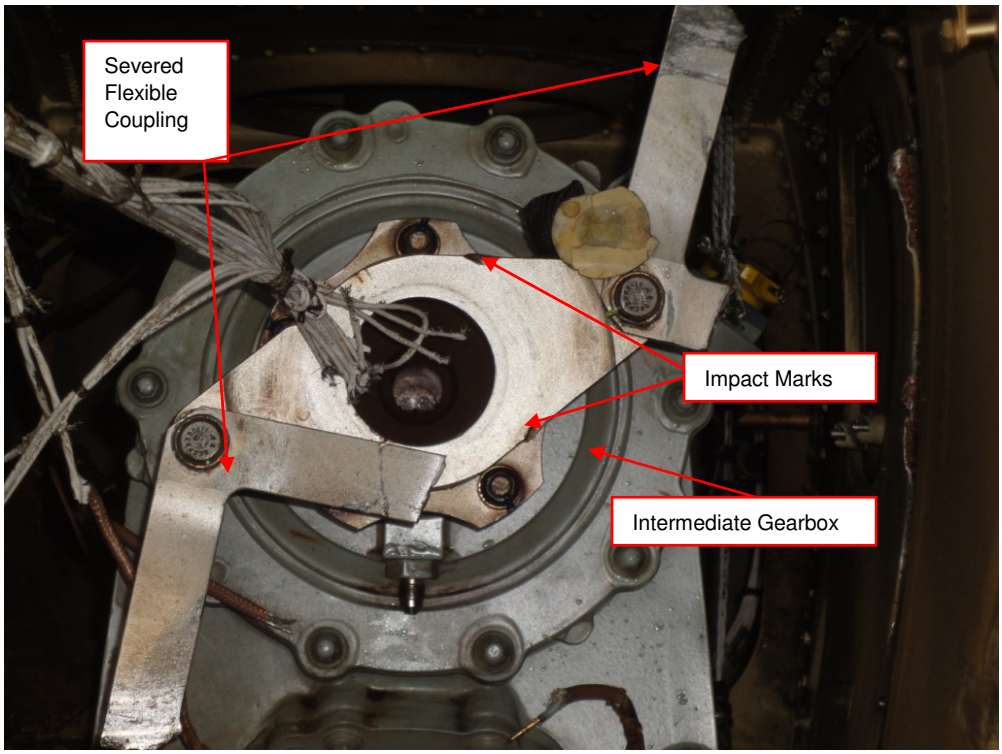

Figure 16 – Impact marks on flexible coupling of intermediate gearbox

1.12.4.4 Apart from damage on the vertical fin, cuts were located on the trailing edge structure of the right side tail plane. Figure 17 shows the cuts on the upper surface of the tail plane whilst Figure 18 shows the ones on the lower surface. In addition, post impact damage was found on the helicopter fuselage:

(a) Loss of left hand nose window transparency panel on the forward fuselage.

(b) Break off of two vent air scoops located at the bottom of rear fuselage.

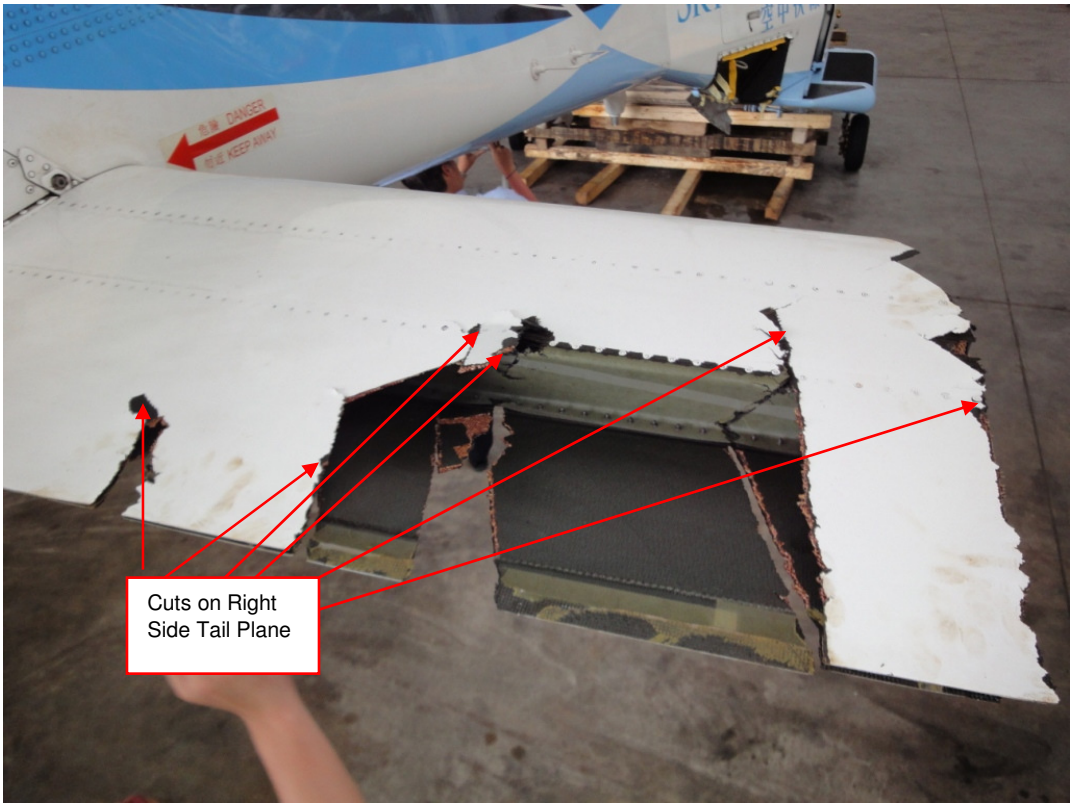

Figure 17 – Cuts on right side tail plane (upper surface)

Figure 18 – Cuts on right side tail plane (lower surface)

1.12.5 Tail Rotor and the Attachment Structure Salvaged

1.12.5.1 During the accident, the tail rotor and the attachment structure had detached from the accident helicopter and fell into the Victoria Harbour. Extensive efforts were expended by the investigation team in the search and location of these missing parts, using Multi-beam Echo Sounder Survey method followed by hand search by divers. However, due to the very small size of the parts and other unfavourable factors, the search and location process was very difficult. Subsequently, the investigation team had found some video tapes of cameras mounted on the buildings nearby the Sheung Wan / Sky Shuttle Heliport. These video tapes captured the point of entry into the harbour of the tail rotor and the attachment structure. With this critical evidence, the investigation was able to locate and recover the parts from the Victoria Harbour on 14 July 2010. Figure 19 refers.

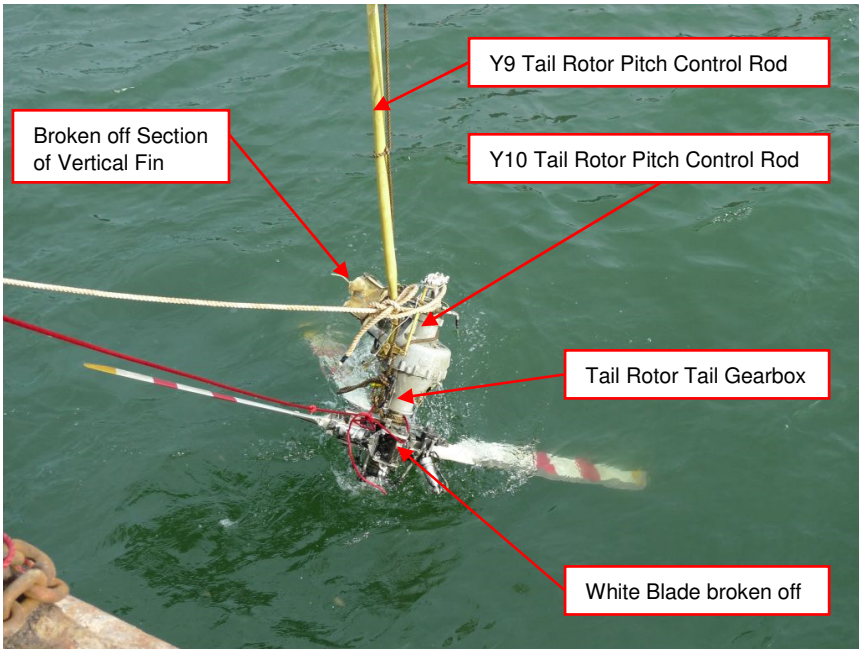

Figure 19 – Salvage of tail rotor and attachment structure

(a) The parts retrieved were as follows:

i. The tail rotor assembly with the White blade severed at its blade root area.

ii. The tail gearbox with a punch hole located in its body flange.

iii. The tail rotor pitch control rod Y9 with the rod end, for connecting to the bellcrank located at the base of vertical fin, severed.

iv. The slightly bent tail rotor pitch control rod Y10.

v. The broken off section of the vertical fin.

(b) The missing parts that could not be found were as follows:

i. The tail rotor drive shaft N.3 that was connecting the tail rotor drive intermediate gearbox and tail gearbox.

ii. The broken off section of the White blade.

1.12.5.2 Condition of the Broken Off Vertical Fin Section

(a) The vertical fin was severed at a point where a hand hole, on the right side of the vertical fin torque box, was located. Figure 20 refers. The broken off section remained attached to the tail gearbox the latter of which remained intact with the tail rotor. As shown in Figure 21, the honeycomb structure was dented inwards on the left side of the broken off structure.

Figure 20 – Broken off section of vertical fin

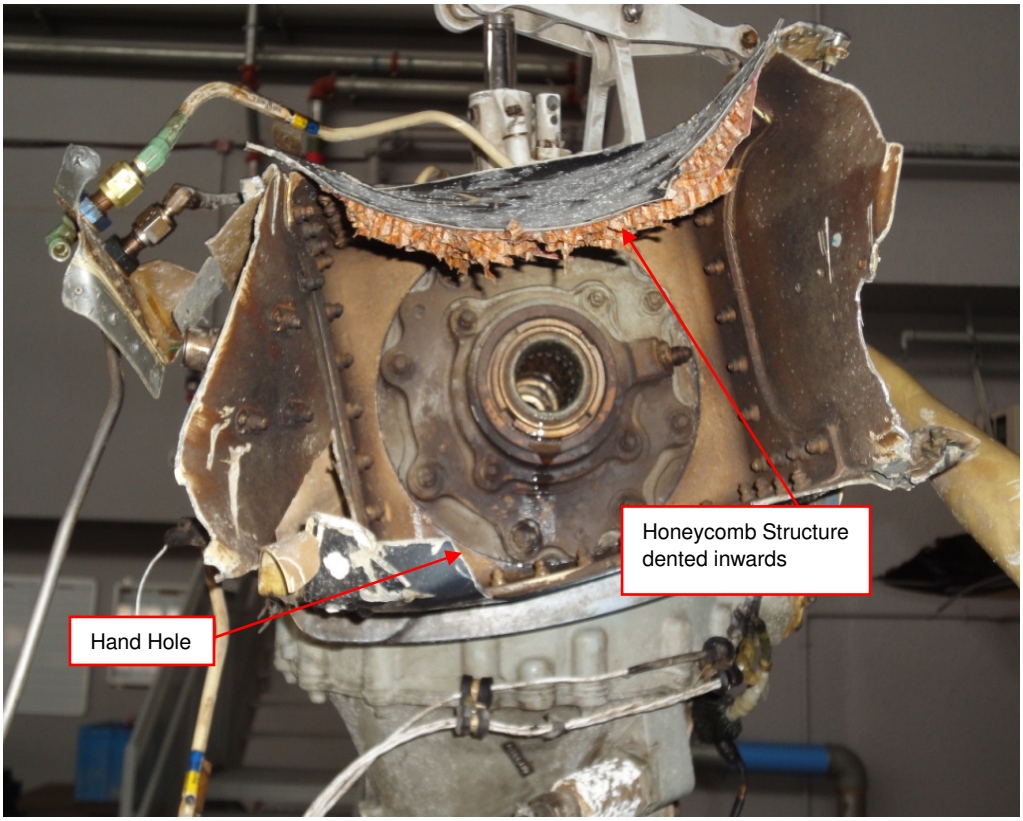

Figure 21 – Broken off section of vertical fin

1.12.5.3 Condition of Tail Rotor Blades

(a) The White blade was severed and broken off at the elastomeric bearing coupling area. The inner portion of the blade root section, retained between the pitch control arm and the elastomeric bearing, had remained properly connected to the tail rotor hub. Figure 22 refers. After recovery, the elastomeric bearing was found to be deflected beyond the normal range of travel, with the pitch control arm lodged against the White blade damper attachment bracket. Figure 23 refers.

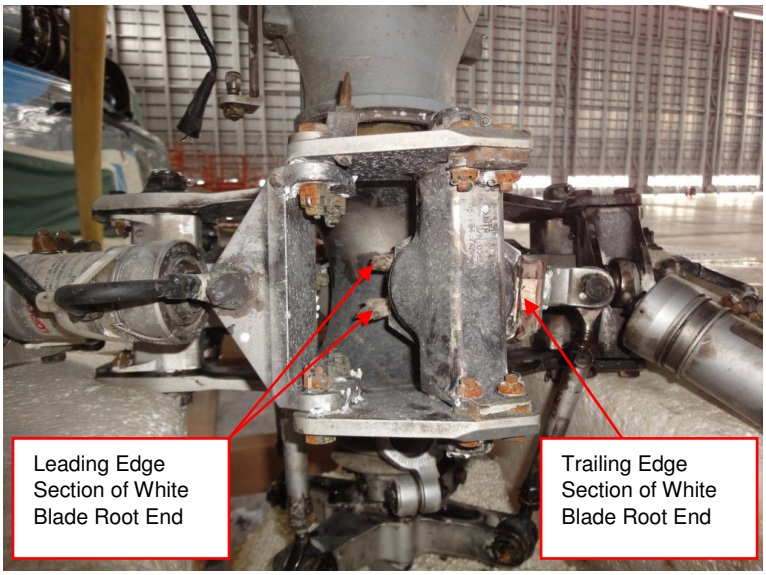

Figure 22 – Remains of White blade beneath elastomeric bearing

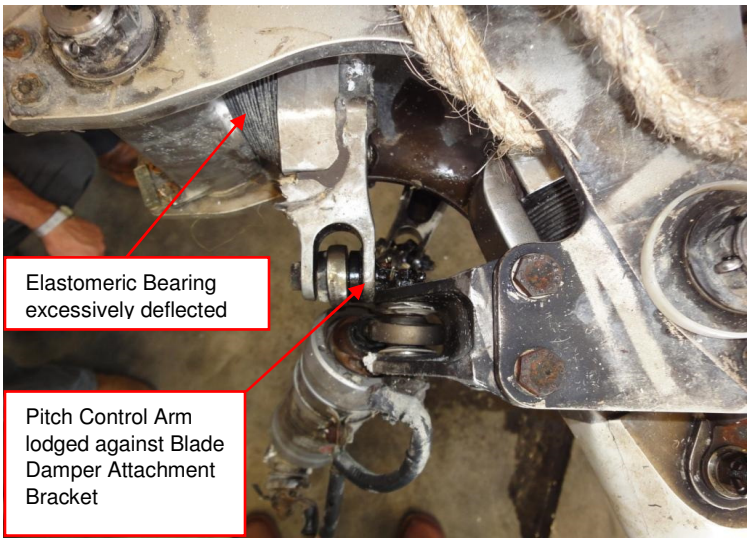

Figure 23 – White blade pitch control arm lodged against blade damper attachment bracket

(b) The Blue blade suffered severe impact damage at blade tip area. The metallic leading edge was flattened and the composites behind were beaten to strips. Figure 24 refers.

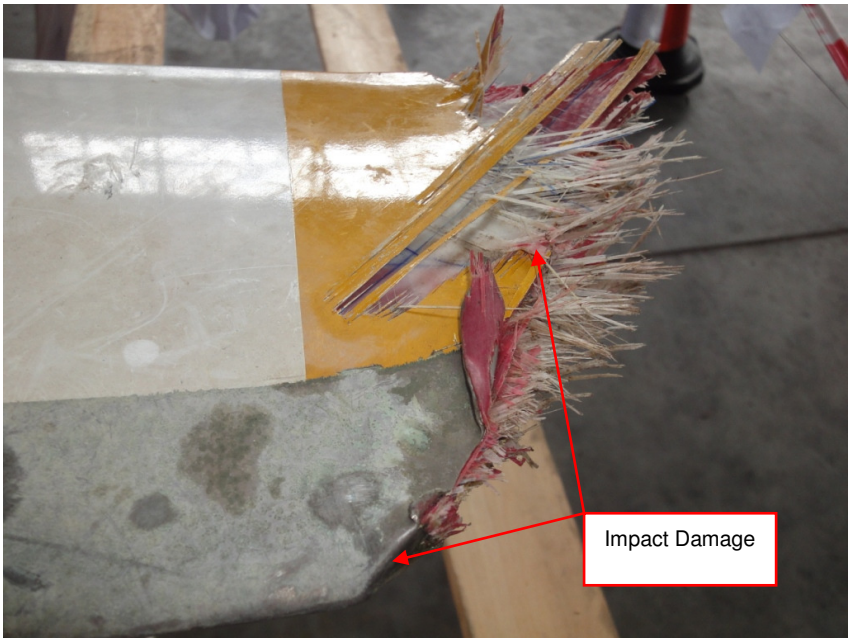

Figure 24 – Impact damage on Blue blade

(c) The Yellow blade suffered minor impact damage at blade tip area. Figure 25 refers.

Figure 25 – Impact damage on Yellow blade

(d) The Red blade had no obvious impact damage.

1.12.5.4 Condition of Tail Rotor Pitch Control Rod

(a) Dents were noted on the tail rotor pitch control rod Y9, on surfaces facing aft and forward, when viewed from aft of the helicopter. Figure 26 and Figure 27 refer.

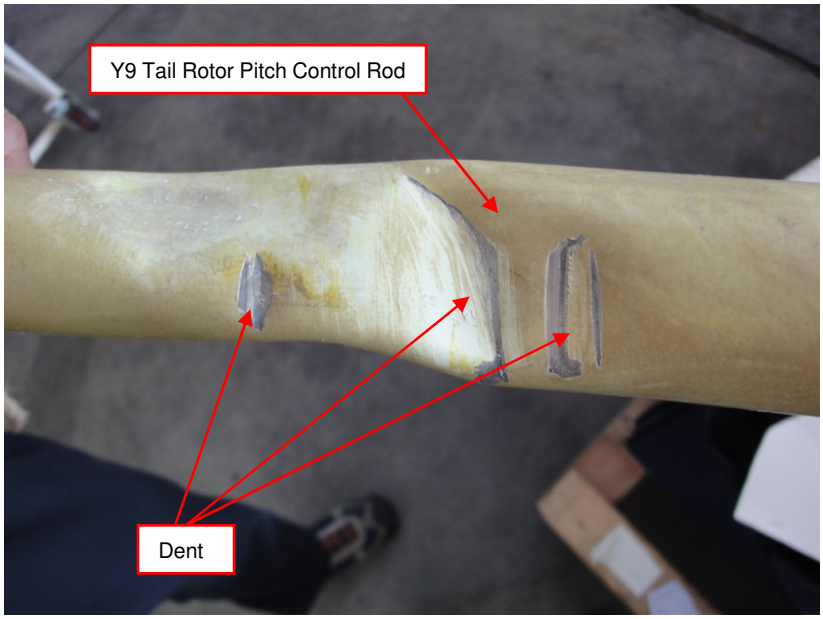

Figure 26 – Impact damage on tail rotor pitch control rod Y9 (facing aft)

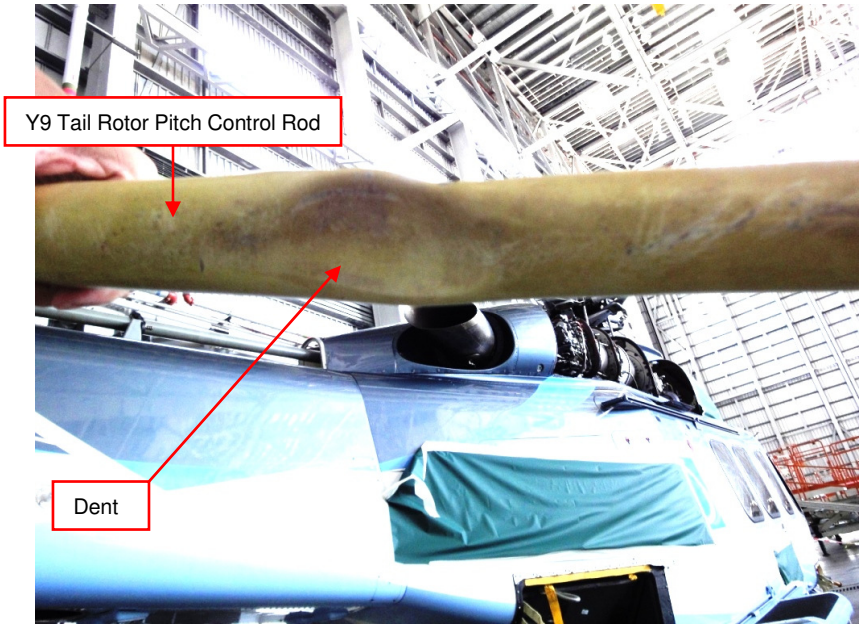

Figure 27 – Impact damage on tail rotor pitch control rod Y9 (facing forward)

1.12.5.5 Condition of Tail Rotor Blade Dampers

(a) The White and Blue blade dampers were separated from the respective blades. See Figure 28 for the dampers.

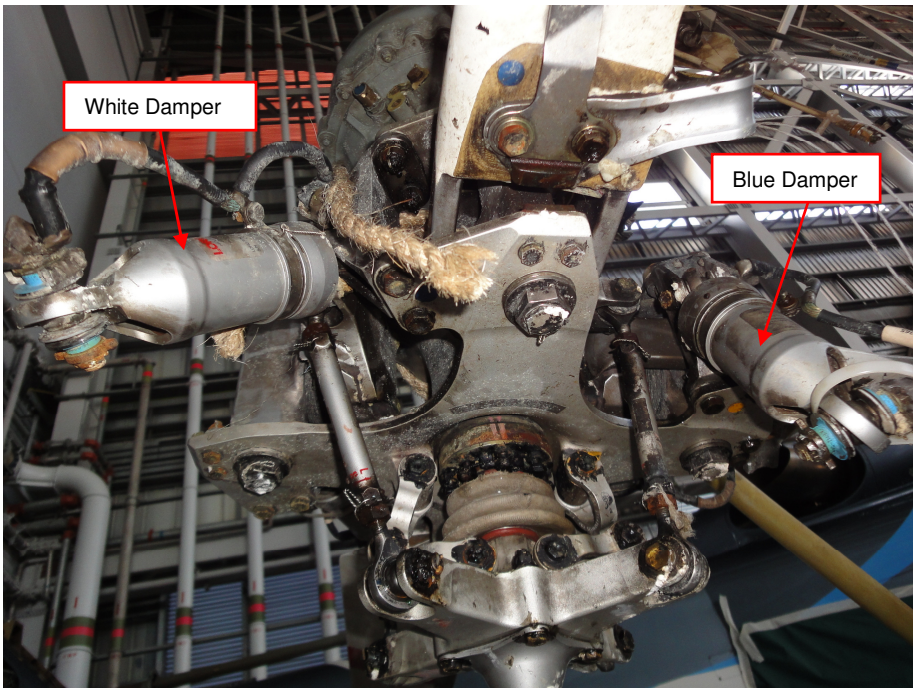

Figure 28 – White and Blue blade dampers

1.13 Medical and Pathological Information

1.13.1 The crew conducted the flight in accordance with the Flight Time Limitations Scheme of the operator. Both the crew members possessed a valid Class 1 Medical Certificate issued by Medical Assessors approved by the AACM. There was no evidence to support that the level of physical fitness of the crew members was a contributing factor to the accident. No medical examination had therefore been conducted, nor was it required.

1.14 Fire

1.14.1 There was no fire or explosion.

1.15 Survival Aspect

1.15.1 Ditching Operation

1.15.1.1 The helicopter is certified for ditching. JAR 29.801(d) requires that it must be shown that, under reasonably probable water conditions, the flotation time and trim of the rotorcraft will allow the occupants to leave the rotorcraft.

1.15.1.2 After ditching, all the four floatation bags inflated automatically and kept the helicopter afloat and upright, though the helicopter was listed to the left with a nose down attitude. In approximately 18 minutes after ditching, the helicopter overturned due to the failure of the right forward floatation bag. By the time it was overturned, all the persons onboard had evacuated from the helicopter. The left forward floatation bag was partially deflated. With the buoyancy provided by the two aft floatation bags and the partially deflated left forward floatation bag, the overturned helicopter remained in a floating condition. Figure 29 refers.

Figure 29 – B-MHJ overturned and remained in floating condition

1.15.1.3 The helicopter was certified for ditching. During type certification, compliance with JAR 29.563 Structural Ditching Provisions had been demonstrated. These provisions require the helicopter to be designed for ditching under the following conditions:

(a) Forward velocities from zero up to 56 km/h (30 kt) in likely pitch, roll, and

yaw attitudes.

(b) Limit vertical descent velocity not less than 1.5 m/s relative to the mean water surface.

(c) Rotor lift, acting through the centre of gravity, not exceeding two thirds of the design maximum weight.

.

1.15.2 Investigation of Forward Float Assemblies

1.15.2.1 After the recovery of the helicopter, the two forward floatation bags were removed and sent for workshop investigation. The following damages were noted.

Description of damage	Left floatation bag	Right floatation bag
Disbonding of the patches that integrate the Kevlar loops from the floatation bag	Yes	Yes
Disbonding of the buck bag from the floatation bag	No	Yes
Failure of the stitchings on the longitudinal ribbon	Yes	Yes
Inflate (swivel) valves torn up from the floatation bag	Yes	Yes

1.15.2.2 Disbonding of the patches that integrate the Kevlar loops from the floatation bag – On both floats, detachment of the patches from the floatation bag was evident. Inspection of the parts revealed the following damage.

(a) failure at bonding interface under the Kevlar tapes due to a low degree of adhesive polymerization. Figure 30 c) refers.

(b) failure at coating-to-weave interface on the remaining area of the patches. Figure 30 b) refers.

(c) patches torn in different points along the stitching of the loops. Figure 31 refers.

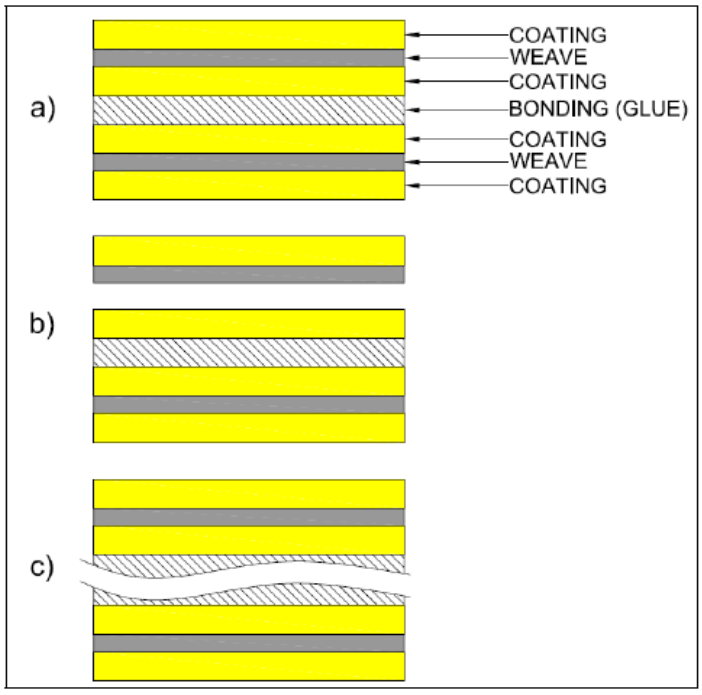

Figure 30 – Sectional views showing:
a) an intact bond between patch and floatation bag, b) and c) a detached patch

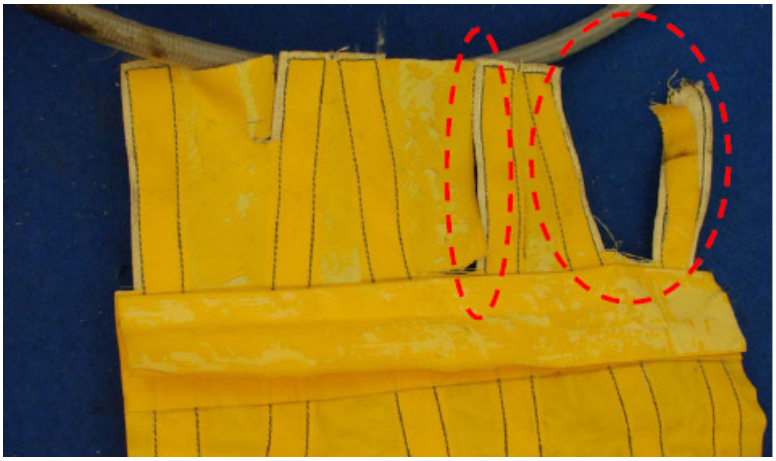

Figure 31 – Fabric torn along stitching

1.15.2.3 Disbonding of the buck bag from the floatation bag - The buck bag on the left side was damaged but still attached to the left floatation bag. The one on the right side was completely detached from the right floatation bag. Figure 32 refers.

Figure 32 – Buck bag detached from the floatation bag

1.15.2.4 Failure of the stitching on the longitudinal ribbon - The failure is in the form of loosening of stitching of the ribbon. Figure 33 refers.

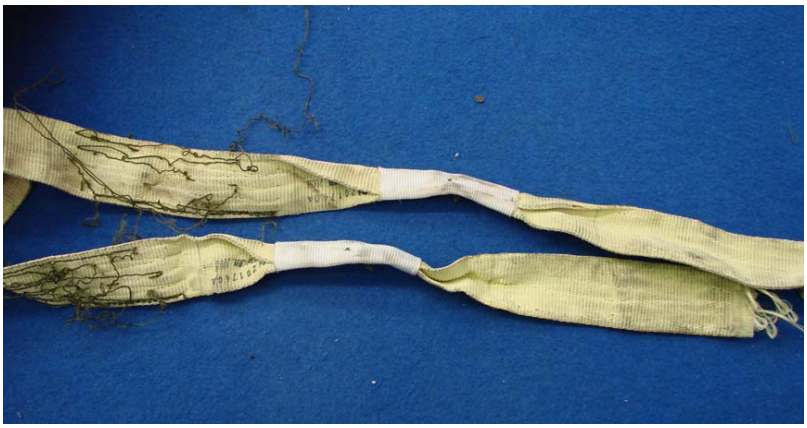

Figure 33 – Failed longitudinal ribbon (Right Forward Float Assembly)

1.15.2.5 Inflate (swivel) valves torn up from the floatation bag. Figure 34 refers.

Figure 34 – Holes for Inflate (swivel) valves

1.15.3 Search and Rescue

1.15.3.1 The accident occurred at approximately 0400 hrs (1200 hrs). Within one minute, a member of the public had made an emergency '999' call to report the occurrence to the Regional Command and Control Centre of Hong Kong Island (RCCC HK) of the Hong Kong Police Force (HKPF) which then alerted the Regional Command and Control Centre Marine (RCCC MAR) of HKPF and Fire Services Communication Centre (FSCC) of the Fire Services Department (FSD) to take corresponding actions. Emergency services personnel of the HKPF, FSD and Government Flying Service (GFS) were also notified and dispatched for the rescue operation.

1.15.3.2 At 0405 hrs (1205 hrs), FSCC notified the accident to CAD duty Aerodrome Supervisor who then initiated alerting actions in accordance with CAD Air Traffic Management Division Emergency Procedures Manual.

1.15.3.3 When Police Launch 43, the first emergency services vessel arrived on scene at 0408 hrs (1208 hrs), only two persons remained in the water and they were subsequently rescued.

1.15.3.4 The two crew members and 11 passengers were rescued by a nearby fishing boat, the first vessel to arrive on scene and a commercial harbour pilot boat within minutes of the accident. See table below.

Vessel	No. of Passengers Rescued
Fishing Boat	5 male passengers and 2 pilots
Harbour Pilot Boat	2 female and 4 male passengers

1.15.3.5 All the two crew members and 11 passengers were conveyed to Central Government Pier adjacent to Sheung Wan / Sky Shuttle Heliport. The 11 passengers were taken to hospital for medical examination. Six passengers received treatment for minor injuries. All the passengers were discharged from hospital on the same day.

1.15.4 Crew interview

1.15.4.1 Both the commander and the first officer were interviewed in the presence of each other by the investigation team on 3 July 2010. Following is the salient survival information of the interviews.

1.15.4.2 According to the statement of the commander, the floatation bags inflated automatically and quickly after the ditching. He evacuated through the emergency exit window. He recalled that two or three passengers had not put on their life jackets when the evacuation was taking place. He knew that there were enough life jackets onboard. He assisted several passengers to put on the lifejackets. The first nine passengers evacuated from the helicopter fairly rapidly. The remaining two passengers complained that they could not find any life jacket. As the commander did not know which seat still had the life jacket attached, he grabbed the seat cushions and told the passengers to use them as floatation means. An arriving boat threw two or three life buoys into the water. The final passenger evacuated from the helicopter had grabbed one of the life buoys. The commander was the last one to leave the helicopter.

1.15.4.3 The first officer advised that the floatation bags inflated automatically after the ditching. He evacuated through the emergency exit window. He saw the commander assisting the passengers and instructing them to get their life jackets out. By using Cantonese and Mandarin, he instructed passengers of where the life jackets were located.

1.15.5 Passenger interview

1.15.5.1 Of the 11 passengers onboard, only two passengers, who travelled together, had accepted the interview by the investigation team. The two passengers were interviewed together on 6 July 2010. During the interview, they had expressed concerns on the sufficiency, design and accessibility of the passenger life jackets onboard. They had also elaborated the difficulties encountered in opening the life jacket valise. One of the two passengers advised the investigation team that he had used his teeth to rip open the valise but was unsuccessful. He recalled that the life jacket was in a white bag with Velcro on top and found it very difficult to rip off the Velcro from the bag.

1.15.5.2 The investigation team had attempted to interview the other nine passengers onboard but was unsuccessful. Subsequently, two of the nine passengers had responded to the passenger questionnaire issued by the investigation team through their representing lawyer.

1.15.6 Investigation of Life Jackets

1.15.6.1 Two crew life jackets and eight passenger life jackets were recovered during the rescue operation. After the recovery of the helicopter from sea, another four passenger life jackets were found remained inside the compartment where the life jackets were stowed.

1.15.6.2 The two crew life jackets recovered are of Part Number 08819001, Model Number 102 MK 2BA and United Kingdom Civil Aviation Authority (UKCAA) Approval Number E11522. The twelve passenger life jackets recovered are of Part Number A312305A01RFD, Model Number MK 20 SV and UKCAA Approval Number E11638. The date of manufacture of these fourteen life jackets is May 2008 and the due date of next shop inspection is May 2018.

1.15.6.3 In light of the concern raised by the two interviewed passengers on the accessibility of passenger life jackets, the investigation team had performed an assessment on an in-service AW139 helicopter of EAA having the same cabin layout of B-MHJ on 21 Oct 2010. The assessment standard was JAR 29.1411(f) Life Preservers, which requires that:

"Each life preserver must be within easy reach of each occupant while seated."

(a) The assessment did not identify any difficulty in accessing the passenger life jackets on all the 12 installed locations.

1.15.6.4 The two interviewed passengers had also raised concern on the opening of the passenger life jacket valise. A test was carried out on passenger life jacket, Serial Number (S/N) 14621-130. This passenger life jacket had dropped to the cabin floor from its stowage position inside the stowage compartment underneath the left-hand most seat of the first row. Figure 35 refers. During the test, the tear opening strap of the valise was pulled manually and any abnormality identified was recorded. The test confirmed that the strap could be pulled open without any difficulty.

Figure 35 - Passenger life jacket, Serial Number 14621-130

1.15.6.5 Passenger life jacket, Serial Number 14621-125 remained inside its stowage compartment underneath the second from left seat of the last row. However, the life jacket had also dropped from its stowage position to the cabin floor and was tampered by seawater. Figure 36 refers.

Figure 36 - Passenger life jacket, Serial Number 14621-125

1.15.6.6 Workshop investigation of the life jacket Serial Number 14621-125 revealed the following:

(a) The tear opening strip of the valise had remained intact. When pulled, it detached from the valise cleanly, leaving a large exit gap for the life jacket to be removed.

(b) The life jacket remained a fully functional and operational piece of equipment.

(c) Water entered the valise through the tear present under the Velcro tape glued to the life jacket valise. It is unclear whether the tear occurred as a result of the removal of the life jacket from its stowage position or if it was made in error by someone trying to open the valise at a later date.

(d) The inclusion of the Velcro tape is not a modification authorised by the manufacturer of the life jacket. Its inclusion and the subsequent tear are ultimately responsible for water entering the lifejacket valise.

1.15.6.7 The AACM requirement for the approval of modification is published in Paragraph 2.1 of Macao Aviation Requirements MAR-1 Airworthiness Procedure No. AP5 Issue 3 Dated 20 February 2009, which stipulates that:

"Modifications other than those made mandatory by the Authority and not traceable to any approved continuing airworthiness information

disseminated by the manufacturer, such as Service Bulletin, shall be approved by the Authority."

(a) The investigation did not identify any AACM approval for the modification of the passenger life jackets with Velcro tape glued on jacket valise.

1.15.6.8 In a standard installation approved under a Service Bulletin of the helicopter manufacturer, the lifejacket is stowed as a standalone unit inside a container attached to the floor beneath the seat without the use of Velcro tape.

1.15.6.9 After the accident, AACM had conducted a thorough review with EAA on the stowage method of the life jackets. Subsequently, EAA submitted a modification for "Relocation of passenger life jacket stowage position" to AACM for approval on 4 April 2011. The modification was approved by AACM on 29 April 2011.

1.15.7 Performance of ADELT

1.15.7.1 After ditching, the ADELT was ejected from the helicopter. The transmitted 406 MHz signal was picked up by the COSPAS/SARSAT distress alerting system. It was subsequently recovered from sea. The exact location of the recovery was not known. However, the investigation team was informed by the rescue party that it was somewhere close to the ditching point of the helicopter. Therefore, the ditching point of the helicopter can fairly accurately represent the recovery location of the ADELT.

1.15.7.2 The Latitude and Longitude of the ditching point of the helicopter was 22º 17' 37.6" N and 114º 08' 48.7" E while the encoded position of the ADELT picked up by the COSPAS/SARSAT distress alerting system satellite was 22º 16' 00" N and 114º 08' 00" E

1.16 Test and Research

1.16.1 Forensic Engineering Examination

1.16.1.1 The recovered parts of the tail rotor assembly and the fractured parts of the vertical fin were sent to QinetiQ, a forensic engineering company that was contracted by the CAD to perform the necessary tests and examinations of these parts.

1.16.1.2 Examination of Parts

(a) All of the parts sent were examined visually and numerous detailed photographs were taken of potentially significant features, with particular emphasis on the relative positions of components and any damage marks prior to further dismantling.

(b) Samples from the root ends of the White, Blue and Yellow blades were radiographed to examine and record the condition of the glass fibre composite before and after the attempts to remove the bonded metal pitch control arm.

(c) 3-dimensional X-ray tomography was carried out under contract to a university. Scans were completed on samples from the White and Blue blades. The results were presented as sets of still images representing slices through each object, moving along X, Y and Z axes in steps of approximately 45µm, and as video animations. The university's analytical software was used to estimate dimensions and porosity within the 3D models.

(d) Image analysis for fibre density and porosity was carried out using proprietary Olympus image analysis software and high resolution images of polished micro-sections through the root regions of the White, Blue and Yellow blades. Measurements of porosity were made at these sections. An estimate of the number of glass fibres (~9µm in diameter) in the straps of the White blade was made by counting the fibres in several small regions, at high magnification.

(e) The fracture surfaces of the broken White blade were first examined under a binocular optical microscope. Detailed examination of broken fibres was carried out in a Field Emission Scanning Electron Microscope (FESEM). Some metal parts were examined optically and in a conventional Scanning Electron Microscope (SEM).

(f) Two samples were removed from the White blade remains for measurement of the glass transition temperature (Tg) by Differential Scanning Calorimetry (DSC).

(g) A burn-off test was carried out on samples from the two straps of the White blade to determine the proportions of fibre and resin in the unidirectional material.

1.16.1.3 Observations on Fracture Surfaces of Vertical Tail

(a) Visual examination of both fractured sections of the vertical fin identified considerable deformation. The structure remained attached to the tail rotor gearbox was more deformed. The deformation showed that the detached section of the vertical fin (attached to the tail rotor gearbox) had departed from the tail in a starboard direction. This section had also suffered some post-failure deformation.

(b) Detailed visual examination was carried out on both halves of the fracture surface using a stereo optical microscope to determine the mode of crack growth. Particular attention was paid to areas around fastener holes where progressive cracks such as fatigue typically initiated. Examination showed that both halves were relatively clean, apart from some deposits which were likely the result of immersion in seawater. There was no evidence of thumbnail-shaped oxidation that may be associated with progressive crack growth. Most of the fracture surface was dull, fibrous and angled at 45° to the sheet surface.

1.16.1.4 Witness Marks Indicating Relative Movement of Parts

(a) The root of the White blade, specifically the pitch link fastener, impacted the rotor hub centre as a result of the blade moving in lag direction. The pitch link impacted the outboard plate of the hub and the rod end was bent.

Figure 37 refers. After recovery, the elastomeric bearing was found to be deflected, with the pitch control arm lodged against the White damper attachment bracket. Figure 23 refers.

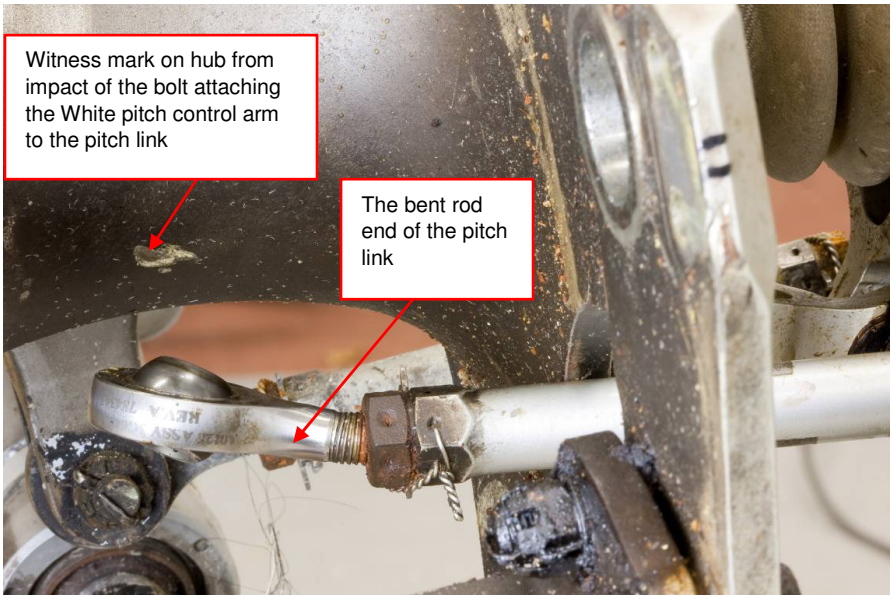

Figure 37 – Witness mark on tail rotor hub

(b) There were marks on the inboard face of the outboard plate of the rotor hub which resulted from contact of the pitch control arm. Figure 38 refers.

Figure 38 – Witness mark caused by flapping of White blade

(c) The Blue blade had impact damage at the tip and had experienced abnormal movement in the lag direction, as evidenced by the damage to

the Blue blade damper and bracket. The bending of the damper rod end was not as great as on the White blade damper and there was no impact mark on the hub centre. The lag movement is almost certainly related to the impact at the blade tip.

(d) The Yellow and Red blades are scratched on the surface. The lead-lag movement was much less than on the White or Blue blades and the damper attachments were still intact.

(e) There were impact marks in the form of dents on both sides of the Y9 tail rotor pitch control rod. Figure 26 and Figure 27 refer.

1.16.1.5 Tail Rotor Blades

(a) The remaining part of the White blade consisted of a small piece of the glass fibre composite from the loop at the root end. Figure 39 refers. This was still bonded to the metal pitch control arm. The fractures of the White blade straps on the leading edge side were long and fibrous. The trailing edge fractures were flatter and, on close examination, exhibited a combination of tension and compression failures.

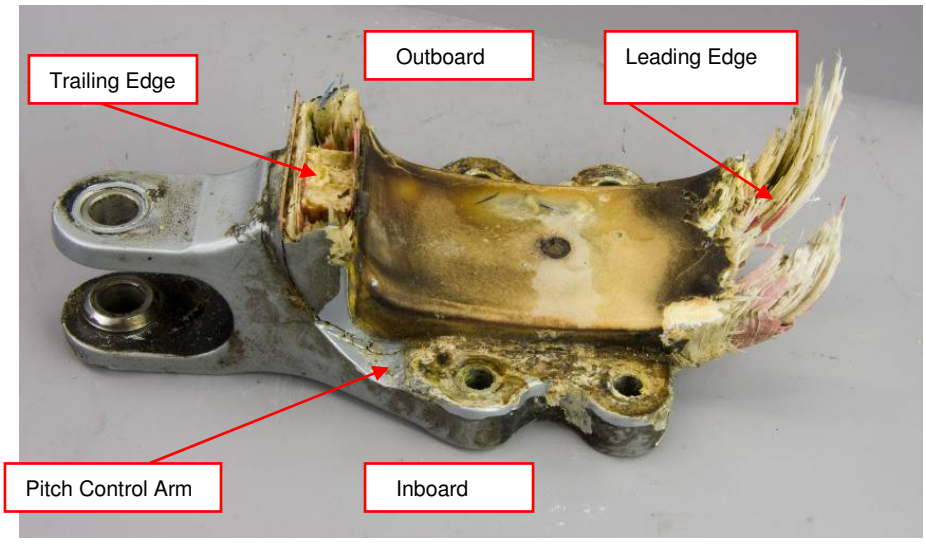

Figure 39 – Remains of White blade with pitch control arm attached

(b) The Blue blade was immediately behind the White blade as the tail rotor rotated. It suffered significant tip damage and the GFRC material failed parallel to one of the 45° direction indicators in the over-wrap. There

was also deformation of the nickel erosion strip on the leading edge and local buckling of blade skin material in the mid-section. Figure 40 refers.

Figure 40 – Impact damage at tip of Blue blade

(c) Both Red and Yellow blades showed evidence of surface scratching. Figure 41 refers. Neither their dampers nor the attachments to these blades was damaged.

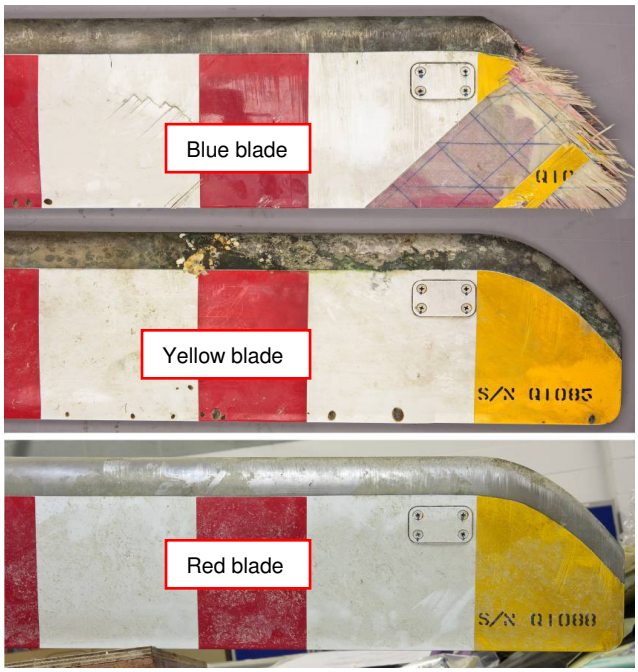

Figure 41 – Blue, Yellow and Red blades

1.16.1.6 Condition of the Dampers

(a) The White damper rod end at the hub end was bent. The rod end has a spherical bearing, so could only be bent after being levered against a hard contact point; the hub attachment bracket. It was evident that the damper

was compressed as the White blade rotated in the lag direction, until it became a rigid link. The blade attachment bracket then failed at one end and the rod was bent at the other. Figure 42 refers.

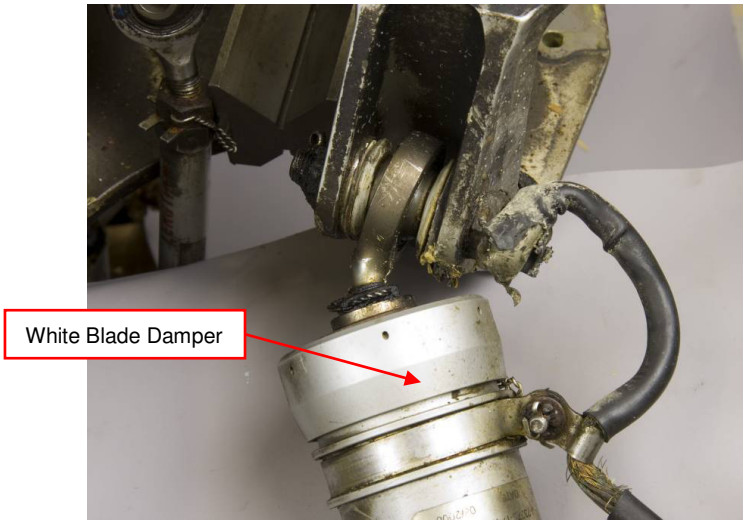

Figure 42 – Bent rod end on White blade damper and damage on hub damper bracket

(b) The damper manufacturer's report on the condition of the White and Blue dampers advises that the elastomers appeared to be in serviceable condition.

1.16.1.7 Build Quality of Tail Rotor Blades

(a) Measurements were made of the cross-sections taken through the root ends of the White, Blue and Yellow blades. See Figure 43 for typical view where cross-sections were taken. These cross-sections were taken as they remained intact after the accident and their build quality should represent that of a typical production tail rotor blade. AW commented that the periodic destructive tests required for quality assurance verification by STAP 106 did not include this area, because it was considered not relevant as the area was clamped between metal parts.

(b) All of the root filler dimensions conformed to the drawing tolerances (20 ± 0.25 x 10 ± 0.25 mm). The specified dimensions and tolerances for the straps are 10 ± 0.25 x 10 ± 0.25 mm. Thus the cross-sectional area should be 100 ± 5mm². For each blade, the cross-sectional dimensions of the two straps were measured. On the White blade, all eight measured dimensions were under-sized, with the result that both cross-sectional

areas were significantly under-sized, at 89.7 mm² and 86.5 mm² (i.e. 89.7% and 86.5% of the nominal area). For the Blue blade, two measurements were under-sized and one measurement was slightly over-sized. For the Yellow blade, three linear measurements were under-sized and the cross-sectional area of one strap was under-sized, at 91.6 mm².

Figure 43 – Typical view of blade root end area showing where cross-sections were taken

(c) The cross-section dimensions measured were compared with manufacturing records supplied by AW for the White blade; top (outboard) and bottom (inboard) straps. For both straps, the measurements of width and thickness at the root end, after the straps were cured, were recorded as being within the allowable tolerances. According to AW's test, it was verified that further spar assembly curing phase could possibly affect the strap dimensions.

(d) On all three blades sectioned at the root: White, Blue and Yellow, the alignment of the straps and the filler core was poor, with the filler core closer to the pitch control arm than the straps. Figure 44 refers. Furthermore, the position of this structural subassembly within outer ±45°

layers was asymmetric. In each case, the over-wrap was considerably thicker on the face adjacent to the elastomeric bearing than on the face bonded to the pitch control arm, hence the core was much closer to the pitch control arm. On the thicker side, it was apparent that there was much more resin and there were wrinkles/waves in the outer wrap.

Figure 44 – Cross-section through the root end of the White blade

(e) A section taken through the side of the loop on the Blue blade, roughly equivalent to the fracture position on the White blade showed that the lay-up was not as badly misaligned as at the root end. There was no intact material in this failure location on the remains of the fractured White blade and so its construction quality and condition prior to the accident cannot be determined. Unfortunately, no other parts of the White blade were recovered.

(f) Measurements were made on the White, Blue and Yellow blade micro-sections of fibre size and the number of fibres per unit area in the straps was estimated by counting the numbers of fibres in small areas under high magnification. This was not conclusive because of the small areas examined and the variability apparent through the material. However, the number of fibres per unit area appears to be as expected in areas with visibly even fibre distribution. The manufacturing records indicate that the correct number of turns (230) of glass fibre tape was applied during the tape winding operation. The number of fibres per tow/turn is not specified and AW has not been able to supply this information at the time. The measured diameters of the fibres appeared to be to the correct specification. According to AW, the proper number of fibres is ensured by the compliance with the procurement specification of the raw split tape material including the resin and fibre content. Material compliance is assured by batch

acceptance tests.

(g) For White, Blue and Yellow blades, numerous voids were noted in the adhesive bonds. Some were located at the points where the straps and the filler core were misaligned, and are considered likely to have been present since manufacture. Other cracks in bonds may have been formed or enlarged during the accident sequence and so it is not possible to determine the extent to which they are quality issues or consequential damage.

1.16.1.8 Porosity

(a) High levels of porosity were measured by 2-D optical analysis of physical cross-sections of the White, Blue and Yellow blades, and by 3-D volumetric analysis of the data from X-ray tomography. For both types of analysis, minimum thresholds were selected, based on pixel or voxel size, to distinguish between real features and possible picture noise. The porosity measurements were found to vary between the blades and different straps from the same blade. However, the area of voids larger than 250 μm^2 on the sections examined was seen to range from 11.3% to 23.9%; all apparently much higher than the allowable limit (2.5% volume). The highest levels of porosity were measured on the sample from the White blade. X-ray tomography of an 83mm^3 volume of the White blade resulted in lower estimates of porosity (between 4.1% and 8.7%) but still more than the allowable level. The differences between the volumetric analysis and the porosity measurements on polished cross-sections could indicate variations in the porosity in different volumes and may well also be influenced by differences in resolution between the two techniques. It was noted that some very long pores were detected parallel to fibre direction. They may have been interpreted as allowable cracks in production X-radiographs taken side-on. The porosity was noted to be associated with localized poor wetting of fibres by the resin matrix. According to AW specification, voids content measurement has to be performed using the calcinations method (Burn-off). Reliable void assessment comparison cannot be performed between different methods of evaluation. Refer 1.6.1.11 for Burn-off test performed on the White blade samples.

1.16.1.9 Cracking

(a) In addition to the cracking close to the bond with the metal pitch control arm, cracks parallel to the fibre direction were observed in the straps. Figure 45 and Figure 46 refer. These mostly appeared to be associated with long strings of porosity. Other cracks were noted in bond lines between the straps and the outer ±45° wrap and at the corners of the bond with the filler core. X-ray tomography also found some transverse cracks through the section in the root filler. Figure 47 refers. These features were not confined to the failed White blade.

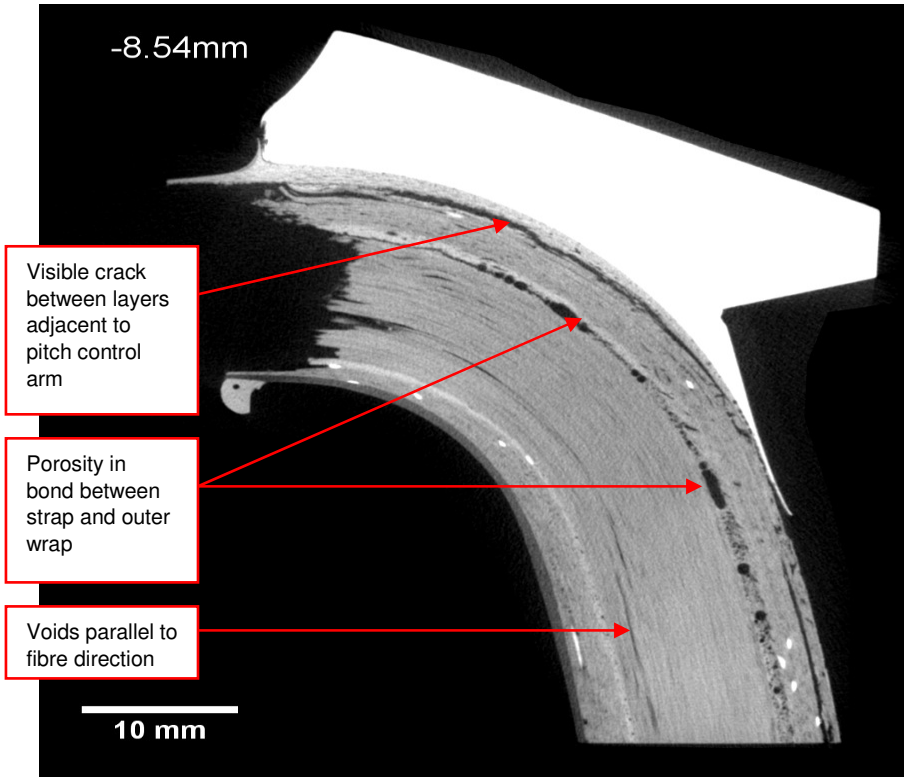

Figure 45 – Section through White blade strap using X-ray tomography

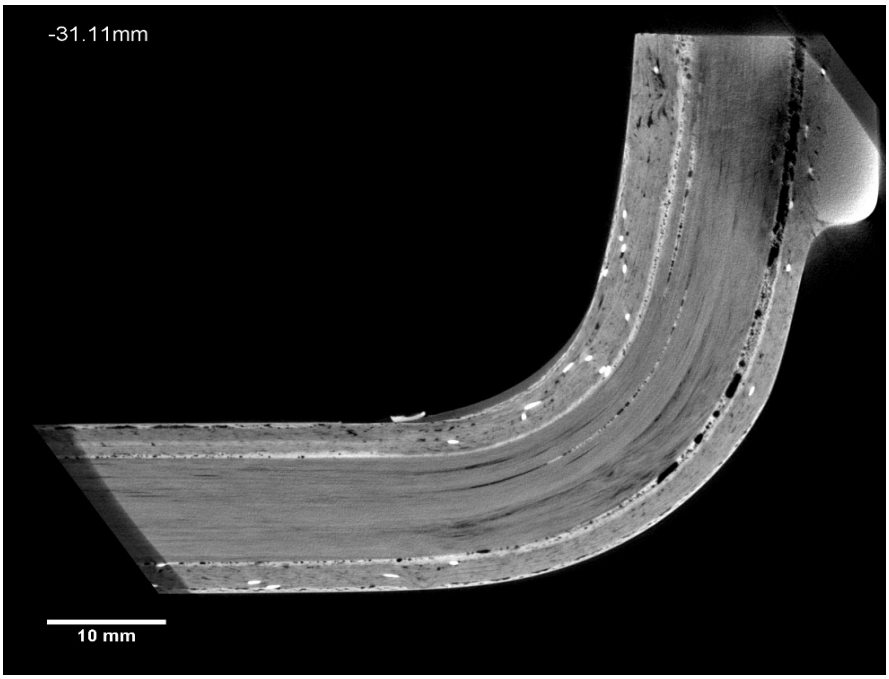

Figure 46 – Section through Blue blade strap using X-ray tomography, showing porosity and cracks parallel to the fibres and in the adhesive layer

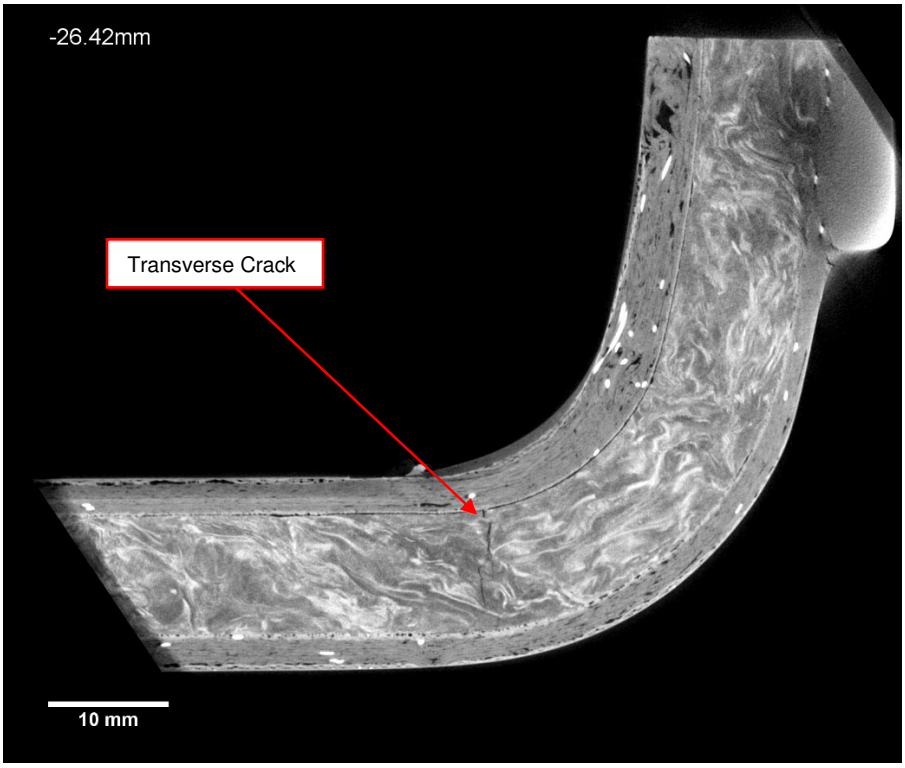

Figure 47 – Section through Blue blade root filler using X-ray tomography, showing traverse crack

1.16.1.10 Fractography

(a) A fractographic examination of the two failed straps of the White blade indicated that both straps failed in a predominantly tensile mode on the leading edge. Figure 48 refers. On the trailing edge, some fibres were observed to have failed in tension, others in compression. Figure 49 refers.

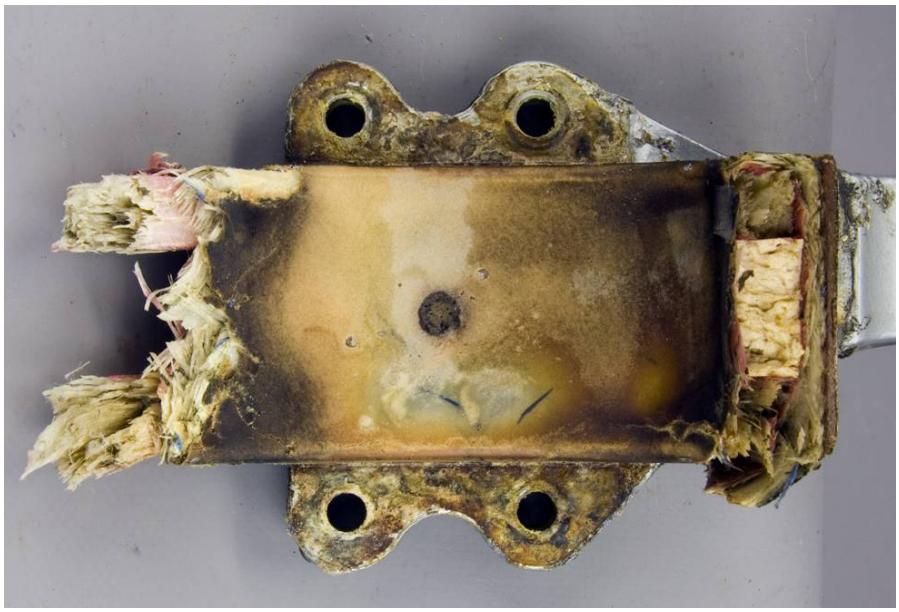

Figure 48 – Fracture surfaces of the White blade

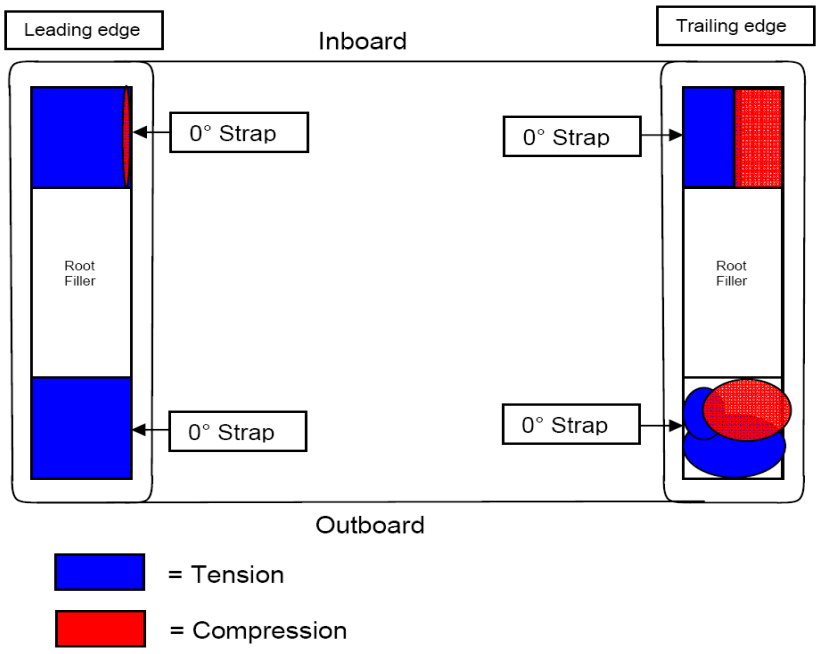

Figure 49 – Approximate zones of compressive and tensile failure

1.16.1.11 Differential Scanning Calorimetry (DSC) and Burn-off

(a) The DSC analysis of samples taken from the straps did not show any very distinct transitions, but the Tg of the resin was interpreted to be between 134°C and 139°C. This was very similar to the Tg of 140°C measured by AW on production samples. The Tg value for ±45° outer wrap (142°C) was also similar to this value. All measurements exceeded the minimum specification of 110°C.

(b) Burn-off tests were conducted on two samples of strap material, one from each strap of the White blade. However, the test was unsuccessful due to the incomplete burn-off achieved.

(c) Two more samples were later cut from the straps on the inboard and outboard surfaces of the White blade to further determine their void content using the Burn-off test. Void content using density determined by machined block method were 5.54% and 3.97%, whilst using density determined by immersion method were 3.4% and 2.55%. The measured figures were above the maximum void content of 2.5% specified in AW manual STAP106. It was apparent from the results that the immersion method gave conservative values of void content. With the immersion method it is thought that some voids within the composite probably were filled with water, leading to an under-estimate of the void content. According to AW, voids content is periodically verified by destructive test on production blades. The check did not include the root area between the pith control arm and elastomeric bearing. Further assessment on production blades in the same area provided the evidence of similar void content in this root blade area as typical figure of production standard, the tested blades for certification were therefore re-assessed as representative of the manufactured blades.

1.16.2 Supplementary Examination of Parts

1.16.2.1 Subsequent to the examination of the tail rotor parts prescribed in Section 1.16.1, two further accidents have occurred involving the failure of AW139 tail rotor blades. Paragraph 1.18 refers. These subsequent accidents have drawn attention to features and combinations of features that are very likely

to be of significance to the B-MHJ investigation, which primarily relate to manufacturing defects and composite failure modes.

1.16.2.2 In conducting this supplementary investigation requested by CAD, QinetiQ has performed the following tasks:

(a) A review of the X-ray tomography data on the fractured White blade and a comparison with additional cross-sections.

(b) A review of the X-ray tomography data on the Blue blade and a comparison with additional cross-sections.

(c) A review of the cross-sections from the Yellow blade and a comparison of features with those identified on the White and Blue blades.

1.16.2.3 X-Ray Tomography of Fractured White Blade

(a) The X-ray tomography images in Figure 50 and Figure 51 show side view slices through the fractured trailing edge bottom (inboard) strap and the top (outboard) strap from the White blade. These slices were taken close to the inboard and outboard edges of the straps, i.e. just inside the straps. The images show a reduction in the thickness of the ±45° GFRC torsion box on the internal corner radii of the component, i.e. the mating surface with the elastomeric bearing attachment bracket. Figure 50 and Figure 51 also show the presence of a resin filler material on the inner surface of the blade root. Plan view slices taken through the fracture location also confirmed the reduction in the wall thickness of the ±45° GFRC torsion box and the addition of the resin filler on the inner surface of the blade root. Figure 52 and Figure 53 refer. The inset image in Figure 53 shows “cut” plies at the inner corner of the GFRC torsion box, which are evidence of blade profile adjustment in this location. The thickness of the filler resin on the inner surface was greater at the inboard corner, probably to make up for the removed GFRC torsion box plies in this location.

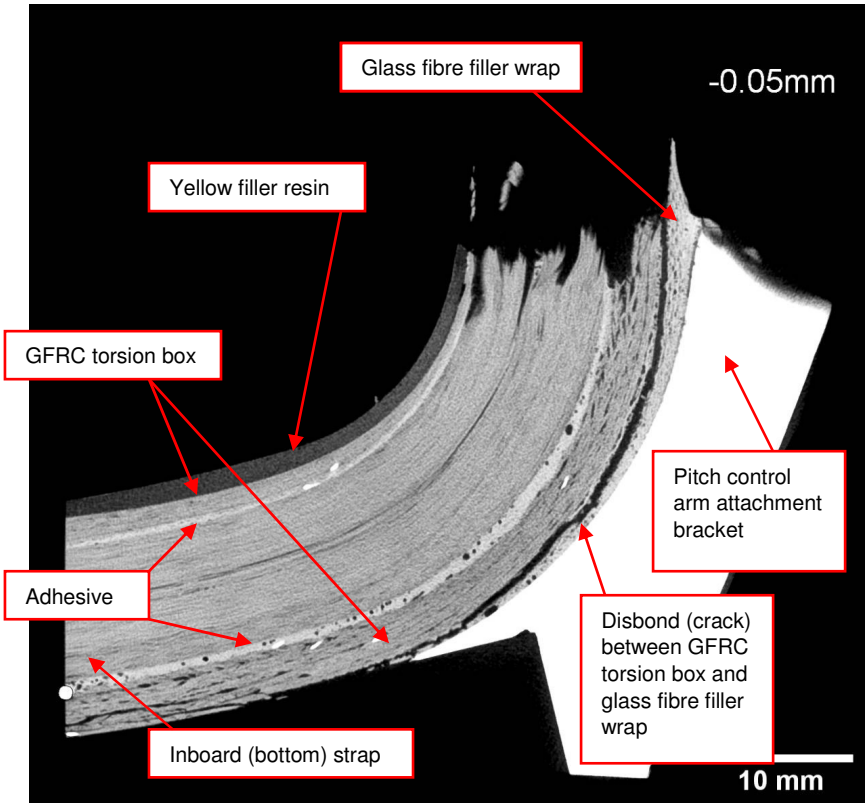

Figure 50 – X-ray tomography image showing a side-view slice through the bottom (inboard) strap of the White blade, trailing edge fracture location, approximately 3.5 mm from the inboard edge of the blade arm

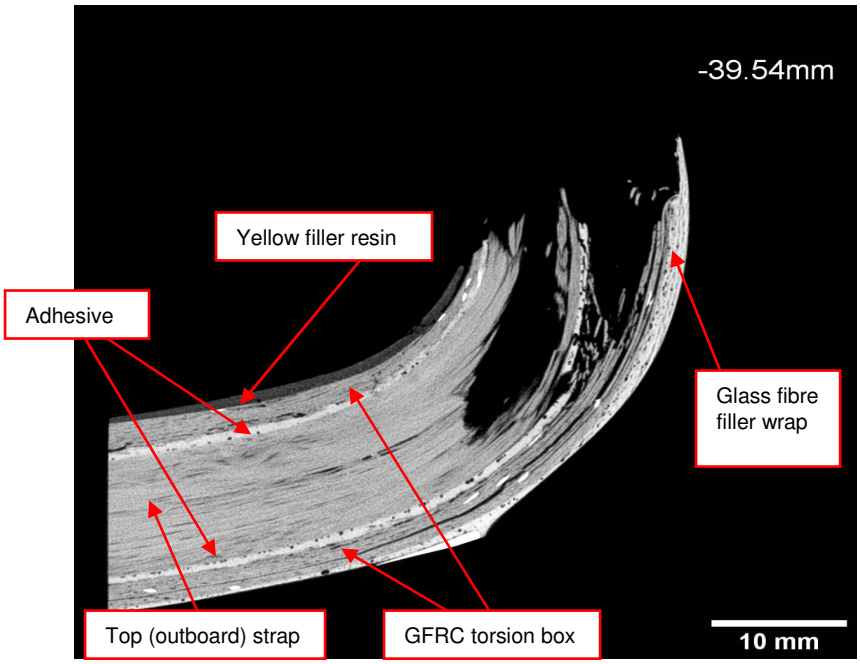

Figure 51 – X-ray tomography image showing side-view slice through the top (outboard) strap of the White blade, trailing edge fracture location, approximately 4 mm from the outboard edge of the blade arm

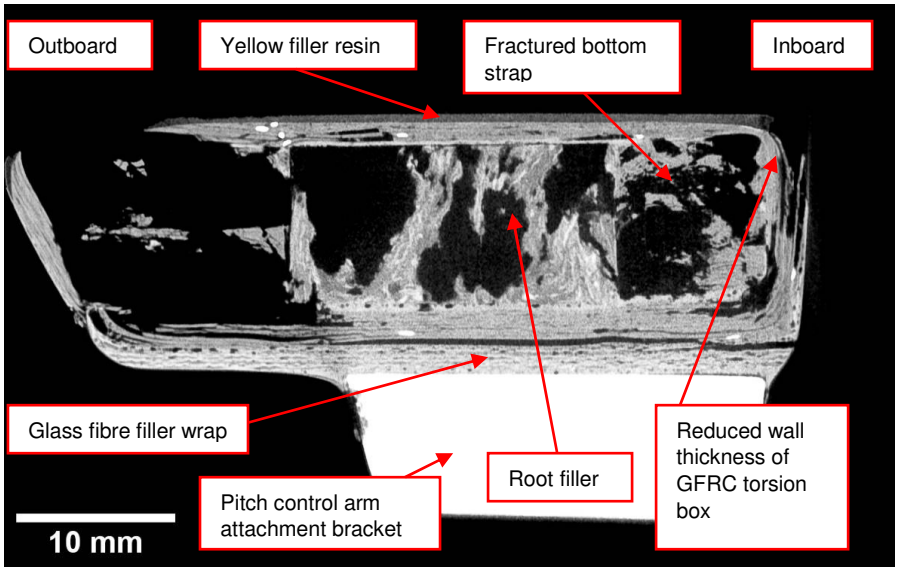

Figure 52 – X-ray tomography image showing a plan-view slice through the fractured trailing edge arm of the White blade, fracture zone approximately 4.1 mm below the top of the pitch control arm horn

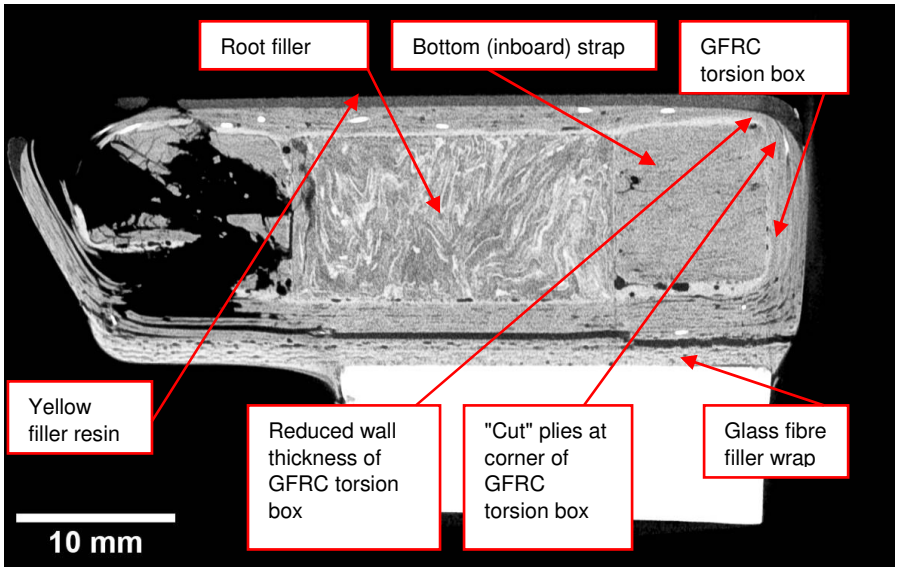

Figure 53 – X-ray tomography image showing a plan-view slice through the fractured trailing edge arm of the White blade; slice taken just below fracture zone approximately 8 mm below the top of the pitch control arm horn

(b) Figure 54 shows a side view slice through the root filler material in the fractured White blade trailing edge sample. The image again shows a reduction in thickness of the ±45° GFRC torsion box plies on the internal radii of the blade root. The X-ray tomography slice also shows evidence of pinching of the external plies of the ±45° GFRC torsion box on the trailing edge side of the blade adjacent to the horn of

the pitch control arm attachment bracket. The glass fibre filler wrap used as a shim to adjust the profile of the blade root to the pitch control arm bracket was observed standing proud of the trailing edge. This corresponds to a disbonding of the filler wrap from the blade handle at this location. The disbond propagated from the pinched plies of the torsion box and then migrated into the plies of the GFRC torsion box at this location. This crack was also observed on the inboard trailing edge slice shown in Figure 50; however, in this image the crack appeared to propagate between the GFRC torsion box and the glass fibre filler wrap. The plan view slices show this crack to change direction from within the GFRC torsion box to the interface between the GFRC torsion box and the glass fibre filler wrap in the location of the bottom (inboard) strap. Figure 52 and Figure 53 refer.

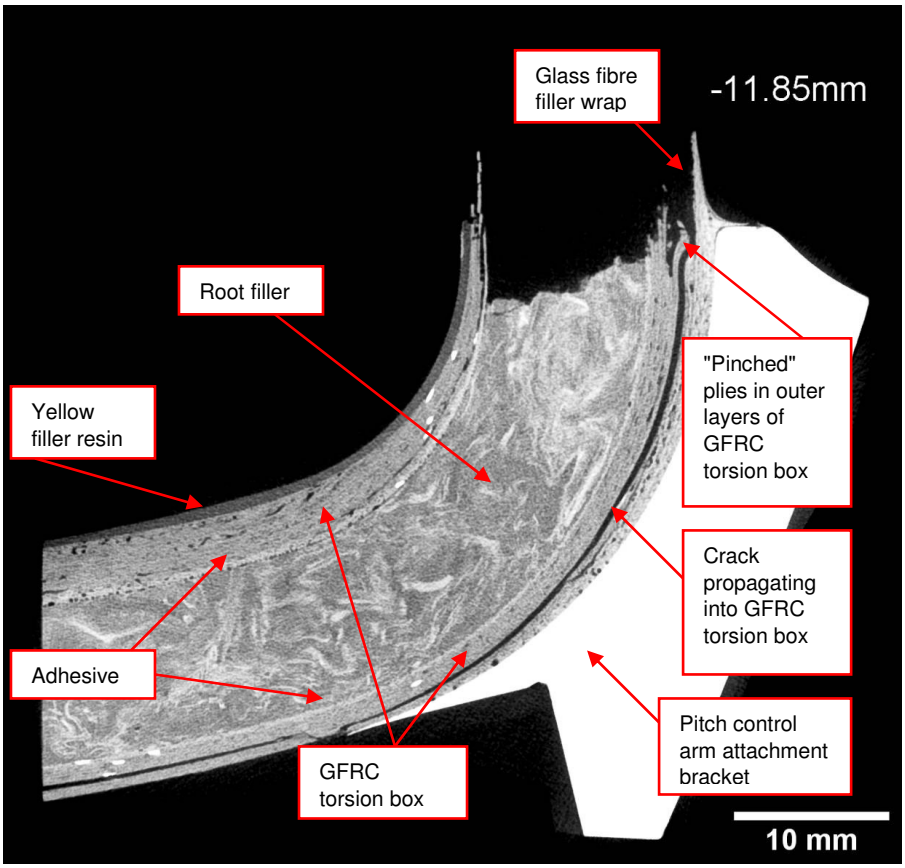

Figure 54 – X-ray tomography image showing a side-view slice through the root filler of the White blade, trailing edge fracture location, approximately 15.4 mm from the inboard edge of the blade arm

(c) Examination of a series of plan view slices through the bottom (inboard) trailing edge strap of the fractured White blade showed the presence of

linear features across the strap close to the fracture surface. These linear features appeared to correspond to the “delaminations” observed on the polished micro-sections taken from this location.

(d) The X-ray tomography images from the leading edge location on the fractured White blade were dominated by longitudinal splits and delaminations within the material, the majority of which were attributable to fracture in this region. The torsion box on the inner corner radii of the blade at this location appeared to be thicker than that observed on the trailing edge and the filler resin was also present on the inner surface.

(e) The reduction in the number of plies in the ±45° GFRC torsion box on the inner corner of the bottom (inboard) trailing edge location can be seen in the inset images in Figure 55 and 56. The number of plies present in this region was estimated to be three or four, when ten plies are required by blade design. The presence of the yellow coloured filler resin on the inner surface of the blade root is also shown in the photographs. The thickness of this filler resin appears to vary across the inner surface, with the tracer fibres within the ±45° GFRC torsion box occasionally visible in the thinner areas. Figure 57 refers. The glass fibre filler wrap standing proud of the fracture surface is indicated in Figure 57 and Figure 58. The surface breaking crack indicated in Figure 58 corresponds to the delamination/disbond crack aforementioned. The photograph shown in Figure 58 also illustrates the “cut” plies of the ±45° GFRC torsion box at the inner corner of the inboard trailing edge location.

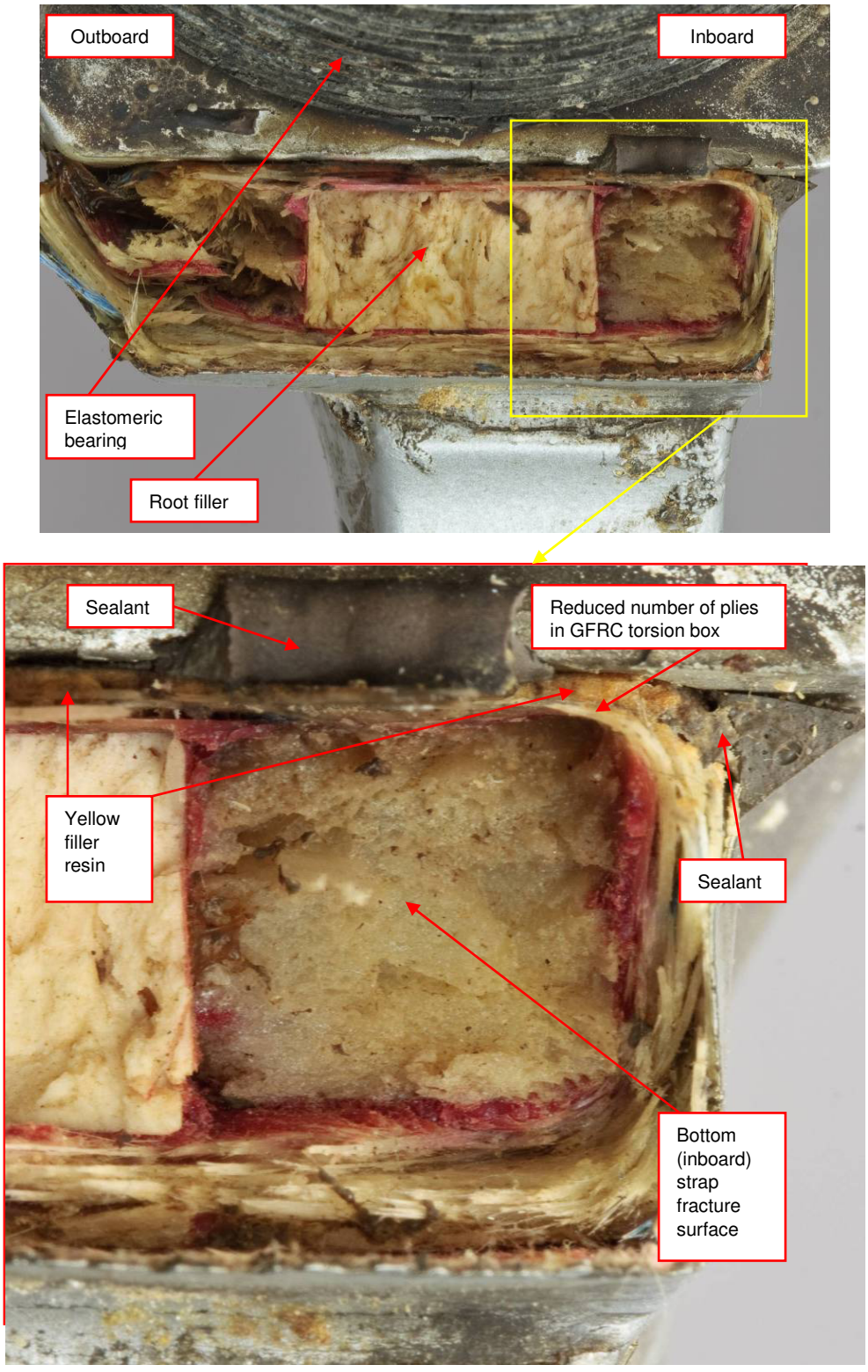

Figure 55 - Photographs showing the trailing edge fracture surfaces of the White blade prior to the removal of the elastomeric bearing, the insert photograph shows detail of the bottom (inboard) strap illustrating a reduced number of plies in the GFRC torsion box at the inner surface of the root.

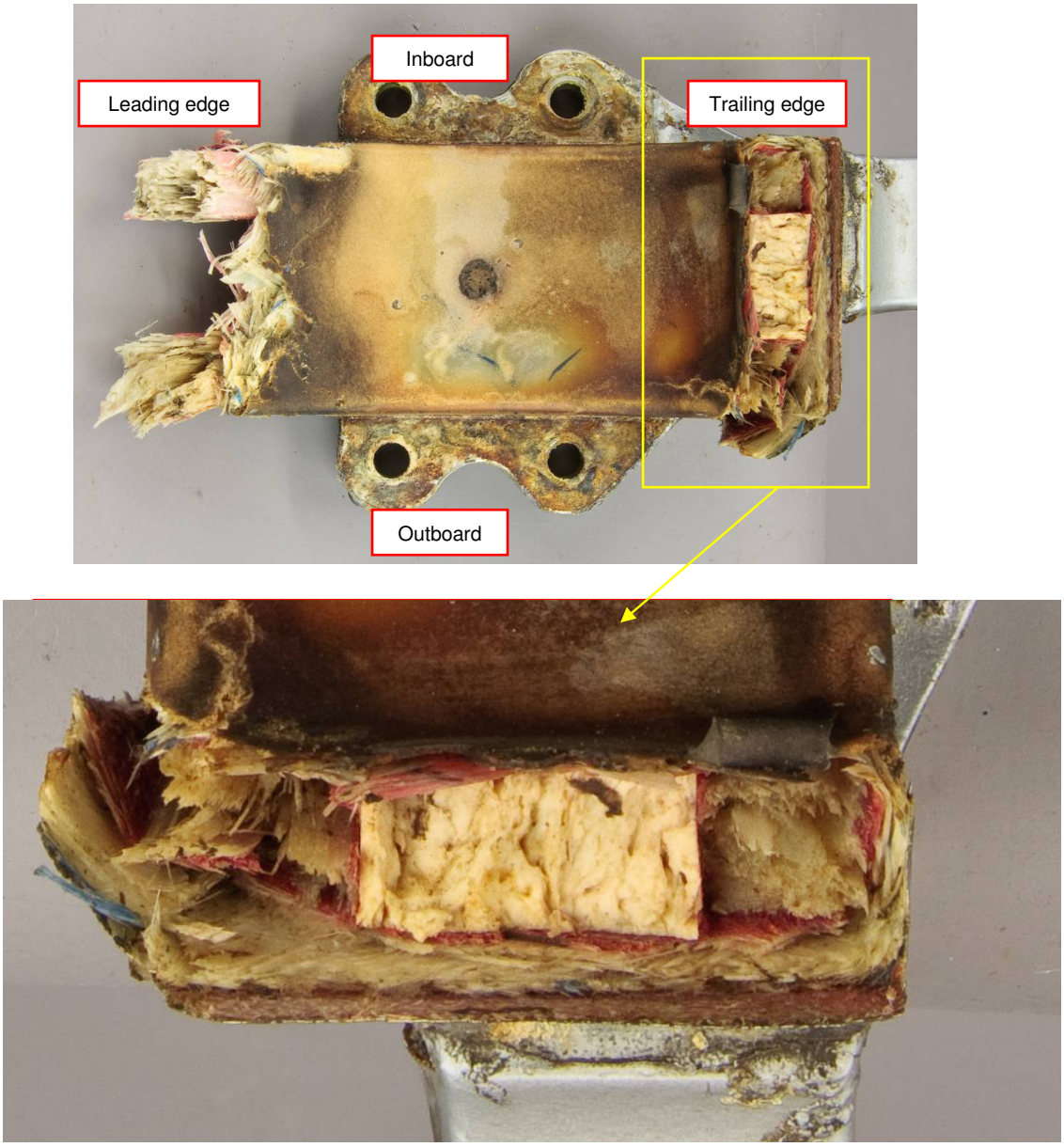

Figure 56 - Photographs showing a plan view of the fractured root area of the White blade after removal of the elastomeric bearing, with detail of the fractured trailing edge arm shown in the bottom insert image

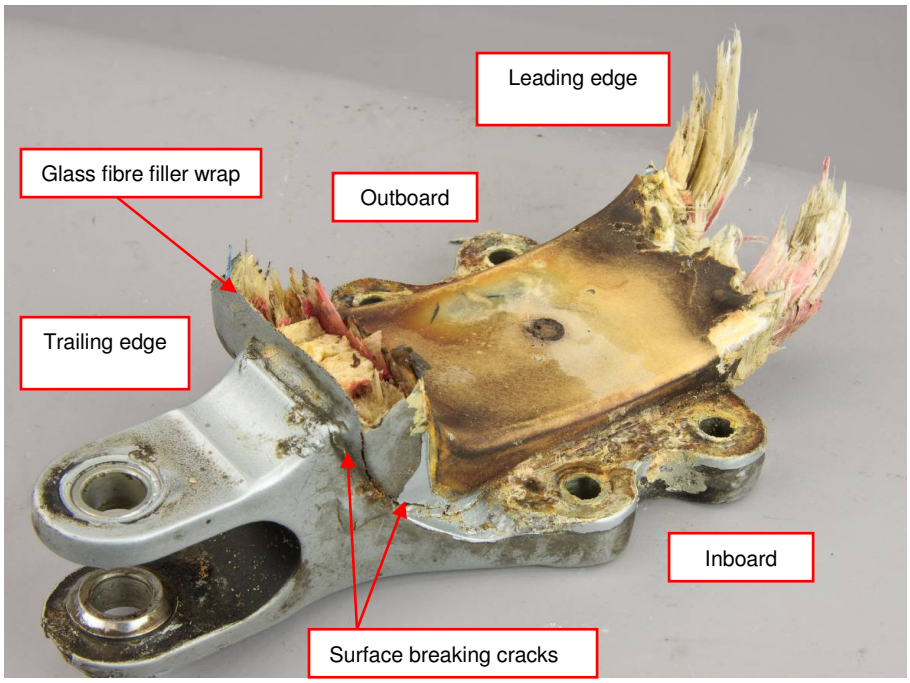

Figure 57 - Photograph showing the fractured root area of the White blade after removal of the elastomeric bearing

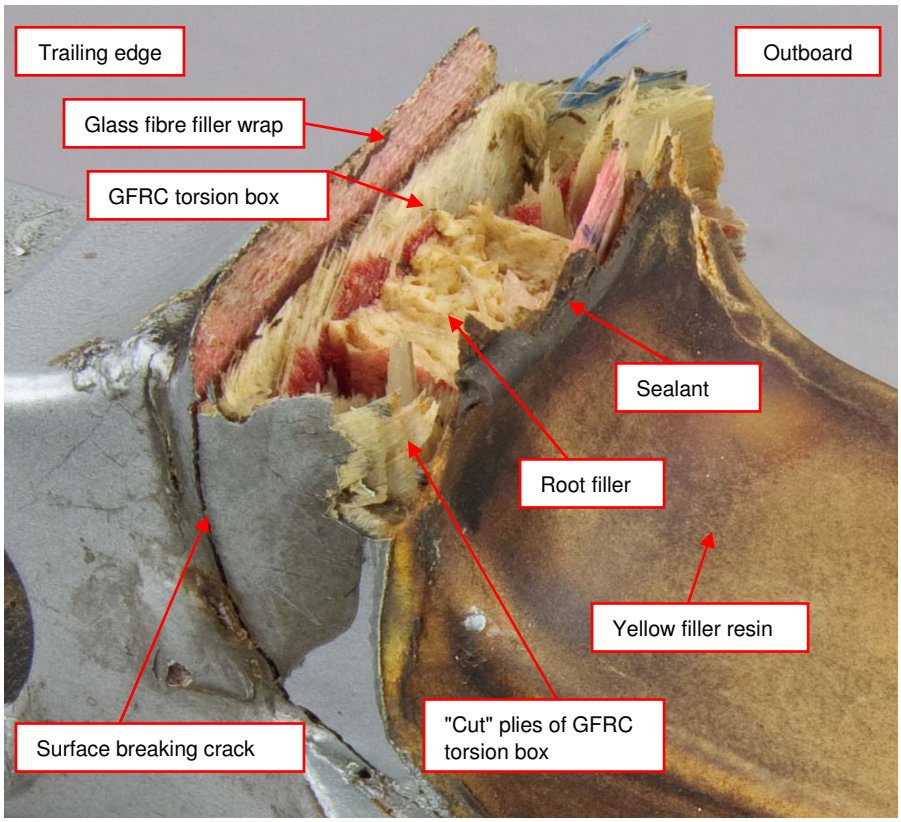

Figure 58 - Macro photograph showing detail of the White blade trailing edge arm fracture after the removal of the elastomeric bearing

1.16.2.4 Fractography

(a) Following the re-assessment of the tomography data, and cross-sections from the White blade, Yellow blade and Blue blade, a section of the transverse fracture present within the strap at the inboard trailing edge of the White blade was cut to facilitate a more detailed fractographic examination. Figures 59 and 60 show the views of the section removed from the root end of the blade.

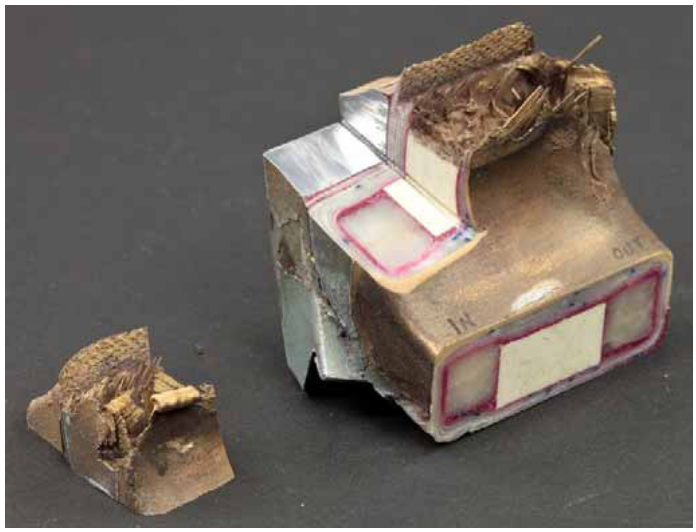

Figure 59 - Section cut from inboard trailing edge of the White blade for detailed fractographic examination

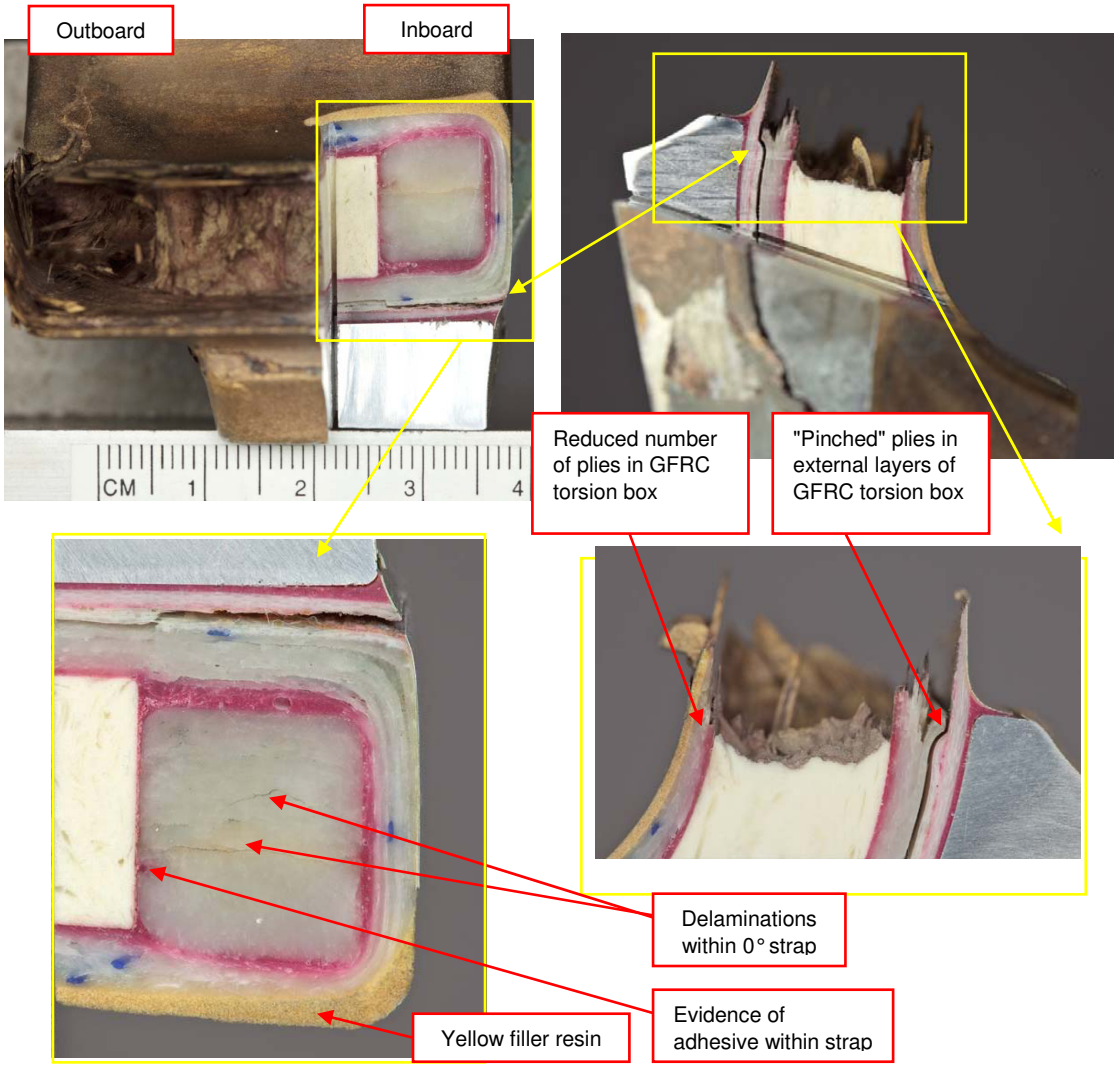

Figure 60 - View of section cut from trailing edge of White blade showing delaminations within the strap, cracking associated with 'pinched' plies and reduced ply thickness on inner radii

(b) Macroscopic examination of the cut surfaces, made in both the vertical and horizontal directions, revealed a number of features that were similar to those described above. The features identified included:

i. Two large delaminations with the bottom (inboard) trailing edge strap.

ii. A reduction in the number of plies present within the ±45° GFRC torsion box on the internal corner radii.

iii. "Pinching" of the external ±45° layers within the GFRC torsion box at the top of the pitch control arm bracket attachment. This was associated with cracking propagating into the torsion box plies.

iv. Evidence of adhesive bleeding into the strap.

(c) The White blade section shown in Figure 59 was further cut into three samples, namely FE1083, FE1084 and FE1085, for analysis.

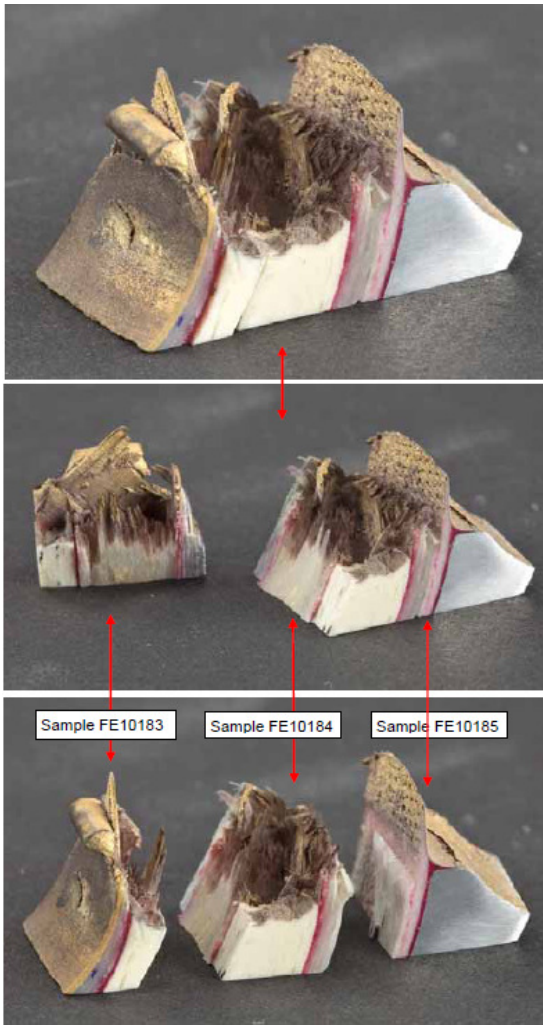

Figure 61 – Samples FE1083, FE1084 and FE1085 (Left to Right)

(d) The fracture surfaces associated with the delaminations within the strap and ±45° GFRC torsion box were separated and examined using scanning electron microscopy.

(e) Figure 62 shows an electron micrograph of the delaminated surface of sample FE1084 taken within the strap from bottom (inboard) trailing edge of the White blade. The fracture was covered with significant quantities of surface debris. Abrasion of the resin and fibres was also observed which was consistent with fretting between the mating fracture surfaces.

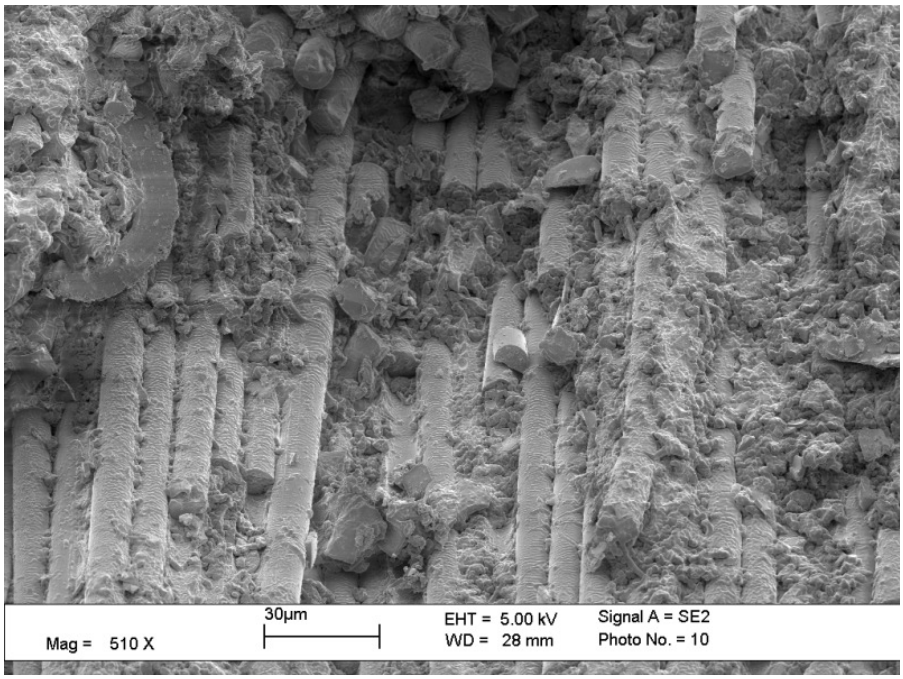

Figure 62 - Electron micrograph of delaminated surface (sample FE1084) within the strap showing close-up view of fretting debris

(f) Figure 63 shows an electron micrograph of the delaminated surface towards the centre of sample FE1084. The delaminated surface in this region also exhibited signs of fretting due to shearing. Some longitudinal voids were also observed at the interface between the delaminated surfaces.

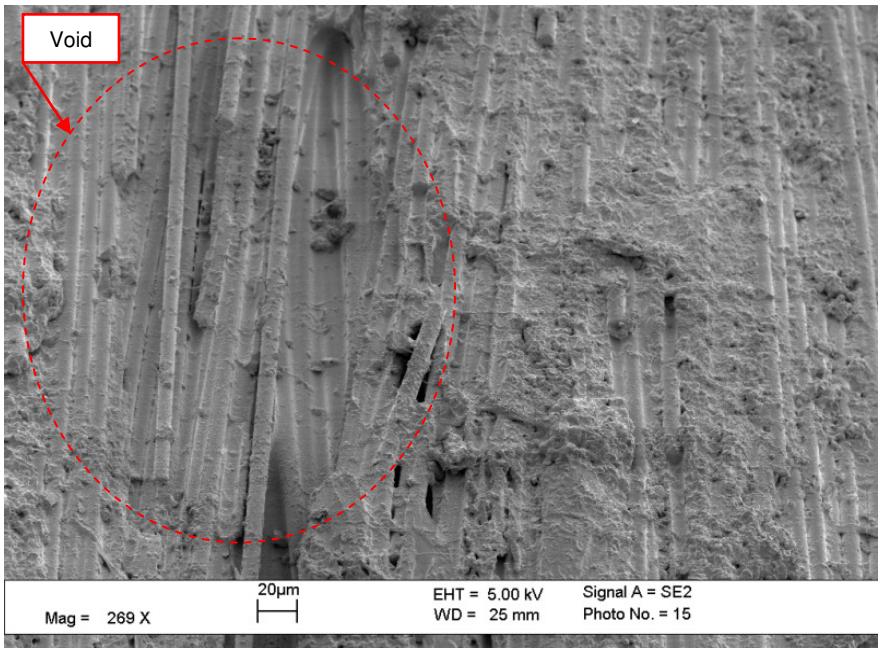

Figure 63 - Electron micrograph of delaminated surface (sample FE1084) within the **strap showing close-up view of fretting debris and void within strap**

(g) Figure 64 shows an electron micrograph of the fracture surface near the centre of the delamination, in a location where the fretting between the surfaces was less apparent. In some areas within the matrix, occasional zones of striations, consistent with localised cyclic advance of the delamination were observed. These striations, which were only rarely identified, can be seen more clearly in Figure 64.

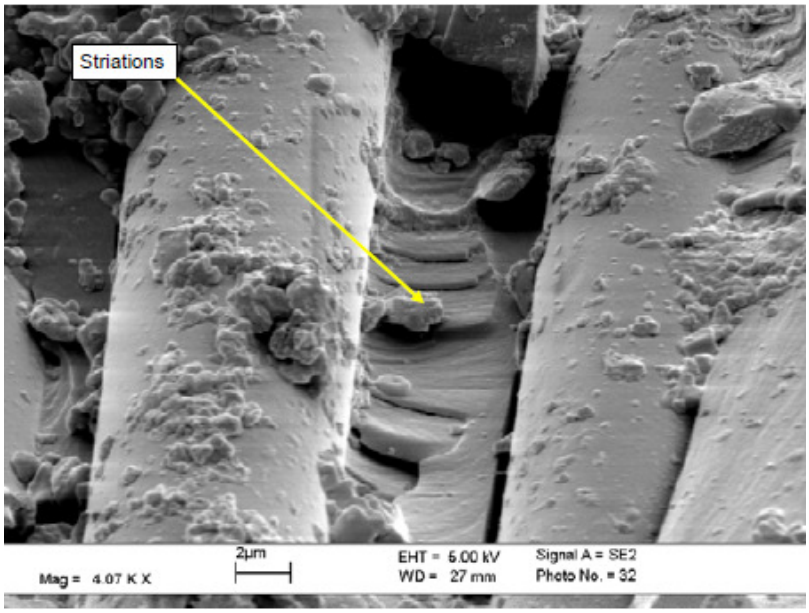

Figure 64 - Electron micrograph of delaminated surface (sample FE1084) within the **strap showing close-up view of fretting debris and striations**

(h) Figure 65 shows the delaminated surface towards the back of specimen FE1084. This region was located closer to the centre of the corner radii. Significant surface fretting, consistent with cyclic fretting, between the surfaces was visible. Smoothing/polishing of the surface, due to abrasion between the mating surfaces, and damage to the fibres was apparent.

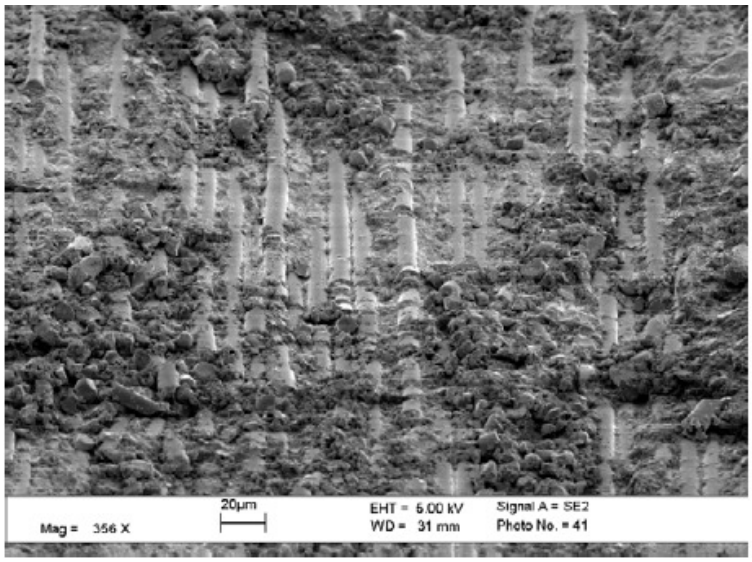

Figure 65 - Electron micrograph of delaminated surface (sample FE1084) within the strap showing close-up view of fretting debris and damage to fibres

(i) Figure 66 and Figure 67 show electron micrographs of the delaminated surface of sample FE1085 within the ±45° GFRC torsion box, where pinching of the ply was observed. Close examination of the fractures within the resin revealed that fracture had occurred primarily due to overload under the action of mixed-mode stresses (tension + shear), as evident by the presence of flattened shear cusps (hackle) features within the resin.

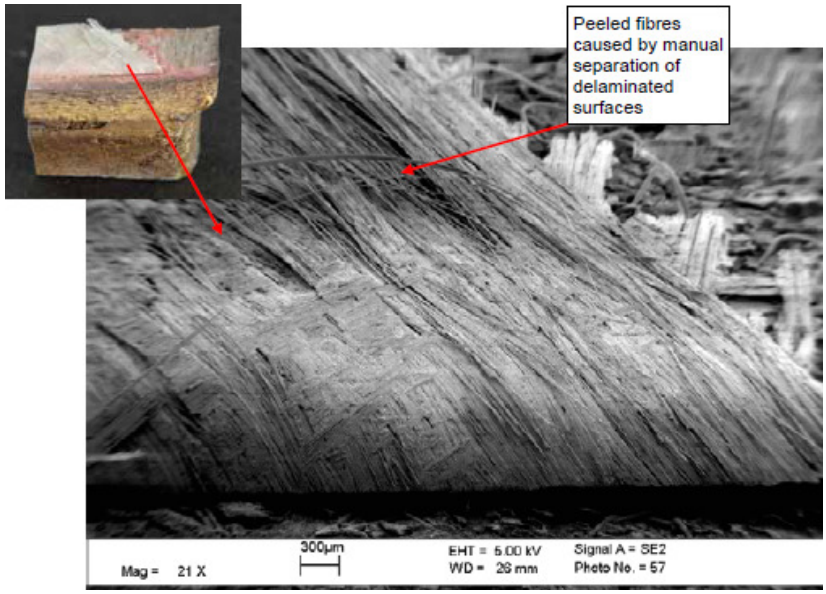

Figure 66 - Electron micrograph of delaminated surface (sample FE1085) within ±45° 'pinched' ply

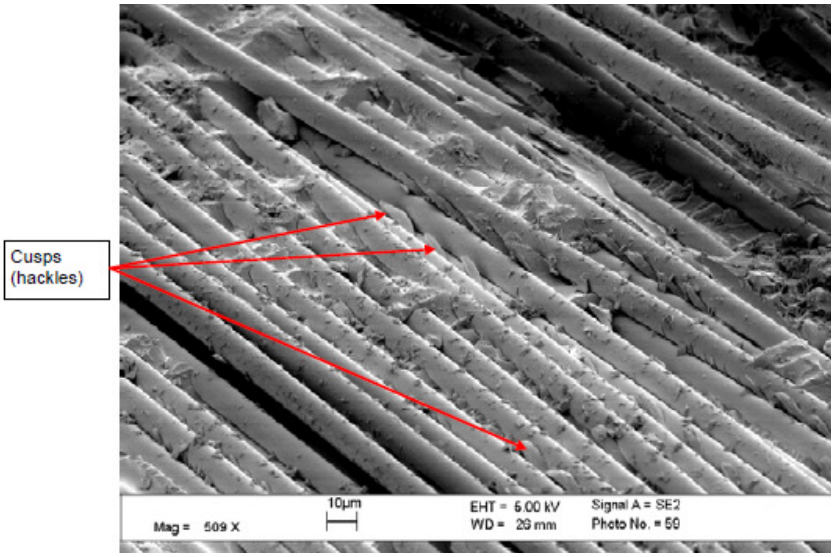

Figure 67 - Electron micrograph of delaminated surface (sample FE1085) within ±45° 'pinched' ply

(j) Figure 68 shows micrograph of the delaminated surface located towards the back left corner of sample FE1085. Severe fretting, consistent with cyclic shearing between the surfaces, was observed. It was noted that on the right side of the specimen, fracture had propagated into the interface between the ±45° GFRC torsion box and glass fabric filler. Figure 69 refers. This interface (which contained adhesive) also showed evidence of fretting. The pockets of adhesive present within the weave often had a smooth, polished, appearance due to abrasion between the surfaces. Occasional striations were also observed on this interface although many had a softer appearance due to surface abrasion. Figure 70 refers.

(k) A summary of findings of the supplementary examination is included in Appendix 3.

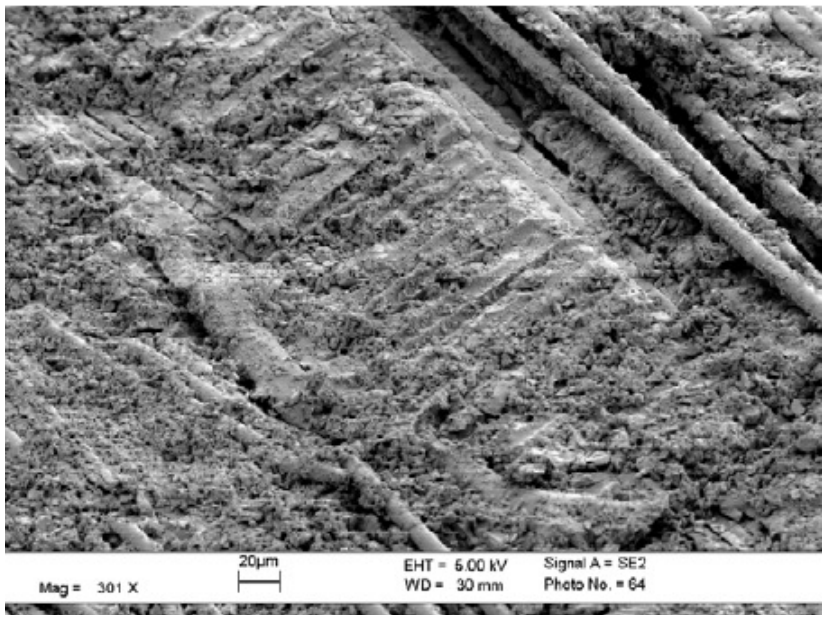

Figure 68 - Electron micrograph of delaminated surface (sample FE1085) within ±45° 'pinched' ply showing fretting

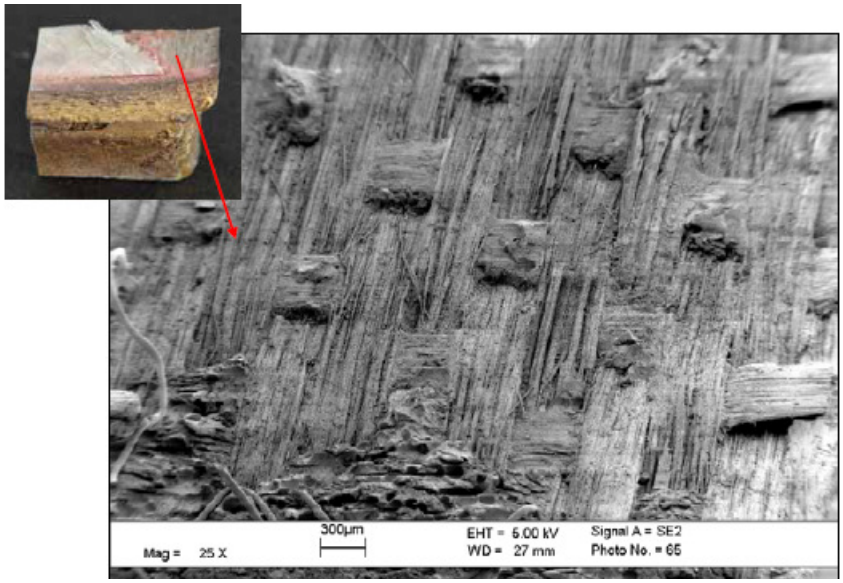

Figure 69 - Electron micrograph of delaminated surface (sample FE1085) of 'woven region' ply showing fretting

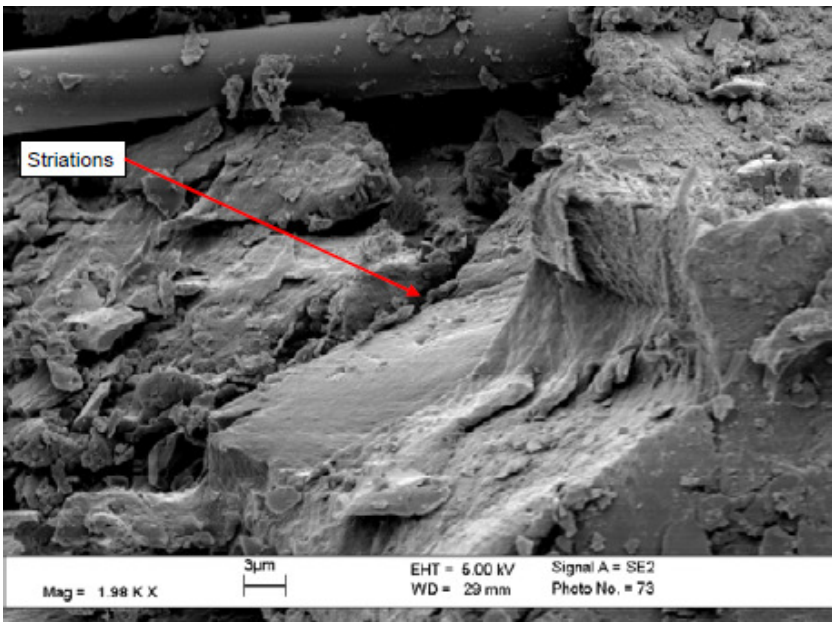

Figure 70 - Electron micrograph of delaminated surface (sample FE1085) of 'woven region' ply showing fretting and striations

1.16.3 Research and Test Activities Carried out by AW

1.16.3.1 Fatigue and Static Test

(a) After the accident that occurred on 2 May 2011 involving a Qatar AW139 helicopter of registration mark A7-GHA, AW performed fatigue and static tests on a tail rotor blade with one of the four straps section severed. According to AW, this confirmed the fail safe approach adopted to assure the airworthiness of the fleet based upon damage tolerance capability. It also confirmed that torsion box fatigue limit were much lower than the fatigue allowable for the straps.

1.16.3.2 Evaluation of Reduced Strap Section and Torsion Wrap

(a) AW has carried out an evaluation of reduced strap section and torsion wrap using two detailed linear finite element (FE) models. The first (pristine model) is a FEM validated with a dedicated strain survey performed on an AW139 helicopter tail rotor blade with nominal dimensions in the root area. Starting from the pristine model, the second modified FEM has been generated having the trailing edge upper and bottom straps with section dimensions reduced by 1 mm height and width. The same boundary condition and load case were used to load and constrain both models. The

load case used is the limit load condition for the root corresponding to the flight condition at -40 degree Celsius having the maximum centrifugal force. The forces/bending were, congruently, calculated and applied at STA 215 and on pitch control arm.

(b) The analysis showed a percentage of stress increase of 11% in the longitudinal direction and 36% in the radial direction, between the modified and pristine FEM, which still maintains big safety margins even when compared to the aged material allowable limits. In addition, the torsion box wrap was tested for its contribution to the strength of the blade root section. The result of the test showed an increase of the strength by a factor of 2.44 between the bare strap and the strap wrapped on three sides.

1.16.3.3 Blade Production, Certification and Design Review

(a) Several tests, on full scale tail rotor blade specimens or strap structural element, were performed by AW and have been able to reproduce the in-flight failure mode. AW presented that the most probable cause of the strap failure originates from an inter-laminar shear phenomenon as a result of a local bending moment.

(b) In addition, the following aspects, that could play a secondary role when alone, become considerable when present in conjunction with reference to the tail rotor blade strength reduction in the root area:

i. Allowable defects in the root curved area (porosity, marcel and separation).

ii. Local bending stress at the root area portal configuration as a result of external load applied in flight.

iii. Bending stress increasing caused by pitch control arm de-bonding.

iv. Strength reduction as a result of torsion box de-bonding, delamination or under thickness particularly in the trailing edge inner side root area.

v. De-bonding of the tail rotor blade elements interfaces.

(c) In relation to the pitch control arm de-bonding, the elastomeric bearing over shimming installation was identified as the possible cause. See Figure 71 for elastomeric bearing shim installation. An improper over shimmed installation could result in pitch control arm de-bonding or torsion box delamination in the underneath area.

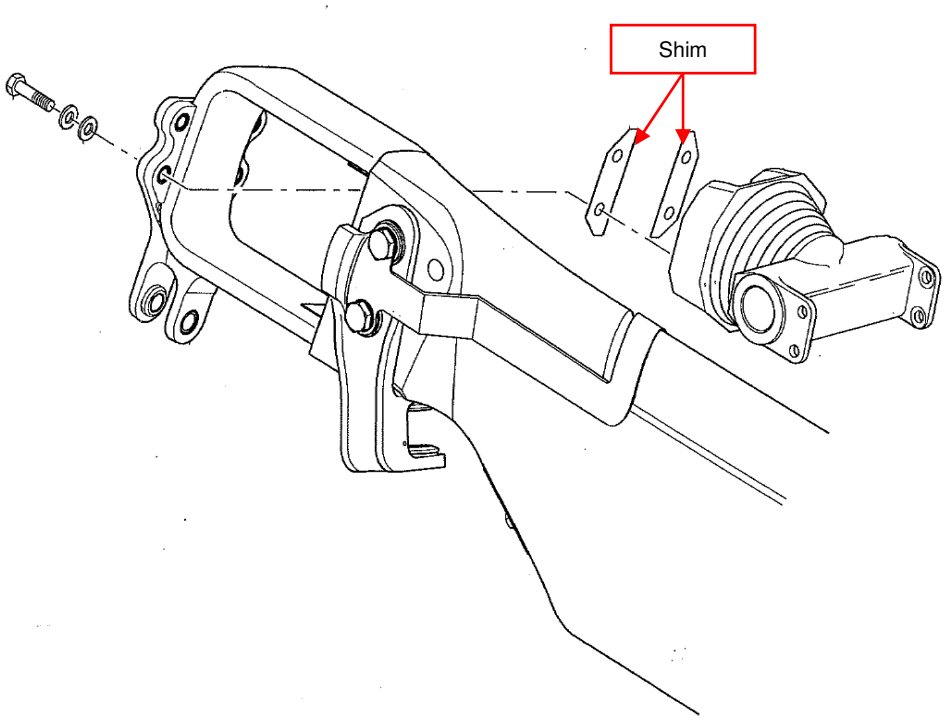

Figure 71 - Elastomeric bearing shim installation

1.16.3.4 Evaluation of Tail Rotor Blade Strap Defect Assessment

(a) A "Round Robin" statistical evaluation of the strap defect assessment by X-Ray was performed by AW. Although the reliability of the inspection system was confirmed, some cases of +/- 1 and just one case of +2 defect grade tolerance (under estimation) have been pointed out.

1.16.3.5 Result of Test Campaign and Analysis

(a) AW has consolidated the following overall considerations as result of the test campaign and analysis prescribed in above:

(b) The origin of the tail rotor blade failure mode was understood and reproduced by test on strap structural elements and tail rotor blade specimens.

(c) The nucleation of the strap damage is driven by Strap Interlaminar Radial Stress (ILRS) and the propagation by Interlaminar Shear Stress (ILSS).

(d) Strap structural elements tests identified that the interlaminar property is more affected by the porosity defect than the marcel.

(e) Low Frequency (Start Stop) cycles represent the significant fatigue load condition.

(f) Blade strength is affected mainly by local stress due to chord bending at the trailing edge root blade section.

(g) Pitch control arm de-bonding significantly increases (+40%) the bending stress at the trailing edge root section as verified by flight stress survey.

(h) Torsion box degradation issues (de-bonding, delamination, under thickness) at the root area significantly over stress the trailing edge straps with worst condition on the bottom one.

(i) As at October 2011, retirement life limitation (quarantine) 600 flight hours or 1,500 landings whichever comes first, was confirmed for the existing blade configuration by statistical analysis of the relevant in service data and tests by including torsion box degradation and pitch control arm de-bonding.

(j) Positive Fail Safe test with a trailing edge bottom strap severed proved conservatively the blade strength and as at October 2011, the life limitation in case of coalescence of defects exceeding the allowable levels and in the presence of pitch control arm de-bonding.

1.16.4 Research and Test Activities Carried out by EASA

(a) Subsequent to another AW139 accident occurred in Doha on 2 May 2011, EASA have worked with AW to establish the most appropriate precautionary and corrective actions, aiming at ensuring safety of the AW139 operations. These activities are summarized below. Refer to Appendix 4 for details.

i. Temperature survey.

ii. In-flight blade strain-stress/load survey.

iii. Full scale fatigue tests and static test survey.

iv. Blade Dynamic Stability Evaluation.

v. Finite Element Method model analysis of the blade root area.

1.16.4.1 Temperature Survey

(a) The result of the survey excluded any damaging effect related to the different coefficient of expansion of the materials of the metallic pitch change arm and composite tail rotor blade.

1.16.4.2 In-Flight Blade Strain-Stress/Load Survey

(a) According to EASA, specific measurements of strain and stress on the tail rotor blade root handle was not performed in the load survey of the original certification of the helicopter. This was justified by the results of some initial flights where a tail rotor blade root handle partially instrumented did not show any specific critical values of strain and stress. The most stressed location was the transition area of the blade where flight bending moments (beam and chord) were maximum. Subsequent to this and another similar AW139 accident, an in-flight blade strain-stress/load survey was performed using a blade instrumented with additional strain gauges in the root area. The result of the survey showed that a local bending moment at the trailing edge area was evident with tensile stress in the inner side and compressive stress on the outer torsion box skin. Also, significant load condition was associated with engine start-stop conditions.

(b) On 23 June 2011, AW was required to perform a new survey with different positions of the strain gauges in order to confirm correctness of the load assumptions of the original certification and of the damage tolerance test on the tail rotor specimen with the cut strap.

(c) On the basis of the information provided, and after review of the test proposal, EASA Continuing Airworthiness (CA) Structures Expert agreed that the new test would have to be performed considering:

i. Upper trailing edge strap completely severed, this decision was driven by consideration that the trailing edge bottom strap presented a high level of manufacturing discrepancies.

ii. Strain application and distribution fully consistent with values and distributions found during load survey.

(d) AW presented on 27 July 2011 two new elements of paramount importance:

i. The new in-flight strain-stress/load survey allowed to accurately measure the strain level in the failed section of the tail rotor blade root area as result of the known load condition. The values obtained were found consistent with the level assessed during certification. The critical section was originally defined by the lowest margin of safety and identified as the blade transition area, on which the certification test was performed. The strain survey allowed to appraise the strain comparability between the root and transition area while confirming the original criticality assessment. What identified, during the initial damage tolerance test performed on the instrumented blade following the accident, was the inability of the test rig to provide the correct strain in the failed section as result of the application of the known external load (centrifugal force and bending); the strain difference was recognized as about 35%. Following this finding, the test rig has been modified in order to obtain proper local strain level in the failed section.

ii. The strain levels along trailing edge bottom strap thickness were not uniformly distributed, varying from high tension value on the inner side to low compression on the outer side (local bending).

(e) On 29 August 2011, AW informed EASA CA Team that the tail rotor blade subjected to the new test (with loads determined during the recently completed in-flight blade strain-stress /load survey), failed after the

application of 3302 flight cycles. The tested blades included the trailing edge upper strap severed, the lower strap critical section with 30J impact damage, strap porosity (grade 4) and marcel (grade 3). The tested blade, despite the relevant damages inflicted and defects included, was able to demonstrate a significant number of flight cycles re-assuring about the interim life adopted for the in service blades. The test result showed the sensitivity of fatigue and damage tolerance characteristics of the tail rotor blade design in case of the severe cumulative damages and under the reassessed test loading conditions.

1.16.4.3 Full Scale Fatigue Tests and Static Test Survey

(a) Several full scale fatigue tests have been carried out with different combinations of production strap defects and possible damages (i.e. torsion box degraded characteristics for plies removal, pitch control arm disbonding and artificial damages in the strap surface). Bending stiffness characteristic of the failed section is mainly dominated by the torsion box that provides about 65% of the stiffness. In addition, extremely severe tests have been performed with a strap totally severed. The fatigue test results performed on the specimen have been plotted and best fitted with a proper curve shape to obtain a "Wholer" curve representative of the blade fatigue strength in presence of relevant defects and damages. Pitch control arm disbonding was assessed in a test stress survey identifying the relevant stress raiser effect in the trailing edge bottom strap area. A pitch control arm disbonding in the curved root area resulted in about 40% of nominal stress increase.

1.16.4.4 Blade Dynamic Stability Evaluation

(a) Complete stability analysis was performed for a 20% reduction of all the straps sections with no evidence of margins reduction. The backlash of tail rotor components was checked, verified and found not significantly affecting the dynamic stability of the rotor. Sudden failure of one strap section was also evaluated for dynamic effects, without evidence of instability phenomena.

1.16.4.5 Finite Element Method (FEM) Model Analysis of the Blade Root Area

(a) A very detailed FEM of the root blade area was developed to properly represent stress/strain condition in the root area including the local bending in the trailing edge bottom strap. Validation of the FEM model was made by comparing the predicted strains in the critical condition of the tail rotor blade root handle trailing edge with the values recorded at the same locations on an instrumented tail rotor blades installed on the helicopter. In particular the detailed FEM model was able to estimate the magnitude of the interlaminar stresses (radial and shear) acting on the tail rotor blade and their contribution to initiate interlaminar damages that eventually lead to the failure of the tail rotor blade section. The FEM model confirmed the correlation between chord bending stiffness and magnitude of the radial and shear stresses (i.e the lower the chord bending stiffness the higher the magnitude of the stresses). The FEM model also indicated that under the most critical loading condition and in presence of macroscopic defects such as reduction of the external box and disbond of the pitch control arm, it is possible that the magnitude of the interlaminar radial stresses exceed the maximum allowable and cause a delamination onset (Open MODE I) in the curved area of the tail rotor blade root handle. Delamination could then grow and propagate due to Inter Laminar Shear Stress (Shear MODE II). The combination of the above failure modes (ILRS and ILSS) can lead to possible subsequent multiple delaminations in the radius area, through the complete thickness.

Note: Under normal conditions with a torsion box intact and a pitch control arm correctly bonded, the maximum values of interlaminar transverse stress in the critical region of the tail rotor root handle was evaluated not exceeding the fatigue allowable value for interlaminar transverse stress. In the case of a reduction to zero of the thickness of the torsion box in the critical region of the tail rotor root handle combined with a disbond of the pitch control arm, the maximum value of interlaminar stress exceeds the fatigue allowable. Presence of allowable manufacturing defect results in further degradation of the strength capability. Under these circumstances, it is expected that a separation among the fibres and along the thickness of the strap could propagate up to the point that the longitudinal fibres, not

being supported along the transverse direction, are not capable to withstand the axial loads.

1.16.4.6 Basic Certification Activity

(a) The tail rotor blade root section, where failures were experienced, had a demonstrated infinite fatigue life on the basis of the full scale certification fatigue tests, where the critical loading condition for static and fatigue are largely dependent on the application of the centrifugal force and therefore on the start-stop cycle.

(b) As demonstrated during the fatigue test of the original certification, the level of strain associated to the centrifugal force was relatively low (about 3000 με) and not damaging the tail rotor blade root section which failed on the field. However, because of the potential degree of discretion associated to the manufacturing X-Ray inspection applied to the tail rotor blade strap, EASA CA Team concluded that there could be a possibility that tail rotor blades installed on AW139 fleet could contain defects and flaws in excess of those assumed during the static and fatigue tests performed for the certification.

1.16.4.7 Inspection Procedures and Acceptability Criteria – Tail Rotor Blade

(a) As a result of the information shared by QinetiQ, on 4 July 2011, a dedicated meeting was called at ENAC Headquarters in Rome on the tail rotor blade production issues that had been identified. The main conclusion of this meeting was the request to AW to perform a production process review, to assess reliability of production inspections and verifications. In particular, AW was required to perform a review of robustness of X-Ray methodology used for the strap, through a so called "Round Robin" exercise.

(b) With the fatal accident happened on another AW139 helicopter, another meeting was requested on 8 and 13 September 2011 to review with AW the status of production quality and of on-going investigations in the aftermath of the aforementioned accident. The following actions were identified as key factors for reducing the risk of subsequent failure:

i. Review of the contents of the AW technical specification STAP106, in order to verify adequacy of the maximum allowable defects and inspection methods in the light of the occurred in-service events.

ii. An inspection procedure to be established for the in-service tail rotor blades.

iii. Performance of a "health check" internal review of the production inspection records of the in-service tail rotor blade straps. This aimed at identifying any blades that might have been delivered with strap defects in excess of those acceptable per STAP106 as result of assessment variability.

1.16.4.8 Findings of EASA

(a) The following is a summary of EASA's findings from the research and test activities on the AW139 tail rotor blades:

i. The tail rotor blade section where failures occurred is subject to high strain levels through thickness gradient as generated by a bending moment. This bending moment is alternating in nature and generated by the offset of the centrifugal force with respect to the tail rotor blade pitch axis. Figure 72 refers.

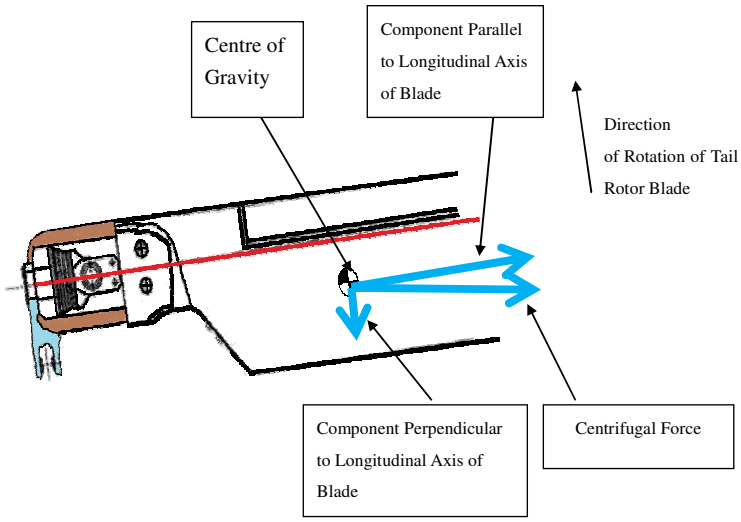

Figure 72 – Bending moment associated with centrifugal force application

ii. Different types of defects can be found in this tail rotor blade section: voids, fibres waviness, filler dislodging/disbond, torsion box defects (thickness reduction, missing plies, disbond).

iii. The inter-laminar shear stress within the tail rotor blade strap, as produced by the bending moment, could be a decisive factor to the strap failure.

iv. Pitch control arm disbond can increase strain in the area of the failure up to 40%.

v. Sub-component fatigue tests highlighted that combination of at least three type of defects play a significant role in determining blade fatigue strength: presence of voids in the straps, torsion box degraded conditions (missing plies), pitch control arm disbonding.

vi. Inter-laminar shear stress (ILSS) fatigue test on AW139 strap indicates that, as result of the Wohler curve shape flatness, small increase in the magnitude of applied stress can significantly reduce the fatigue life for ILSS failure mode.

vii. The combination of more than one defect in the area appears to be necessary to generate the failure.

1.16.5 Bird Strike Resistance

1.16.5.1 The review on tests performed confirmed compliance of the tail rotor blade against bird strike.

1.16.6 Review of the Manufacturing Process by Ente Nazionale per l'Aviazione Civile

1.16.6.1 A number of actions and investigations were initiated by ENAC jointly with AW to fully understand the causes and devise the necessary mitigation actions to ensure the safe operations of the AW139 helicopter fleet. In the frame of the investigation, allowable production discrepancies were identified as one of the main contributing factors to the failures of the AW139 tail rotor blades as experienced in service.

1.16.6.2 After June 2011, a complete review of the tail rotor blade manufacturing process has been carried out by ENAC. Special focus was put on production standards, conformity documents, design data and traceability of production records relevant to tail rotor blades P/N 3G6410A00131 installed on the helicopters that were involved in this and two other similar accidents.

1.16.6.3 Dedicated meetings were held with the participation of ENAC/EASA Project Certification Manager and Structure experts, to review, along with the design characteristics, the production specification and manufacturing process of the composite material tail rotor blades. This review permitted to highlight three elements that, based on the tests and analysis performed, were supposed to be the main contributing factors to the failure pattern:

(a) Manufacturing defects inside the straps (voids, porosity, delaminations and waviness) at the maximum allowable value as a result of the assessment variability.

(b) Torsion box thickness reduction.

(c) Pitch control arm disbonding from the torsion box as this has the potential to cause an increase of the level of strain in the area of the failure.

1.16.6.4 The tests and analysis showed that, the other production issues (under dimensions of the strap cross sections, dislodging of the filler between the two straps), although representing non conformities to the drawings, have no direct effect on the failure pattern. In the light of the above, the ENAC/EASA investigation focused on the following main areas of the production process:

(a) Production records relevant to top and bottom straps.

(b) Conformity of raw material to technical data requirements.

(c) Records relevant to dimensional inspections of top and bottom straps in order to check conformity to approved design data.

(d) Conformity of polymerization process parameters to technical specification requirements.

(e) Non-destructive tests performed on straps which are subject to x-ray inspection to detect delaminations, voids and waviness (also defined as "marcels") during the production process.

(f) Installation and bonding of pitch control arm

1.16.6.5 These activities resulted in the following findings:

(a) Straps:

i. The average production distribution of defects in the straps, in particular voids and waviness, was found to be positioned, very close to the upper limit of the maximum allowable.

ii. The defectology grade, assigned through the X-ray inspection, can be affected by subjectivity assessment method. This was confirmed by the re-evaluation of the X-ray grade carried out on ENAC request, where 100 blade strap X-ray records were re-assessed by AW inspectors not involved in the production.

iii. In the production specification, there was no specific limitation for the presence of combined defects (combination of waviness, porosity and delaminations). In the absence of dedicated instructions and acceptability criteria devised for multiple defects, the quality control inspector allowed, as intended, the maximum acceptable value for each defect.

iv. The maximum allowable defects grade for porosity and marcels was defined for the whole tail rotor handle root region, where a maximum porosity grade of 4 was identified as permissible defect, regardless of any geometrical consideration and presence of marcels, and the blade would have been accepted in production if it had met these criteria.

(b) Torsion box:

i. It was confirmed that its integrity cannot be checked in an effective way after the production phase and therefore required special attention and dedicated production procedures.

1.17 Organisational and Management Information

1.17.1 EAA is the operator of the accident helicopter. AW is the manufacturer of AW139 helicopters. EASA is the authority responsible for the type certification and continuous airworthiness of the AW139 helicopter. ENAC is the authority responsible for the production organization approval of AW139 production facilities.

1.18 Additional Information

1.18.1 During the investigation of the B-MHJ accident, the CAD had become aware of the two similar AW139 helicopter accidents as follows.

1.18.1.1 Accident happened on 2 May 2011 involving a Qatar AW139 Helicopter

(a) The helicopter had just completed the Engine Power Assurance check and was ready for the taxiing phase. The commander heard a loud bang from the back of the helicopter followed by sense of severe vibrations on pedals. The tail rotor detached from the tail fin and dropped on ground. One tail rotor blade was found detached and recovered from about 66 m from the helicopter at about 30° azimuth. A fire ignited in the tail fin upper area. The aircraft engine was shut down and the fire was promptly extinguished by ground personnel. Passenger and crew left the helicopter without any injuries.

1.18.1.2 Accident happened on 19 August 2011 involving a Brazil AW139 Helicopter

(a) During the climb, when the helicopter was passing approximately 1800 ft, the crew declared emergency to the approach control, and then informed that they had a failure in the hydraulic system. Later, the helicopter

crashed into the sea, sustaining severe damage. The four occupants were fatally injured. A tail rotor blade, which was the first piece of wreckage in the line of projection of the flight path, was found at 240 m from the tail rotor assembly. This blade broke between the blade root and the fork, with the remainder of the blade found intact. The tail rotor assembly, the second piece of wreckage found in the line of projection of the flight path, was at a distance of 560 m from the fuselage.

1.18.1.3 Pitch Control Arm Attachment Bolts Preload and Shimming

(a) In the two aforesaid AW139 accidents related to tail rotor blade failure, the investigation has identified issues on pitch control arm attachment bolts preload and shimming. CAD has enquired AW on the following:

i. What would be the effect on the torsion box if one or more of the pitch control arm attaching bolts is/are not shimmed properly such that there is no preload on the bolt(s) to predetermined value?

ii. Would the loss in preload cause any fretting wear on the handle portion, in particular on the inner radii area, and induce excessive stress in that area?

iii. Would the loss in preload act together with the repetitive cyclic load on the radii area to cause delamination during Interlaminar Transverse Stress (ILTS) tests?

(b) Advice from AW was as follows:

i. Improper shimming either under or over shims installation has no relation with the bolt torque (bolt preload). In case of under shimming the bolt preload results in a compression of the blade root area clamped between the bonded pitch control arm and the assembled elastomeric bearing. In case of over shimming there is compression of the interposed shims possibly leaving a gap, depending on the over shimming entity, between the blade root area and the elastomeric bearing. Application of centrifugal force in this condition could result in a pitch control arm de-bonding from the facing root area or

delamination of the underneath interface (pitch control arm blade root) bonded zone of the torsion box.

ii. Wear fretting can result from relative small movements between clamped parts. The condition of clamping could therefore affect the fretting development. With reference to the root inner corner area, wear is expected also to be related to the different stiffness of the blade composite structure and the metallic constraint realized by the elastomeric bearing attachment area causing deformation under loads.

iii. Cyclic loads (high frequency) were measured to be not significant (about 10%). The local stress in the corner area is mainly related to the start stop cycle (low frequency) caused by the centrifugal force. The strap delamination test was performed in accordance with a standard procedure to induce bending in curved composite beams. The test is normally used to define ILTS allowable in composite curved beam. The blade straps failures always occurred just outside of the clamped root area in the curved section where the ILTS is maximum. In this section the root blade strength in relation to the ILTS is mainly dominated by the torsion box integrity and can be affected by local strap manufacturing defects.

(c) As for the effects of a not properly applied pre-load on the four bolts on pitch control arm, EASA Certification Team do not have information to quantify its effect on the vibratory loads and therefore on the interlaminar stresses.

(d) It is noted that preliminary FEM models made by AW nonetheless indicate only a modest increase in longitudinal strain (along fibre direction) in case of a strap not in contact with the elastomeric bearing outer face. A strap not in contact with the elastomeric bearing outer face is believed to represent an extreme condition more severe than that one derived from a not proper application of the pre-load on the four bolts.

1.19 Useful or Effective Investigation Techniques

1.19.1 To allow an in-depth understanding of failure characteristics of the White blade, the Investigation Team had applied the following forensic engineering techniques during the failure analysis of the B-MHJ tail rotor and tail gearbox assembly.

1.19.1.1 Optical Microscope – A type of microscope which uses visible light and a system of lenses to magnify images of small samples.

1.19.1.2 Scanning Electron Microscope (SEM) - A type of electron microscope that images the sample surface by scanning it with a high-energy beam of electrons in a raster scan pattern. The electrons interact with the atoms that make up the sample producing signals that contain information about the sample's surface topography, composition and other properties such as electrical conductivity.

1.19.1.3 Image Analysis - The extraction of meaningful information from images; mainly from digital images by means of digital image processing techniques.

1.19.1.4 3-D X-ray Tomography - A quick and non-destructive method to produce three dimensional images that correspond closely to serial sections through an object. Sequential contiguous images are compiled to create three-dimensional representations that can be manipulated digitally to perform efficiently a large array of measurement and visualization tasks.

1.19.1.5 Differential Scanning Calorimetry (DSC) - A thermoanalytical technique in which the difference in the amount of heat required to increase the temperature of a sample and reference is measured as a function of temperature. Both the sample and reference are maintained at nearly the same temperature throughout the experiment. Generally, the temperature program for a DSC analysis is designed such that the sample holder temperature increases linearly as a function of time. The reference sample should have a well-defined heat capacity over the range of temperatures to be scanned.

1.19.1.6 Burn-off Test – A method to determine the fiber volume of the composites being investigated.

2 ANALYSIS

2.1 Flight Operations

2.1.1 Crew Qualifications

2.1.1.1 The two crew members were properly licenced and qualified to operate the flight.

2.1.2 Crew Medical Fitness

2.1.2.1 The crew conducted the flight in accordance with the Flight Time Limitations Scheme of the operator. The two crew members were in possession of valid medical certificates issued by AACM. There was no evidence to support that the level of physical fitness of the crew members was a contributing factor to the accident.

2.1.3 Operational Procedures

2.1.3.1 The time between the loud bang heard by the pilots and the touchdown of the helicopter on water was about 16 seconds. Taking into account the limited response time allowed for the crew to handle the emergency and the number and the complexity of tasks of the subsequent actions that had to be accomplished prior to the touchdown, the overall outcome of the ditching operation was highly successful. The prompt response of the commander and his skills in controlling the speed and attitude of the helicopter to ensure a controlled ditching deserves compliment. For the issue on the transmission of the Mayday call by the commander, refer to 2.4.

2.2 Weather

2.2.1 The prevailing weather at the time of the accident was generally fine and considered not a contributing factor to the accident.

2.3 Air Traffic Control

2.3.1 The ATS provided is considered adequate and in accordance with established procedures.

2.4 Communications

2.4.1 The aircraft was equipped with the required communication equipment and they were serviceable during the accident flight. Throughout the accident flight, the VHF radios of the commander and the first officer were set to transmit with the FOCC and the Hong Kong Zone Control respectively, thus the Mayday call made by the commander was not received by the latter. This operational practice did not comply with the requirement of Paragraph 4 (Reporting hazardous conditions), Part II, Eleventh Schedule, ANRM.

2.4.2 As the Hong Kong Zone Control did not receive the Mayday call, notification of the accident to other search and rescue units could not be done immediately.

2.4.3 After the accident, EAA had revised the SOP to require that during the significant phase of departure, between take-off and levelling off in the cruise, both pilots should have their respective VHF radio transmission set to the appropriate ATC frequency (COM 1). The action taken by EAA is appropriate.

2.5 Aids to Navigation

2.5.1 The accident flight was operated under Visual Flight Rules, during which the aircraft remained clear of cloud and the pilots maintained visual contact with the surface.

2.6 Aerodrome

2.6.1 Not relevant.

2.7 Aircraft

2.7.1 Aircraft Maintenance

2.7.1.1 The aircraft held a valid Certificate of Airworthiness and was maintained in accordance with AACM regulations. Review of its maintenance history did not identify evidence of overdue items nor significant defects recorded on the tail rotor system.

2.7.2 Aircraft Performance

2.7.2.1 Not relevant.

2.7.3 Mass and Balance

2.7.3.1 The aircraft was operated within both longitudinal and lateral C of G limits and below the MTOW. Weight and balance is considered not relevant to the cause of the accident.

2.7.4 Aircraft Instrumentation

2.7.4.1 Not relevant.

2.7.5 Aircraft Systems

(a) The accident happened with loss of tail rotor in flight leading to loss of yaw control. Hence, the fracture analysis of vertical fin broken parts and the separation of the White blade at the root area became the key elements of this investigation. Unfortunately, the broken portion of the White blade could not be recovered, the investigation team had to rely on the limited evidence from the small portion of the White blade remained and other available wreckage parts.

2.7.5.1 Movement of the White blade

(a) There were marks on the inboard face of the outboard plate of the rotor hub which was resulted from contact with the pitch control arm of the White blade. This indicates a flapping movement of the White blade inboard,

beyond the normal limits of the flap stops. It suggests that a large force had acted on the blade and caused pivoting about the inboard flap stop and further deflection of the elastomeric bearing. The witness marks indicate that the blade was in a lag position when it came in contact with the plate and was rotating in the lead-lag plane.

(b) The elastomeric bearing was found to be deflected, with the pitch control arm lodged against the White damper attachment bracket. This indicates that the White blade had rebounded in the lead direction.

(c) The fractures of the White blade straps on the leading edge side were long and fibrous, indicating that they had failed in a primarily tensile mode. The fractures on the trailing edge were flatter and exhibited a combination of tension and compression failures. The evidence is consistent with the blade tip moving in lag direction and flapping inboard, until contact of the blade root with the rotor hub.

(d) The overall impression is that the blade was subjected to a significant force in the lag direction and towards the inboard surface. This is consistent with the witness marks noted on the tail rotor hub.

2.7.5.2 Damages on Other Tail Rotor Blades and Y9 Control Rod

(a) The scratches on the surface of the Yellow and Red blades are believed to be the result of the secondary damage when they cut through the trailing edge of the right side tail plane whilst still rotating, after the tail gearbox attachment structure had parted from the vertical fin.

(b) The impact marks on the Y9 tail rotor pitch control rod are consistent with contact with one or more of the rotating tail rotor blades.

(c) The impact damage to the tip of the Blue blade and the deformation of the nickel erosion strip on the leading edge indicates an impact with a relatively hard object. Other cracks and damage noted in the over-wrap layer are consistent with bending in the lag plane and torsion, resulting from the impact at the tip, and consequent local buckling of blade skin material in the mid-section. The bending of the Blue blade damper rod end was not as great as on the White blade damper and there was no impact mark on the

hub centre; indicating that the lag movement on the Blue blade was of lesser magnitude than that of the White blade.

2.7.5.3 Build Quality of Tail Rotor Blades

(a) The examination of the samples of the Blue blade, Yellow blade and the remaining portion of the White blade indicates that these blades did not comply fully with AW's specifications in the root end area. Manufacturing discrepancies including undersize and high level of voids of the upper and lower straps of the blade samples were identified. Also, reduction of torsion box thickness was also noted from the remaining portion of the White blade. The discrepancies found were not in conformity with the manufacturing specifications published by AW. Also, disbond of pitch control arm was also noted. AW commented that the periodic destructive tests required for quality assurance verification by STAP 106 did not include this area, because it was considered not relevant as the area was clamped between metal parts.

(b) In light of the findings, CAD considered that the manufacturing process of the AW139 tail rotor blades should be reviewed. Also, further static, fatigue, dynamic and aerodynamic tests and analyses would be required to determine the cause of the breakage of the White blade and the subsequent detachment of the tail rotor and tail gearbox assembly. The performance of these review, tests and analyses would require reference to proprietary and confidential manufacturing, design and certification data of AW139 helicopters which are maintained by AW (the manufacturer of AW139 helicopters), ENAC (the Competent Authority responsible for the Production Approval of AW) and EASA (the Type Certification Authority of AW139 helicopters), and beyond the access of CAD. Safety Recommendation 2011-3 and Safety Recommendation 2011-4 were therefore issued to ENAC and EASA respectively on 21 November 2011.

(c) In addressing the two Safety Recommendations and also upon the request of CAD, ENAC, EASA, and AW have provided reports and relevant information to support the completion of the investigation by CAD.

2.7.5.4 Supplementary Examination of the Fractured White Blade

(a) During the supplementary examination of remaining portion of the fractured White blade, the X-ray tomography data has identified two manufacturing defects which are of technical significance:

i. A reduction in the number of the ±45° layers within the GFRC torsion box on the internal radii of the trailing edge arm of the blade in the corresponding locality of the fracture observed on the White blade. Evidence of cut plies indicates that structural material had been removed, possibly by a machining operation. At the inner corner radii of the inboard strap, cut fibre ends on the GFRC torsion box plies were observed, which could potentially initiate delamination. The missing structural material of the torsion box had been replaced by a resin applied to the inner surface of the blade root.

ii. There was a 'pinch' point (associated with fibre ply waviness) in the outer plies of ±45° GFRC torsion box on the trailing edge side of the blade adjacent to the horn of the pitch control arm attachment bracket. The crest of the pinched layers had been removed, severing the outer plies and exposing the plies to potential delamination.

(b) These manufacturing defects occurred in locations very close to the horn of the pitch control arm on the bottom (inboard) trailing edge. This also corresponds to the location of maximum bending moment at the blade root radii area.

(c) Further sectioning of the White blade revealed the presence of delaminations within the bottom (inboard) trailing edge strap. Fractographic examination of the delaminated surfaces indicates that fretting due to cyclic shear loading had occurred. In a few areas, striations which are features of fatigue, were also observed.

2.7.5.5 Joint Review of Tail Rotor Blade Investigation Findings by EASA/ENAC

(a) The joint review by EASA/ENAC on the tail rotor blade investigation findings has identified three elements that are the main contributing factors to the failure:

i. Manufacturing defects inside the straps (waviness, porosity and delaminations) at maximum acceptable values as a result of the assessment variability.

ii. Torsion box thickness reduction.

iii. Pitch control arm disbonding caused by over shimming of elastomeric bearing installation and manufacturing quality lapses as this have the potential to cause an increase in the level of strain in the area of the failure.

iv. The failure analysis of the remaining portion of the White blade has identified evidence relevant to these three elements (i, ii. and iii).

(b) The join EASA/ENAC review also identified the following significant findings:

i. Other production issues (under dimensions of the strap cross sections, dislodging of the filler between the two straps), although representing non conformities to the drawings, had no direct effect on the failure pattern.

ii. In the production specification of the straps, there was no specific limitation for the presence of combined defects (combination of waviness, porosity and delaminations).

iii. The integrity of the torsion box cannot be checked in an effective way after the production phase.

2.7.5.6 Load Survey During Original Certification of AW139

(a) According to EASA, specific measurement of strain and stress on the tail rotor blade root handle was not performed in the load survey of the original certification of the helicopter. This was justified by the results of some initial flights where a tail rotor blade root handle partially instrumented did not show any specific critical values of strain and stress.

The most stressed location was the transition area of the blade where flight bending moments were maximum.

(b) Subsequent to this and another similar AW139 accident, AW had carried out a new in-flight blade strain-stress/load survey on the failure area of the tail rotor blade. While confirming the criticality of the blade transition area defined by the original certification of the helicopter, the new strain-stress/load survey allowed to appraise the strain comparability between the root and transition area while confirming the original criticality assessment. It also identified that the strain levels along trailing edge bottom strap thickness were not uniformly distributed, varying from high tension value on the inner side to low compression on the outer side (local bending).

2.7.5.7 Bending Loads on Tail Rotor Blade Root

(a) Bending loads measurement on another AW139 helicopter indicated a localised bending moment acting on the blade root handle in the lag direction. This bending moment is alternating in nature and generated by the offset of the centrifugal force with respect to the tail rotor blade pitch axis. Three possible causes are considered relevant:

i. Loads during start-up and shut-down. The blades tend to droop when stationary and will tend to bend in the lag direction during acceleration with no dominant centrifugal force initially.

ii. There will always be a tendency to bend in the lag direction as a result of the drag of the blade versus the driving torque. The drag will increase with the increase in pitch.

iii. When at full speed, the centrifugal loads will tend to straighten the curve in the blade root handle structure with a resultant bending moment in the lag direction.

2.7.5.8 Bending Stiffness at Tail Rotor Blade Root

(a) The chord bending stiffness of the tail rotor root handle is mainly provided by the torsion box that contributes 65% of the overall bending

stiffness. The remaining 35% of the bending stiffness is provided by the straps and the root filler.

(b) With the reduced thickness of torsion box, cuts of the plies and pinched plies found, the bending stiffness of the White blade at the blade root area would have been lowered. Moreover, delamination formed within the straps and the fatigue fretting of the fibres in the matrix would also reduce the bending stiffness.

2.7.5.9 Interlaminar Failure Mode

(a) As determined by EASA and AW, there is a matrix interlaminar failure mode driven by the stresses associated with the application of a bending moment at the tail rotor blade trailing edge handle generated by the offset of the centrifugal force with respect to the tail rotor blade pitch axis. If the torsion box is damaged, the bending stiffness at the blade root area would be lowered.

(b) The FEM model devised for the investigation confirmed the correlation between chord bending stiffness and magnitude of the radial and shear stresses (i.e. the lower the chord bending stiffness the higher the magnitude of the stresses). It also confirmed that, under the most critical loading condition and in the presence of macroscopic defects such as reduction of the torsion box thickness and disbond of the pitch control arm, it was possible that the magnitude of the ILRS would exceed the maximum allowable limit and cause a delamination onset (Open MODE I) in the curved area of the tail rotor root handle, i.e. blade root radii area. Delamination could then grow and propagate due to ILSS (Shear MODE II). The combination of the above failure modes (ILRS and ILSS) could lead to possible subsequent multiple delamination in the blade root radii area, through the complete thickness.

2.7.5.10 Failure of White Blade

(a) The broken off section of the White blade could not be recovered. The investigation team had to rely on the limited evidence from the remaining portion of the White blade and other available wreckage parts for the determination of the most probable cause of the accident.

(b) Disbond of pitch control arm and reduction in bending stiffness caused by thickness reduction of torsion box, cuts of plies and pinched plies were evident from the remained portion of the White blade. Also, manufacturing defects (waviness, porosity and delamination) at the maximum acceptable values in the production specification were evident inside the straps. The combined effects of these discrepancies would have caused the ILRS at the blade root radii area to exceed the maximum allowable limit, resulting in matrix delamination onset (Open MODE I). The delamination then grew and propagated when ILSS exceeded the fatigue allowable limit (Shear MODE II), resulting in complete matrix degradation that would have left the strap fibres unsupported and the complete failure of the blade.

2.7.5.11 Fracture Failure of Vertical Fin

(a) Visual examination of both fractured sections of the vertical fin identified considerable deformation, which is characteristic of overload failures. Most of the fracture surface was dull, fibrous and angled at 45° to the sheet surface, which are typical features of overload in thin sheet material.

(b) The failure of the White blade at trailing edge bottom strap led to tail rotor imbalance. The vertical fin structure was then subjected to a load of magnitude high enough to part off the section connecting the tail rotor assembly, ie, static overload. This was the most likely failure mechanism as there was no evidence of progressive crack growth, such as fatigue, observed at the fracture surfaces. Due to the thrust generated by the tail rotor, the tail rotor departed in a starboard direction from the vertical fin. With the detachment of the tail rotor, the helicopter lost its directional control.

2.7.5.12 Detachment of Aircraft Parts

(a) The left-hand nose window transparency panel on the forward fuselage the two vent air scoops at the bottom rear fuselage were found detached after the accident. Their detachment can be explained by considering

the structural ditching provisions of JAR 29.563 and the attitude of the helicopter at the point of ditching.

(b) During type certification of the AW139 helicopters, compliance with JAR 29.563 had been demonstrated by the helicopter manufacturer. At the point of ditching, the helicopter fuselage shall sustain a structural load resulting from a forward velocity of 50 km/h (30 kt) and a vertical decent velocity of 1.5 m/s without failure.

(c) The ground speed and vertical descent velocity of the helicopter recorded by the MPFR at the point of ditching were 24 kt and 2.76 m/s respectively. While the ground speed was within the limit of 30 kt prescribed by JAR 29.563, the vertical descent velocity was 1.84 times greater than the prescribed limit of 1.5 m/s. Due to the exceedance in vertical descent velocity, some form of structural damage resulting from impacting with water can be expected and in this case, the loss of the left-hand nose window transparency panel and the break off of the two vent air scoops. Also, the MPFR recorded that the helicopter banked to the left by 6.5 degrees at the point of ditching. This made the left-hand nose window transparency panel mounted on the left forward bottom fuselage more exposed to impact damage.

2.8 Survivability

2.8.1 Passenger Evacuation

2.8.1.1 With the supervision of the commander and the assistance of the first officer, the emergency evacuation was conducted in a timely manner without delay, allowing all the passengers to evacuate from the helicopter before it capsized in about 18 minutes after ditching.

2.8.2 Search and Rescue

2.8.2.1 Within one minute of the accident, a member of the public made an emergency '999' call to report the accident to RCCC HK who then immediately notified RCCC MAR and FSCC. All these emergency services had taken immediate

action and rescue vessels deployed had arrived on scene promptly to assist the rescue operation. FSCC had also notified the accident to CAD.

2.8.2.2 The accident site is located in a busy part of the Victoria Harbour, easily accessible by marine vessels and fishing boats nearby. Therefore, most of the persons onboard the helicopter had been rescued by the Fishing Boat and Harbour Pilot Boat operating nearby before the arrival of the emergency services vessels.

2.8.2.3 Overall, the emergency response and level of attendance of the emergency services were considered efficient. Despite the absence of immediate notification by the pilot in distress, the provision of alerting service by ATS units was in order.

2.8.3 Emergency Flotation System

2.8.3.1 The emergency flotation system kept the helicopter afloat for 18 minutes, allowing sufficient time for the evacuation of all persons onboard. The performance of the helicopter and the associated emergency flotation system met the certification requirement of JAR 29.801(d).

2.8.3.2 Although the sea conditions were compatible with the certification of the equipment, the helicopter was significantly out of balance after ditching due to the loss of the tail rotor and the tail fin section and the ingress of water into the cabin through the opening left behind by the lost left-hand nose window transparency. The out of balance condition subsequently resulted in the overload and damage of the two forward floatation bags.

2.8.3.3 The exact sequence of the failure of the floatation bag could not be determined. However, the probable scenario was that the bonded patches and buck bag detached from the floatation bag. At about the same time of or soon after the detachment, the loss of stability and positioning of the floatation bag against the fuselage caused the longitudinal webbing to work improperly and subsequently failed. Tension then built up on the inflation hoses connected to the Inflate (Swivel) Valves which eventually caused the latter to tear from the floatation bag.

2.8.3.4 The disbonding of the patches which integrate the Kevlar loops from the floatation bag indicates that the bonding in the failed areas were less effective than those of other intact areas. The reduced bonding effectiveness between the patches and the floatation bag can be explained by a low degree of adhesive polymerization caused by a lower level of heat application under the tapes when the patches were adhered to the floatation bag. The failure at coating-to-weave interface suggests a continuity of the coating achieved during the bonding process with proper application of adhesive. The stitching was the weakest line during initial separation and allowed the propagation of the failure along the tapes. This phenomenon, in combination with the reduced effectiveness of the bonding under the tapes, could lead to the failure of the connection between the floatation bag and the structure.

2.8.3.5 The disbonding of the buck bag from the floatation bag was due to the failure of the bonded areas, similar to the failure of the bonded patches on the floatation bags. The failure of the stitching on the longitudinal ribbon is probably the consequence of the reduction and/or loss of stability of the floatation bag when the connection between the floatation bag and the pod failed due to the patch detachment or the buck bag failure. As a result of the detachment of the patch from the floatation bag, transversal loads were applied on the ribbon which subsequently caused the stitching of the ribbon to fail.

2.8.3.6 AW has confirmed that Aero Sekur S.p.A, the float manufacturer has incorporated modifications to improve the AW139 Emergency Floatation System based on the findings of this investigation.

2.8.4 Passenger Life Jacket

2.8.4.1 After the accident, a total of 12 passenger life jackets were recovered, either from the rescue operation or from the cabin of the helicopter. The number is equal to the maximum number of passengers certified to be carried by the helicopter. Therefore, the number of passenger life jackets onboard was adequate.

2.8.4.2 The assessment done by the investigation team on all the twelve installed passenger life jackets based on the requirement of JAR 29.1411(f) Life Preservers did not identify any difficulty in accessibility.

2.8.4.3 The two passengers interviewed by the investigation team had complained on the difficulty in opening the life jacket valise. The investigation team and the life jacket manufacturer had conducted respective test on the tearing strip of life jacket S/N 14621-130 and S/N 14621-125 recovered from the cabin of the helicopter. Both the investigation team and the life jacket manufacturer could not establish similar difficulty encountered by the two passengers. During the interview, one passenger recalled that the life jacket was in a white bag with Velcro on top and he found it very difficult to rip off the Velcro from the bag. Based on his information, it is most probable that the passenger had pulled the Velcro tape instead of the tear strip when attempting to open the valise.

2.8.4.4 Passenger life jackets S/N 14621-125 and S/N 14621-130 had detached from their stowage position under the seat pane and dropped to the cabin floor. However, the investigation team could not determine if the detachment occurred before or after the accident since the helicopter had sustained an impact force at the time of ditching.

2.8.4.5 Investigation of passenger life jacket SN 14621-125 found a tear on the valise. However, whether the tear was made as a result of the removal of the life jacket from its stowage position or was made erroneously by someone trying to open the valise at a later stage could not be ascertained.

2.8.4.6 The operator performed daily inspection of the passenger life jackets in accordance with the requirement of the AMS approved by AACM. Every inspection required the removal of the life jackets and then reinstallation afterwards, through respective unlatching and latching of the Velcro tapes. In a standard installation offered by the helicopter manufacturer, the lifejacket is stowed as a standalone unit inside a container attached to the bottom of the seat pane without the use of Velcro tape.

2.8.4.7 There was no evidence of AACM approval for the modification of the passenger life jackets with Velcro tape glued on jacket valise, indicating that the integrity of the modification might not have been assessed by the authority. After the accident, AACM had conducted a thorough review with EAA on the stowage method of the life jackets and subsequently approved the modification for the relocation of passenger life jacket stowage position.

2.8.5 ADELT

2.8.5.1 After ditching, the transmitted 406 MHz signal was picked up by the COSPAS/SARSAT distress alerting system. The ADELT had performed as per the design of the equipment.

2.8.5.2 Since the ADELT was recovered from a point in close proximity to the helicopter, its recovery position can be taken as the ditching position of the helicopter. The difference in Latitude and Longitude between the encoded position of the ADELT picked up by the COSPAS/SARSAT distress alerting system satellite and the ditching position of the helicopter was 1 minute and none respectively. This is within the encoded position uncertainty of plus or minus 4 minutes of Latitude and Longitude of the ADELT, thus the performance of the ADELT was within the design tolerance of the equipment.

2.8.6 Injuries to Passengers

2.8.6.1 Six of the eleven passengers required medical treatment such as arm bruise or dizziness. The injuries are considered minor.

3 CONCLUSIONS

3.1 Findings

3.1.1 Crew

3.1.1.1 The two crew members were properly licensed.

3.1.1.2 The two crew members were medically fit to perform their duties at the time of the accident.

3.1.1.3 The prompt response of the commander and his skills in controlling the speed and attitude of the helicopter contributes to a controlled touchdown of the helicopter during ditching operation.

3.1.1.4 The commander transmitted the Mayday call to the FOCC, not the Hong Kong Zone Control. This practice did not comply with the ANRM with regard to report of hazardous conditions.

3.1.2 Aircraft

3.1.2.1 The helicopter held a valid Certificate of Airworthiness and was properly equipped and maintained in accordance with AACM regulations.

3.1.2.2 The examination of the samples of the Blue blade, Yellow blade and the remaining portion of the White blade indicates that these blades did not comply fully with AW's specifications in the root end area. Manufacturing discrepancies including undersize and high level of voids of the upper and lower straps of the blade samples were identified.

3.1.2.3 Reduction of torsion box thickness and disbond of pitch control arm were also noted from the remaining portion of the White blade. The periodic destructive tests required for quality assurance verification by STAP 106 did not include this area, because AW considered them not relevant as the area was clamped between metal parts.

3.1.2.4 Supplementary examination of the fractured White blade found reduction of torsion box thickness and disbond of pitch control arm. Also, cut plies and 'pinch' point, which could potentially initiate delamination, were also found.

3.1.2.5 Fractographic examination of the delaminated surfaces of the fractured White blade identifies evidence of fretting due to cyclic shear loading. In a few areas, striations which are features of fatigue were also observed.

3.1.2.6 The joint EASA/ENAC review of the tail rotor blade investigation findings identified three elements that are main contributing factors to the tail rotor blade failure, namely, manufacturing defects inside the straps at the maximum allowable value, torsion box thickness reduction, and pitch control arm disbond possibly caused by over shimming of elastomeric bearing installation.

3.1.2.7 The joint EASA/ENAC review identified that under dimensions of the strap cross sections and dislodging of the filler between two straps, although representing non conformities to the drawings, had no direct effect on the failure pattern of the tail rotor blades.

3.1.2.8 The joint EASA/ENAC review identified that in the production specification of the straps, there was no specific limitation for the presence of combined defects (combination of waviness, porosity and delamination). Also, the integrity of the torsion box cannot be checked effectively after the production phase.

3.1.2.9 The in-flight strain-stress/load survey performed on an AW139 tail rotor blade after the accident confirmed the criticality of the blade transition area defined by the original certification of the helicopter. It also identified that the strain levels along trailing edge bottom strap thickness were not uniformly distributed, varying from high tension value on the inner side to low compression on the outer side (local bending).

3.1.2.10 Reduced thickness of torsion box, cut plies and pinched plies, delamination within straps and fatigue fretting of the fibres in the matrix would reduce the bending stiffness of the White blade.

3.1.2.11 Reduction of torsion box stiffness and disbond of pitch control arm of the blade, when associated with manufacturing strap defects at maximum acceptable values in the production specification, would have caused the ILRS at the blade

root radii area to exceed the maximum allowable limit resulting in matrix delamination onset (Open Mode I).

3.1.2.12 The delaminations grew and propagated when the ILSS exceeded the fatigue allowable limit (Shear Mode II), resulting in matrix complete degradation that would have left the fibers unsupported and the complete failure of the trailing edge bottom strap of the White blade.

3.1.2.13 The failure of the White blade led to tail rotor imbalance that caused static overload of vertical fin structure at magnitude high enough to part off the section connecting the tail rotor assembly. With the loss of the tail rotor assembly, the helicopter lost its directional control.

3.1.2.14 The exceedance in vertical descent velocity of the helicopter corresponding to the design conditions required by JAR 29.563 and the banking left of the helicopter by 6 degrees at the point of ditching could have caused the loss of the left-hand nose window transparency panel and the break off of the two vent air scoops.

3.1.3 Survivability

3.1.3.1 The emergency evacuation was conducted in a timely manner without delay, allowing all the passengers to evacuate from the helicopter before it capsized in about 18 minutes after ditching.

3.1.3.2 The provision of alerting service by ATS units was in order. The emergency response and level of attendance of the emergency services were considered reasonably efficient.

3.1.3.3 The Emergency Floatation System performed as per design and met the certification requirement of JAR 29.801(d).

3.1.3.4 The helicopter was significantly out of balance after ditching, due to the loss of the tail rotor and the tail fin section and the ingress of water into the cabin through the opening left behind by the lost left-hand nose window transparency. The out of balance condition subsequently resulted in the overload and damage of the two forward floatation bags.

3.1.3.5 The number of passenger life jackets onboard was adequate. The assessment on all the twelve passenger life jackets confirmed that the accessibility met the requirement of JAR 29.1411(f).

3.1.3.6 The investigation could not establish difficulty in opening the passenger life jacket valise as encountered by the two passengers interviewed by the investigation team.

3.1.3.7 There was no evidence of AACM approval for the modification of passenger life jacket (Part Number A312305A01RFD and Model Number MK 20 SV) with Velcro tape glued on jacket valise.

3.1.3.8 The ADELT had performed within the design tolerance of the equipment.

3.2 Causes

3.2.1 Causal Factors

3.2.1.1 The failure of the White blade was most probably caused by disbond of pitch control arm and the reduction of torsion box stiffness at the blade root radii area, which when associated with manufacturing strap defects at maximum acceptable values in production specification, caused the ILRS to exceed the maximum allowable limit, resulting in matrix delamination onset and then propagation under ILSS and complete failure of the blade. (Reference: 3.1.2.2, 3.1.2.3, 3.1.2.4, 3.1.2.5, 3.1.2.6, 3.1.2.10, 3.1.2.11, 3.1.2.12)

3.2.1.2 The reduction in torsion box stiffness at the White blade root radii area was most probably caused by manufacturing quality lapses and the lack of effective way for checking the integrity of the torsion box after production. (Reference: 3.1.2.4, 3.1.2.8)

3.2.1.3 Disbond of the pitch control arm could have been caused by over shimming of elastomeric bearing installation. (Reference: 3.1.2.6)

4 SAFETY ACTIONS AND SAFETY RECOMMENDATIONS

4.1 Safety Actions

4.1.1 Safety Actions Taken by AW

4.1.1.1 Aircraft Inspection

(a) On the basis of available evidence, including witness reporting of possible bird strike event, related to the AW139 accident happened in Hong Kong Victoria Harbour, no corrective actions on the helicopter fleet had been considered necessary by AW.

(b) After the accident happened on 2 May 2011 involving a Qatar AW139 helicopter of registration marks A7-GHA, immediate corrective action was undertaken by AW with the issue of Service Bulletin (SB) BT139-251 requiring a detailed visual inspection within 25 hours on the visible portions of the tail rotor blade root with no removal required for blades having logged at least 600 hours. The same SB introduced also a visual and hammer check after tail rotor elastomeric bearing removal within the 25 hours for blades having logged at least 1,200 hours. Detailed visual inspection and hammer tapping check had to be repeated every 25 flight hours and 600 flight hours respectively. The SB was endorsed by EASA AD 2011-0081. The result of compliance of the AD 2011-0081 by operators worldwide showed about 64% of the inspected blades without fault found while the remaining 36% of the inspected blades were discrepant with 34% of which with repairable damages, either at field or in workshop. The remaining blades have been scraped from service as repair was not feasible typically due to the closeness of the composite damages to the metallic parts precluding the application of composite patches of adequate dimensions.

(c) After the fatal accident happened involving a Brazil AW139 helicopter of registration PR-SEK on 19 August 2011, EASA issued AD 2011-0156-E immediately to mandate SB BT139-265 to require the quarantine of tail rotor blades with more than 600 hours or 1,500 landings whichever comes first.

4.1.1.2 Production Specification

(a) Improvement to Production Specification was immediately consolidated, through the issue of an Engineering Technical Instruction in advance to the formal production documentation implementation, on the following topics that affect tail rotor blade strength:

i. Strap X-Ray improvement procedure (lateral view) and assessment (double check).

ii. Automatic straps dimensional check and recording, visual inspection for strap surface defect identification.

iii. Grade reduction for coalescent defects in the same area, separations are not allowed.

iv. Absence of separation verified by transmission Ultrasonic Technique.

v. Present fluoroscopy replaced by X-Ray continuous inspection capable to identify the root filler dislodging.

vi. Root filler dislodging precluded by root filler and filler support pre-bonding.

vii. Proof test followed by Ultrasonic Technique to further exclude weak bonding lines.

viii. Improvement of destructive test through increase in frequency of periodic test, parts dimensions and correct positioning, lower minimum value of ILSS, additional ILSS coupons for strap-torsion box interface, allowable defects reduction in the blade root area and peel test on the pitch control arm bonding.

4.1.1.3 Tail Rotor Blade Configuration Improvement

(a) AW has introduced in service an improved blade configuration, identified by a different Part Number (P/N) 3G6410A00133, providing same fit, form and function. The updated configuration includes an additional

load path in the blade root area that incorporates a carbon fiber root strap replacing the present non-structural root filler. The configuration is certified fully restoring the original tail rotor blade safe life.

4.1.2 Safety Actions Taken by EASA

4.1.2.1 Risk Mitigation Measures

(a) At the conclusion of a meeting with AW on 8-13 September 2011, EASA identified the following main actions as key factors for reducing the risk of subsequent failure:

i. Review of the current contents of the STAP106, in relation to the maximum allowable defect and inspection criteria in the light of the occurred in-service events.

ii. Inspection procedure to be established for the in-service tail rotor blades.

iii. Performance of a "health check" internal review of the production inspection records of the in-service blade straps, aiming at identifying any blades that might have been delivered with strap defects in excess of those acceptable per STAP106 as result of possible variability related to the comparative radiographic assessment.

iv. Statistical analysis of the in-service occurrences, to confirm the quarantine interval of 1500 flight cycles / 600 flight hours taking into account the flight cycle accumulated by the blade failure in the Brazilian AW139 accident.

4.1.3 Safety Actions Taken by ENAC

4.1.3.1 New Production Specification

(a) As a result of the review of the manufacturing process, a number of actions were undertaken by AW in agreement with ENAC to improve the production quality standard and to minimize the uncertainty in the control of the manufacturing process, leading to a new production specification

that became effective for all the blades manufactured from 2 December 2011 onwards.

(b) The new production specification included a number of changes, all aimed at reducing the level of defectology and improving the effectiveness of the inspections performed as part of the production process.

(c) The main changes consist of:

i. Strap X-ray improvement procedure.

ii. Strap maximum allowable combined defect criteria for acceptance of multiple defects defined.

iii. Presence of separations in the straps not allowed.

iv. Changes devised to detect torsion box thickness reduction due to manufacturing problems and/or separations from the straps. A new procedure has been implemented by AW, requesting the check for accidental removal of the external torsion box layer after the machining re-working.

v. Improved non-destructive inspection techniques have been introduced throughout the production process together with more detailed data recording of the results of the tests performed.

vi. Visual inspection for strap superficial defects identification.

vii. Dimensional width and height check at ten locations along the straight and curved sections of each strap and on eight locations of the complete blade after curing of the external torsion box lay-up.

viii. Root filler bonding to strap filler in order to avoid its possible displacement and ensure the correct position during successive lay-up and curing phases.

ix. X-ray inspection to check the correct position of the root filler with respect to the strap support.

x. Frequency of the periodic destructive tests increased and integrated with additional coupons to assess interlaminar shear properties between strap and torsion box.

xi. Introduction of pitch control arm bonding verification during the periodic destructive test.

4.1.3.2 Risk Mitigation Measures

(a) A risk mitigation strategy was put in place to address the continued airworthiness of the AW139 fleet. This strategy was agreed with EASA and was continuously monitored throughout the time to verify its effectiveness taking into account the results of the on-going tests at AW facilities and availability of the results of investigations.

4.1.4 Safety Actions Taken by AACM

4.1.4.1 On 29 Nov 2013, AACM advised CAD that the following safety actions had been taken by the authority after the accident.

(a) AACM noted the importance of having a floatation system and life jackets on a helicopter flying over water in the case of mishap, the authority has amended the ANRM in 2011 to mandate the equipage of life jackets and floatation system for helicopters taking off or landing at a heliport where the take-off or approach path is disposed over water.

(b) Noting that the modification to the life jackets was not properly approved, AACM has conducted a thorough review with EAA on the stowage method of the life jackets. EAA subsequently submitted a modification for "Relocation of passenger life jacket stowage position" to AACM for approval on 4 April 2011. This modification was approved by AACM on 29 April 2011.

4.2 Safety Recommendations

4.2.1 Interim Recommendations

(a) During the investigation, CAD has made the following two Safety Recommendations.

4.2.1.1 Safety Recommendation 2011-3

(a) The following Safety Recommendation 2011-3 was sent to ENAC on 21 November 2011:

Ente Nazionale per l'Aviazione Civile, jointly with AgustaWestland, to review the manufacturing process of the AW139 tail rotor blades to determine the causes of the discrepancies identified in the QinetiQ Report and evaluate their effects.

(b) ENAC replied by fax to CAD on 29 March 2012, with which attached a report titled "ENAC Position on Hong Kong Safety Recommendation No. 2011-03". The actions taken were summarized as follows:

i. Complete review of the manufacturing process of AW139 tail rotor blades.

ii. Review the production specification and manufacturing process of composite tail rotor blades with EASA, along with design characteristics.

Note: For details of these actions, refer to Section 1.16.6.

4.2.1.2 Safety Recommendation 2011-4

(a) The following Safety Recommendation 2011-4 was sent to EASA on 21 November 2011:

European Aviation Safety Agency to require AgustaWestland to perform static, fatigue, dynamic and aerodynamic tests and analyses on AW139 tail rotor blades so as to minimize the possibilities of tail rotor blade

failure which could have been caused by one or the combination of these effects.

(b) EASA replied by fax to CAD on 29 March 2012, with which attached the "EASA Safety Recommendation Reply". The actions taken were summarized as follows.

i. Temperature survey.

ii. In-flight blade strain-stress/load survey.

iii. Full scale fatigue tests and static test survey.

iv. Blade Dynamic Stability Evaluation.

v. Finite Element Method model analysis of the blade root area.

Note: For details of these actions, refer to Section 1.16.4.

4.2.2 Implementation of Safety Recommendations

4.2.2.1 ENAC and EASA, along with AW, have taken necessary safety actions on Safety Recommendation 2011-3 and Safety Recommendation 2011-4 respectively. All the safety actions have been accomplished and no further safety actions are envisaged.

Appendix 1

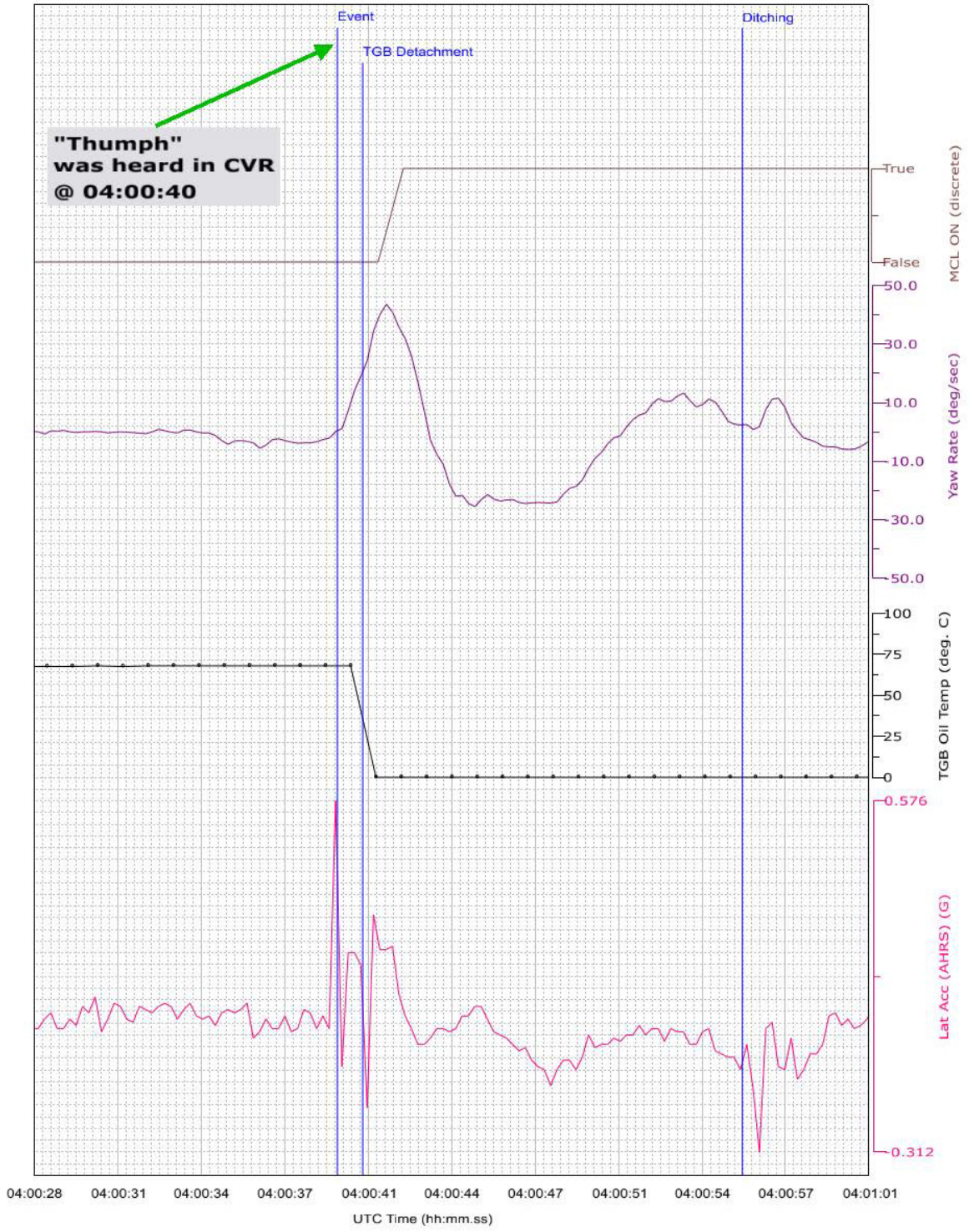

MPFR Data Showing Abrupt Changes in Lateral Acceleration, Yaw Rate and TGB Oil Temperature

Appendix 2

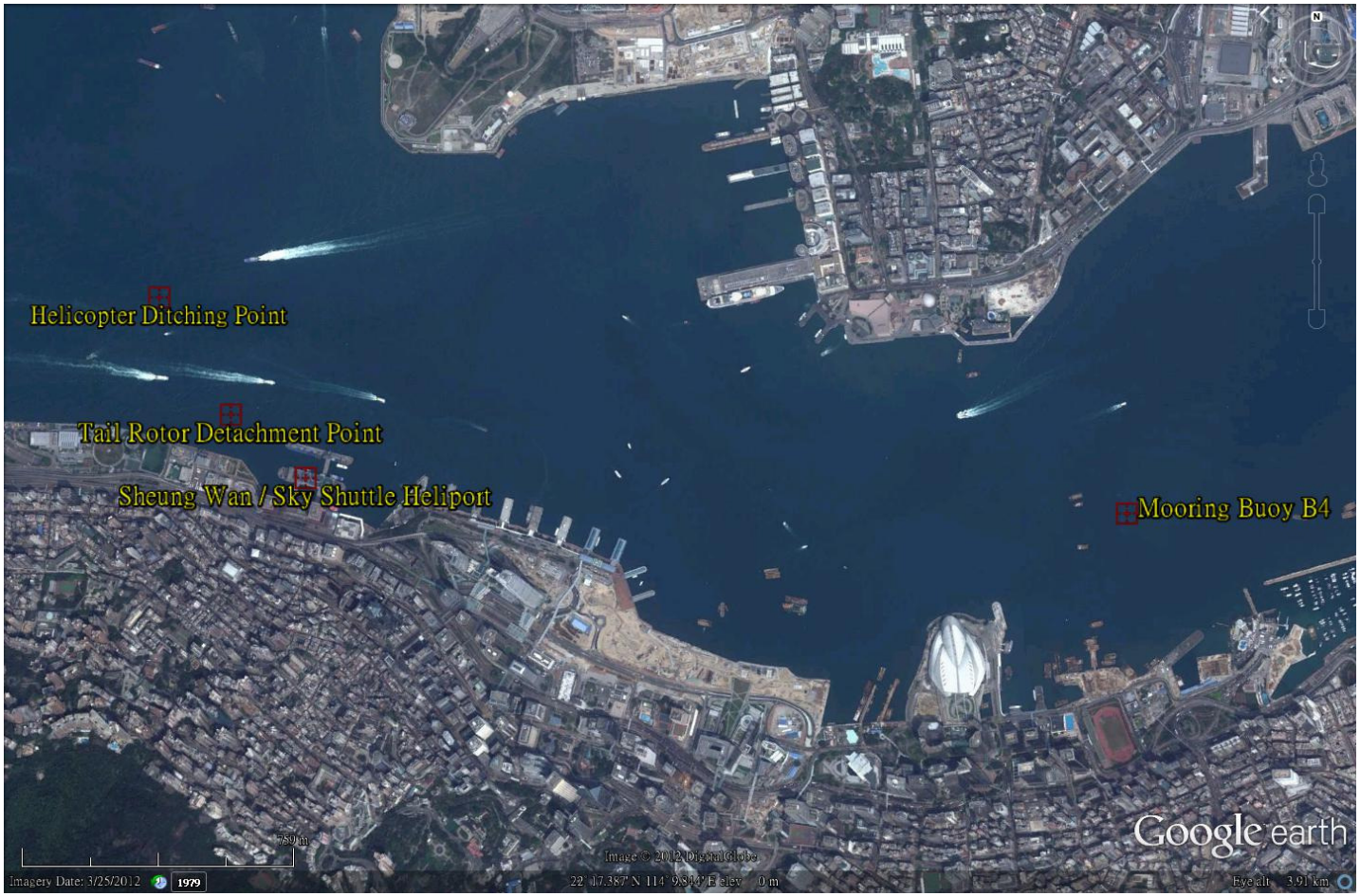

Map showing take-off, accident, ditching and mooring locations of B-MHJ

Findings of Supplementary Examination of the White Blade

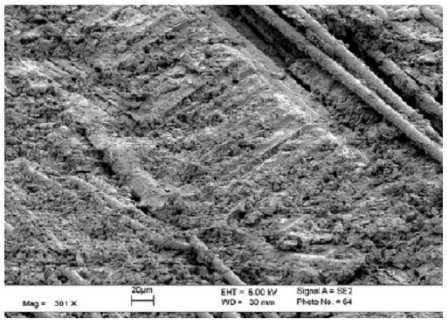

Delaminated surface (sample FE1084) within ±45º "pinched" ply showing fretting (*Fig.68*)

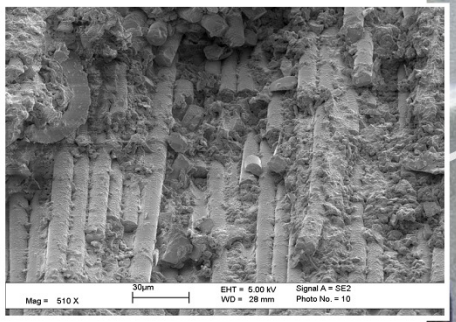

Delaminated surface (sample FE1084) within 0º strap showing close-up view of fretting debris (*Fig.62*)

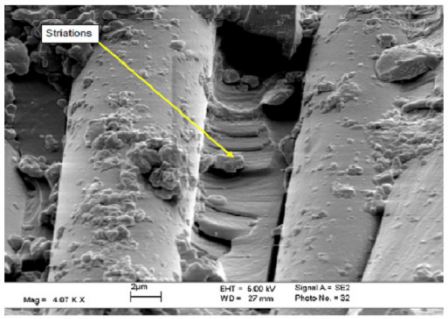

Delaminated surface (sample FE1084) within 0º strap showing close-up view of fretting debris and striations (*Fig.64*)

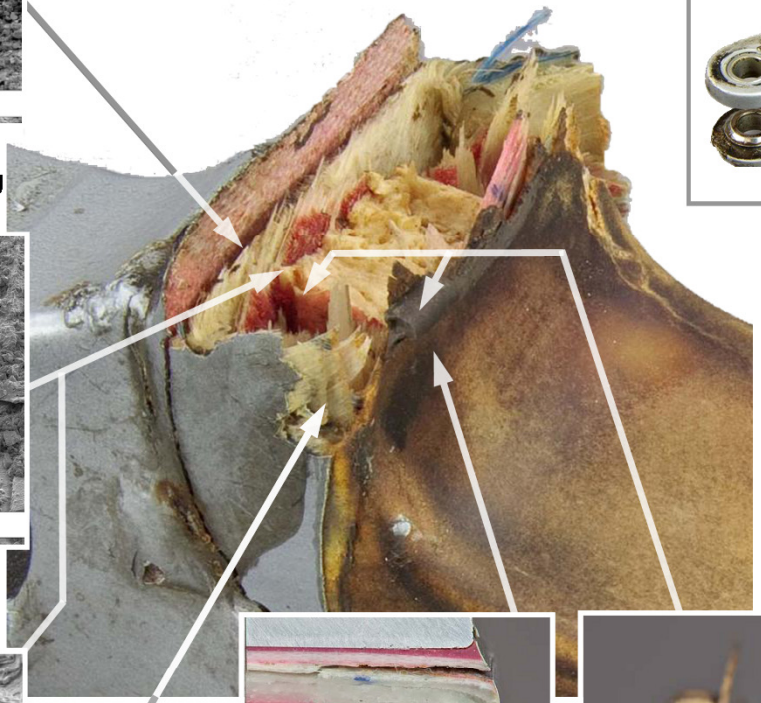

Cut plies

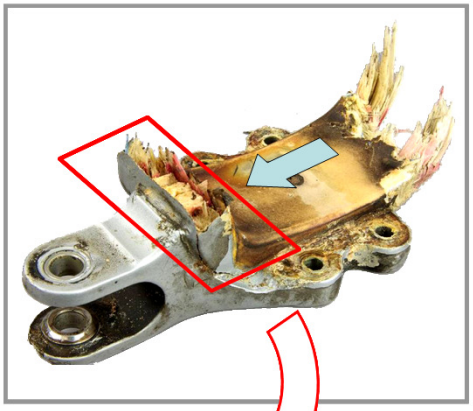

Adhesive bleeding into 0º load bearing trap (*Fig.60*)

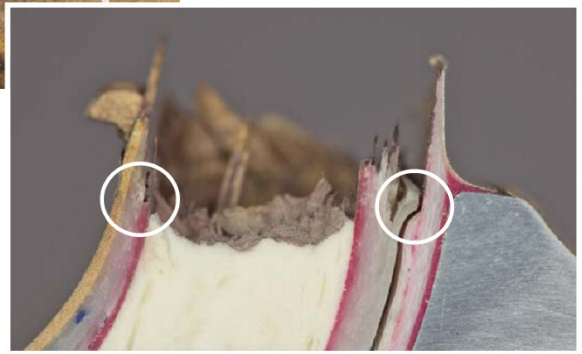

"Pinched" plies in external layers of GFRC torsion box (*Fig.60*)

Reduced number of plies in GFRC torsion box (*Fig.60*)

EASA actions Addressing CAD Safety Recommendation 2011-4

1) Temperature survey

A dedicated test campaign has been performed to assess the maximum blade root temperature while exposed to direct sun light with reference to the external environment.
As reported in the following graph the overheating effect generated by direct sun light exposure was measured in about 5℃ over the OAT and therefore fully addressed in the tail rotor blade certification.

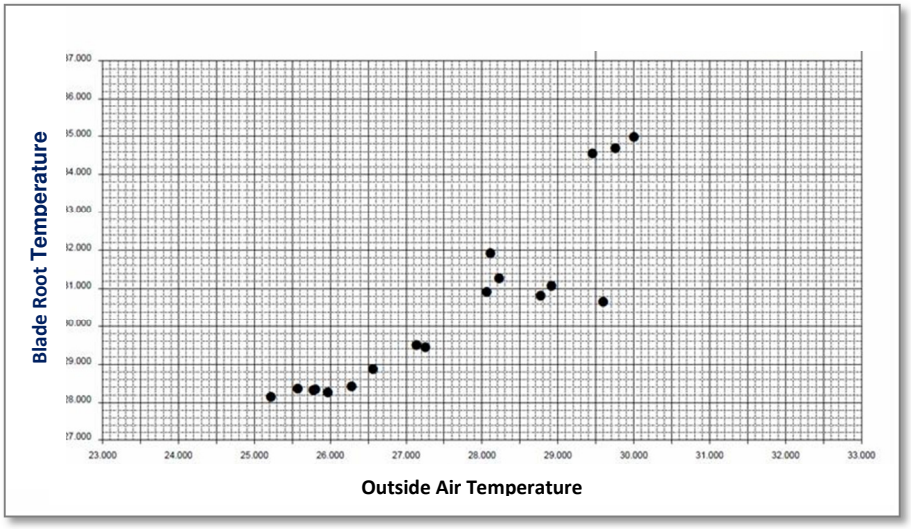

OAT vs Blade root temperature

Thermal fatigue on the root area, as result of the bonding between the metallic pitch change arm and the composite, was also tested up to 70℃ (maximum value for requirements).
Results showed a small percentage in respect to the load condition, therefore excluding any damaging effect related to the different coefficient of expansion of the two materials.

2) In-flight blade strain-stress/load survey

The original certification load survey was performed on an instrumented aircraft including blades with strain gauges bridges able to record beam/chord bending moment.
At that time, the root handle was shown not to be the critical section. The most stressed was the one located in the transition area where flight bending moments (beam and chord) are maximum.
Following these accidents an additional stress/strain survey has been carried out to investigate local stress distribution at the failed section.
A load survey was performed using a blade instrumented with additional strain gauges in the root area.

The stress survey performed included the most significant flight conditions of AW139 spectrum as well as other extreme conditions outside the flight envelope. Instrumentation sampling rate was confirmed adequate to fully and properly record the flight loads.

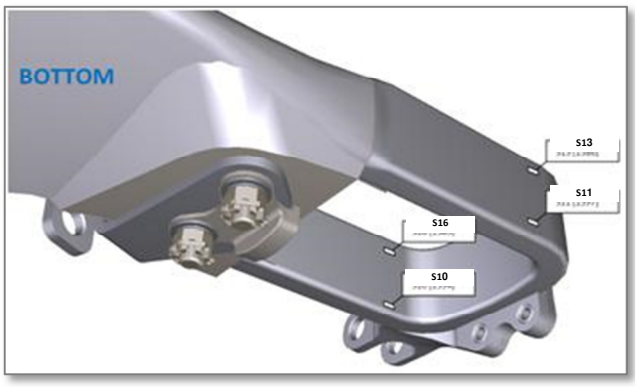

Strain gauges position (Bottom View)

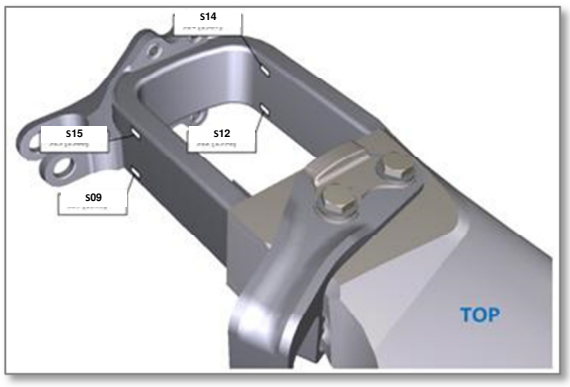

Strain gauges position (Top View)

The results from the flight strain survey highlighted that over 90% of the strain amplitude in the blade root area is mainly due to Centrifugal Force (CF). The strain amplitude associated to vibratory loads is less than 10%. Maximum strain values were measured in autorotation flight condition (110% RPM). A local bending moment at the trailing edge bottom strap area was evident with tensile stress in the inner side and compressive stress on the outer torsion box skin (analysis showed that the straps work always in tension).

Extreme flight and ground conditions did not pointed out any concern in terms of possible overload. The significant load condition is therefore to be associated with the Engine start-stop conditions (see plots below).

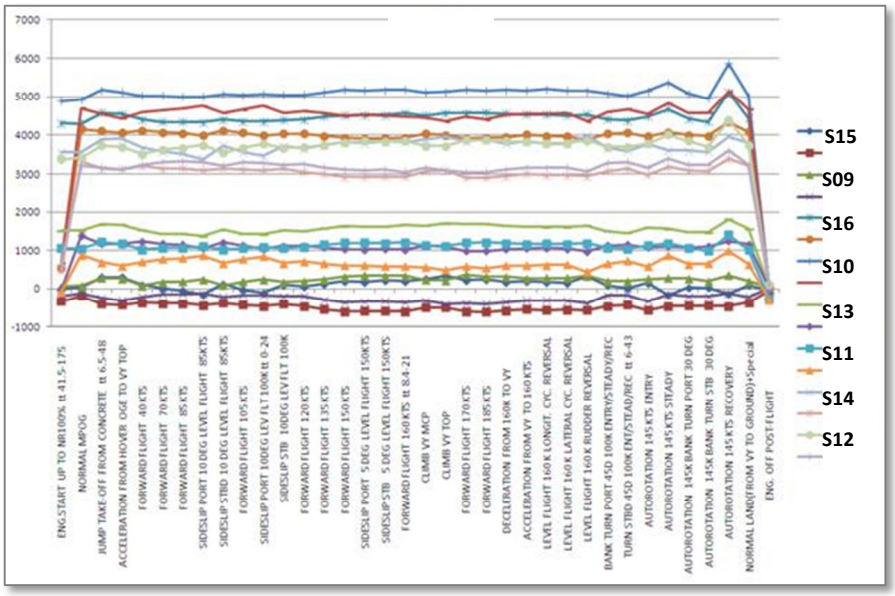

Flight stress survey

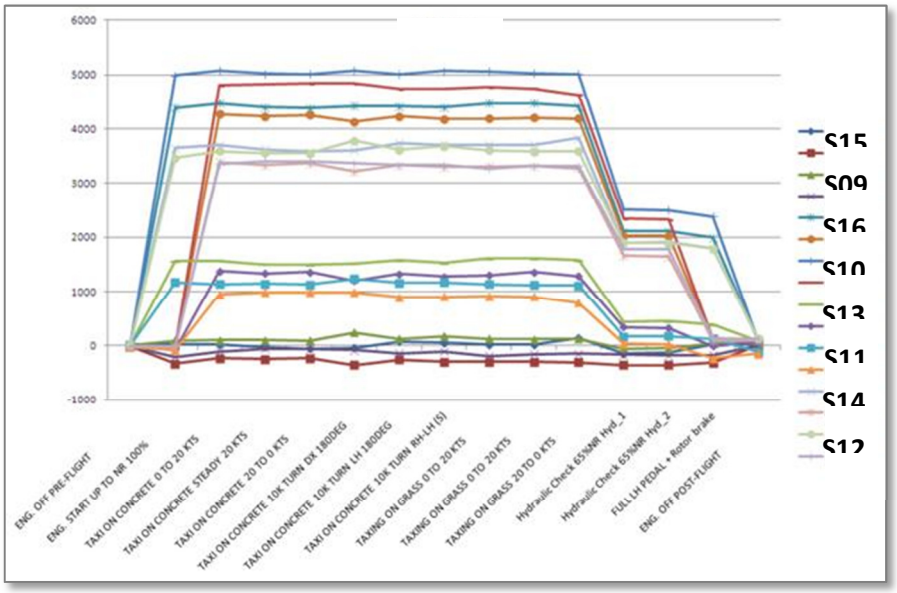

Ground stress survey

Conservatively for the purposes of establishing a reliable quarantine limits these low frequencies conditions have been assimilated to the Ground-Air-Ground cycles.

3) Full scale fatigue tests and Static test survey

Following the flight stress survey an additional static test survey was performed in order to monitor the most critical blade root stress/strain parameters reproducing the maximum values measured in flight. The nominal limit load condition was estimated in terms of strain calculated at 116% RPM (Design Limit Loads).
The autorotation conditions were executed at 110% RPM; to have a conservative approach for the calculation of the target strain value at 116% RPM, the strain is factored by quadratic proportion with respect to the RPM ratio.

The test stand was calibrated with a set of loads (CF, Pitch Link Force, Damper Lateral Force, Chord and Beam Bending) in order to reproduce the target nominal limit strains providing the correct CF value at 116% RPM and maximum Pitch Link Force measured in flight. Then the loads were amplified, monitoring the amplification resulting on the strain values. Several Static Tests were performed both at factored limit and ultimate loads, accounting for environmental factor HTW = 1.8 (fiberglass split tape 5216-S2 per 199-44-006 Ty A, cl S2).

A total of seven blade specimens were tested both before and after fatigue loading. Most of the tested specimens were obtained by blades recovered from service and having accumulated a significant fatigue life in real operational environment. The typical blade test setup applies CF, beam/chord bending moment and torsion load. Due to the amplified load to be applied the original elastomeric bearing was replaced by a dummy one.

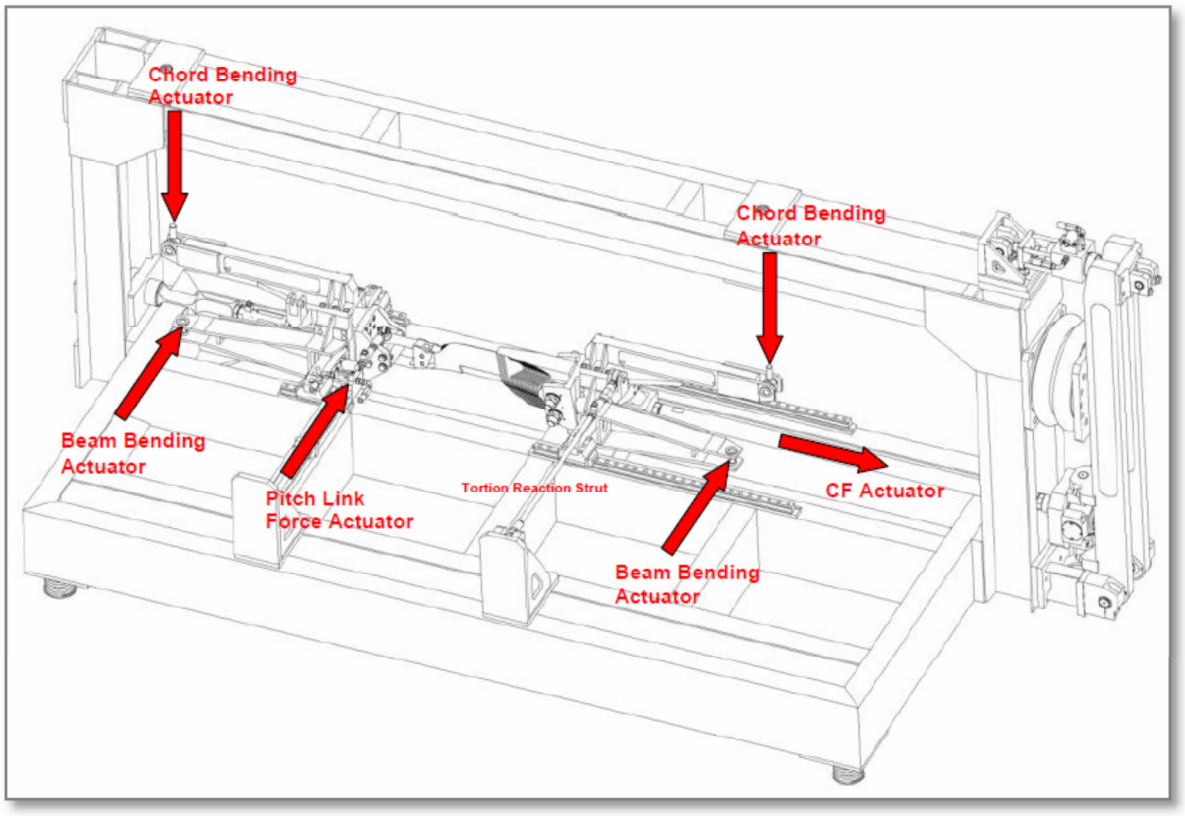

Blade static stress test rig

Several full scale fatigue tests have been carried out by the manufacturer with different combinations of production strap defects and possible damages (i.e. torsion box degraded characteristics for plies removal, pitch change arm debonding and artificial damages in the strap surface).

Bending stiffness characteristic of the failed section is mainly dominated by the torsion box that provides about the 65% of stiffness. In addition extremely severe tests have been performed with a strap totally severed.

The fatigue test results performed on the specimen have been plotted and best fitted with a proper curve shape to obtain a “Wholer” curve representative of the blade fatigue strength in presence of relevant defects and damages.

The proper curve shape was obtained by dedicated coupon fatigue tests performed at R=0.1 load condition representative of GAG cycle. The coupons have been directly obtained by production strap root area and have been fatigue tested in a four point bending condition

obtaining an ILSS failure mode representative of matrix failure dominated mode.

The delta stress/strain recorded close to the failed section was chosen as representative parameter of the bending moment in the section governing the fatigue phenomena.

Pitch change arm debonding was assessed in a test stress survey identifying the relevant stress raiser effect in the trailing edge bottom strap area. In detail, a pitch change arm debonding in the curved root area resulted in about 40% of nominal stress increasing
(see blue curve of the plots below)

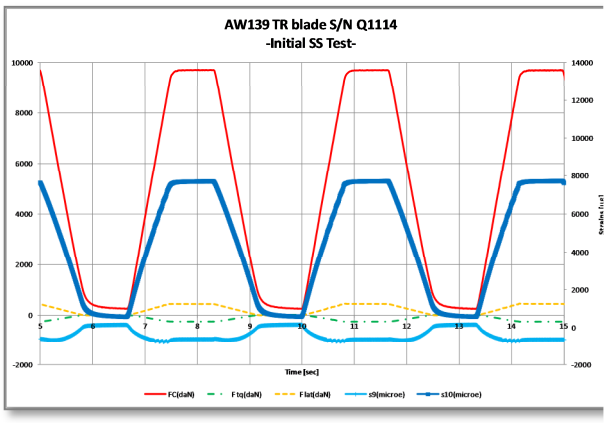

PCA bonded

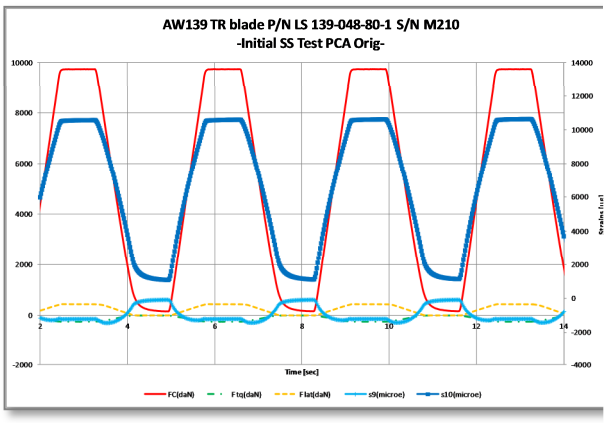

PCA debonded

Considering the strain level corresponding to the worst GAG low frequency cycle (104% NR – Power on green scale), the computed flaw tolerant safe life provides a retirement life greater than the actual quarantine limitation (see fatigue chart below)

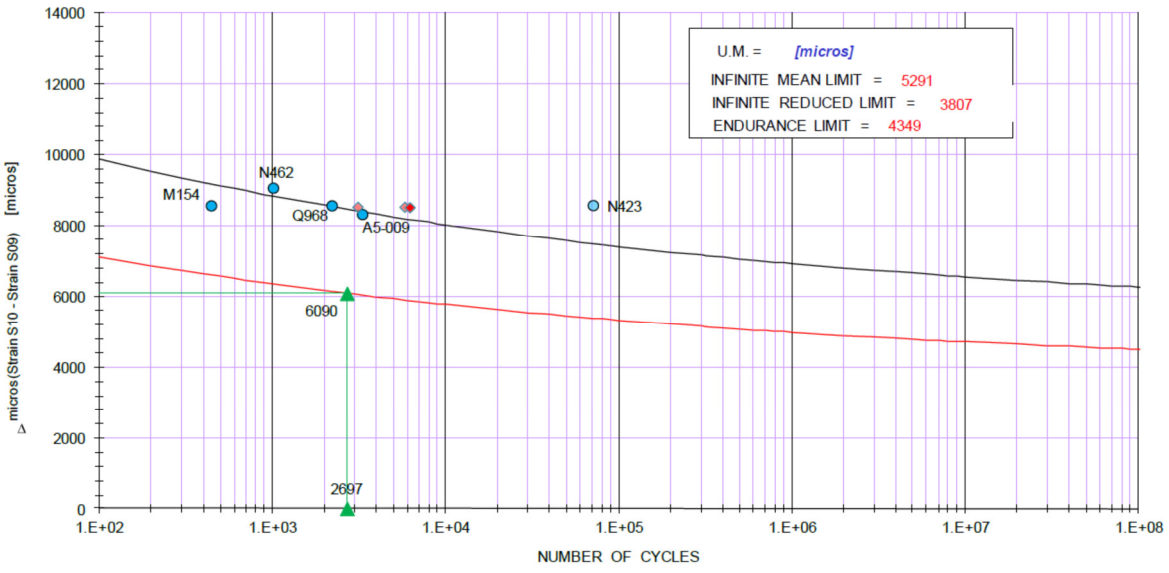

The 25FH periodic inspection requirement of the BT139-265, aimed to detect torsion box degradation and pitch change arm disbonding, provides relevant additional safety margin to the actual quarantine limitation.

4) Blade dynamic stability evaluation

Although the TR dynamic stability presents significant margins, factors possibly affecting the stability have been reviewed.
Complete stability analysis was performed for a 20% reduction of all the straps sections with no evidence of margins reduction. Tail rotor components installation backlash was checked verified and found not significantly affecting the dynamic stability of the rotor.
Sudden failure of one strap section was also evaluated for dynamic effects, without evidence of instability phenomena.

5) Finite Element Method model analysis of the blade root area

A very detailed FEM of the root blade area was developed; the more detailed model was able to properly represent stress/strain condition in the root area including the local bending in the trailing edge bottom strap.

Blade root FEM model

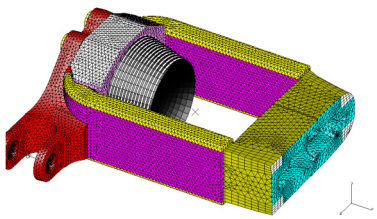

Blade root FEM model

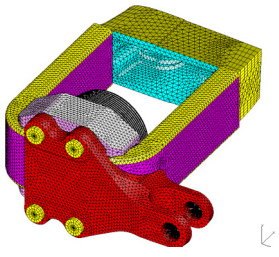

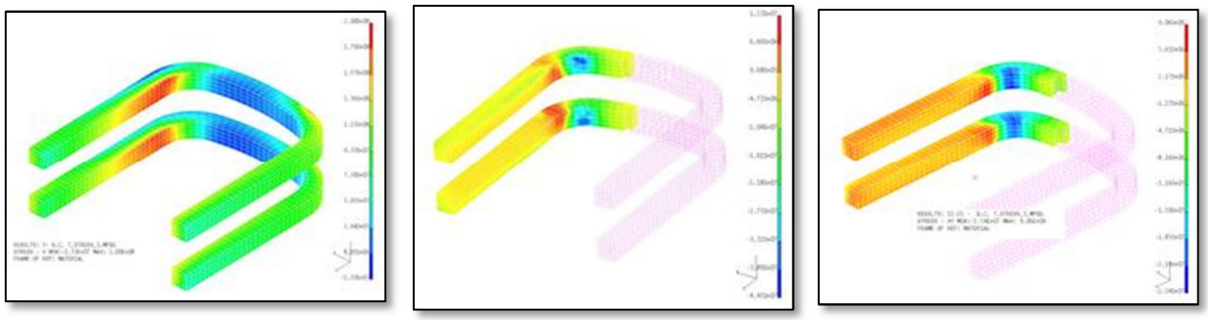

Longitudinal stress

Radial stress

Shear stress

The FE-Model has straps and XLD filler modelled with parabolic brick elements and anti-torsion box modelled with tetra parabolic elements.

The total elements are 125672 and the total nodes are 248700

The bolts have been modelled with solid elements.

Gaps and Contacts are represented; Contacts have been defined between the Bearing and the Blade Root, between the Pitch Arm and the Bearing and between the bolts and the Pitch Arm/Bearing;

The Pitch Arm is bonded to the antitorsional box through a layer of solid elements having the elastic properties of the AF163 adhesive.

Validation of the FEM model was made by comparing the predicted strains in the critical condition of the TR blade root handle trailing edge (see strain gages S10 and S16 in the sketch below)

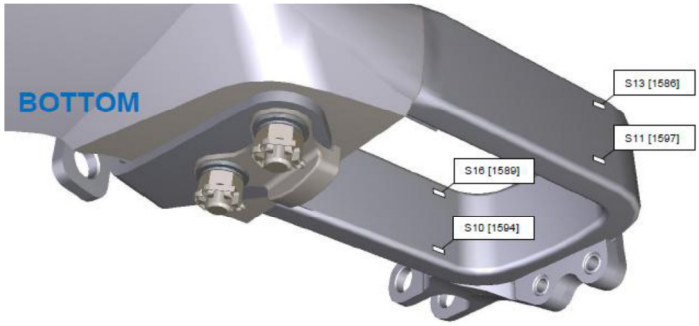

with the values recorded at the same locations on an instrumented tail rotor blades installed on the helicopter (see table below) :

	FEM strain	Flight Strain

S10	4785	4972
S16	4753	4318

The so validated FEM model was then used to estimate the structural strength behaviour and the effects of defects such as reduction of the external box and delaminations under the most critical flight conditions.

As already indicated above the chord bending stiffness of the TR root handle is mainly provided by the external box that contributes by 65 % of the overall bending stiffness-

In particular the detailed FEM model was able to estimate the magnitude of the interlaminar stresses (radial and shear) acting on the TR blade and their contribution to initiate interlaminar damages that eventually lead to the failure of the TR blade section.

The FEM model confirmed the correlation between chord bending stiffness and magnitude of the radial and shear stresses (i.e the lower the chord bending stiffness the higher the magnitude of the stresses).

Namely the FEM model indicated also that, under the most critical loading condition and in presence of macroscopic defects such as reduction of the external box and disbond of the pitch control arm, it is possible that the magnitude on the interlaminar radial stresses exceed the maximum allowable and cause a delamination onset (Open MODE I) in the curved area of the TR root handle.

Delamination could then grow and propagate due to Inter Laminar Shear Stress (Shear MODE II).

The combination of the above failure modes (Radial and ILSS) can lead to possible subsequent multiple delaminations in the radius area, through the complete thickness.

Stress/strain analysis results are consistent with failure mode evidence pointed out by the failure analysis of the failed blade.

For further and more detailed explanation on the failure modes of the TR please refer also to the EASA presentation provided during the ANSV Meeting of 30 May 2012.